Corrosion and tribocorrosion characterisation of Ti13Nb13Zr alloy in oral environment for dental implants

Ione Golvano Escobal

Mondragon Goi Eskola Politeknikoa
Mechanical and manufacturing department

November 13, 2015

Corrosion and tribocorrosion characterisation of Ti13Nb13Zr alloy in oral environment for dental implants

Ione Golvano Escobal

dirigida por:

Dr. Andrea Aginagalde
Mechanical and manufacturing department
Mondragon Unibertsitatea

Dr. Iñaki García Diego
Surface engineering, corrosion and durability department
CENIM-CSIC

para la obtención del grado de Doctor
bajo el programa de doctorado de la Universidad de Mondragon:
Mechanical behaviour and materials.

Tribunal de Tesis:
Presidente: Dr. Stefano Mischler (École Polytechnique Fédérale de Lausanne)
Vocal: Dr. Raquel Bayón (TEKNIKER)
Vocal: Dr. Rafael Rodríguez Trías (Universidad Pública de Navarra)
Vocal: Dr. Ana Conde (CENIM-CSIC)
Secretario: Dr. Wilson Tato (Mondragon Unibertsitatea)

November 13, 2015

Acta de Grado de doctor
Acta de defensa de Tesis Doctoral

Doctorando: D./Dña. Ione Golvano Escobal

Título de la Tesis: "**Corrosion and tribocorrosion characterisation of Ti13Nb13Zr alloy in oral environment for dental implants.**"

El tribunal nombrado por el Excmo. y Magfco. Sr. Rector para calificar la Tesis Doctoral arriba indicada y constituido en el día de la fecha por los miembros que suscriben la presente Acta, una vez efectuada la defensa por el doctorando y contestadas las objeciones y/o sugerencias que se han formulado ha otorgado por _____ la calificación de:

El Presidente: ..... Fdo:_____

El Secretario: ..... Fdo:_____

Vocal: ..... Fdo:_____

Vocal: ..... Fdo:_____

Vocal: ..... Fdo:_____

Doctorando: ..... Fdo:_____

En _____, a _____ de _____ de 200__

Etxekoei

Laburpena

Osasunaren ikuspuntutik, biztanleriaren zahartzeak eta bizitza kalitatearen igoerak biztanleriaren beharrak aldatzera eraman dituzte.

Gero eta dentista gutxiagok hortzordeak jartzen dituzte hortzik gabeko pazienteetan. Honen arrazoi nagusia, inplantologia oralaren garapena hortz inplanteetan jarri duen kalitate zeinua eta iraunkortasuna izan da. Hala ere, eskakizun mailek eta produktuaren bizitzak handiagotze joera dute eta materiala edota gainazal iraunkorragoak eta bateragarriagoak, bai mekanikoki eta biologikoki, garatu behar dira.

Tesi doktoral honetan, hortz inplanteetan erabiltzeko aleazio berri bat karakterizatu dugu. Ti13Nb13Zr aleazioak hezurrarekiko propietate mekaniko antzekoagoak izateaz gain, aleazio elementu biokonpatibleak ere badauzka. Hortz inplanteek mastikazioa jasan behar dutenez ingurune oldarkor batean (listua), korrosio eta tribokorrosioarekiko karakterizazioa aurrera eraman dugu.

Lortutako emaitzak, egun asko erabiltzen den materialaren antzekoak izan dira, CpTi4. Beraz, Ti13Nb13Zr aleazioa inplantologia oralerako material hautagaia bihurtzen da.

Are gehiago, materialaren babesa sustatzeko bi alternatiba ikertu dira. Alde batetik, korrosio inhibitzaileak listuan gehitzea irakuzketen bidez; apustu interesgarri bat, nahitaezko osagarri batean bihurtu litekeela inplanteen korrosio eta degradazioa kontrolatzeko.

Bestalde, oxidazio termikoak Ti13Nb13Zr aleazioan, tratamendu termikoa kostu lehiakorrean, materialearen degradazio abiadura % 200-ean murriztea erakutsi du.

Abstract

Ageing of the population together with the increase of life's quality in developed societies, has lead to a change of population needs from the health point of view.

Dentist placing dentures are increasingly fewer, since the large development in oral implantology has attributed a sign of quality and durability to dental implants. However, the exigency level and product life tend to increase, which attracts attention to the development of more durable materials and surfaces and more compatible, from mechanical and biological viewpoint.

In this thesis dissertation, a promising alloy in the area of oral implantology has been characterised. Ti13Nb13Zr alloy has not only a much many similar mechanical properties comparing to the bone, but it also has biocompatible alloying elements. Corrosion and tribocorrosion characterisation of the alloy has been carried out to study the mechanical request due to mastication events in an aggressive environment such as saliva.

Results were very similar to the widely used materials, *i.e.* commercially pure titanium, which converts Ti13Nb13Zr alloy in candidate material for oral implantology applications.

Two different ways have also been studied to enhance metal protection. On the one hand, the addition of corrosion inhibitors through mouth-rinses, an innovative faith that could became an essential accessory to control corrosion and alloy degradation.

On the other, thermal oxidation of Ti13Nb13Zr, a cost effective thermal treatment, that has shown to reduce the degradation rate in more than a 200 %.

Resumen

El continuo envejecimiento de la población, junto con el incremento de la calidad de vida en las sociedades desarrolladas, han llevado a un cambio en cuanto a necesidades del ciudadano desde el punto de vista de salud.

Cada vez menos dentistas ponen dentaduras en sus pacientes edéntulos. El rápido desarrollo en el área de implantología oral, hace que un implante dental se haya convertido en seña de calidad y durabilidad. Sin embargo, las exigencias y la vida de los productos tiende a incrementarse, lo que llama al desarrollo de materiales y superficies más duraderas y más compatibles, tanto mecánica como biologicamente.

En esta tesis doctoral se ha caracterizado una prometedora aleación en el campo de la implantología oral. El Ti13Nb13Zr no solo ofrece unas propiedades mecánicas mucho más similares a las del hueso, sino que sus aleantes también son biocompatibles. La caracterización se ha llevado a cabo desde el punto de vista de corrosión y tribocorrosión, solicitaciones que inevitablemente van a tener lugar en el entorno oral debido a los eventos de masticación en un entorno agresivo como es la saliva.

Los resultados obtenidos has sido muy similares a los del material más utilizado en la actualidad, el titanio comercialmente puro, lo que convierte a la aleación Ti13Nb13Zr en material candidato para aplicaciones de implantología oral.

También se han estudiado dos vías para mejorar la protección de la aleación. Por un lado la aplicación de inhibidores de corrosión a través de enjuagues bucales, una apuesta innovadora que podría convertirse en accesorio indispensable para controlar la corrosión y degradación de la aleación.

Por otro lado, la oxidación térmica del Ti13Nb13Zr, un tratamiento térmico de bajo coste, mediante el cuál se ha conseguido reducir la velocidad del desgaste en más de un 200 %.

Eskertzak

En estos años he aprendido muchas cosas, de las cuales podría destacar una buena lección: si de una reunión no sales con nuevas ideas que dan al traste con tu plan, es que la reunión no ha terminado.

En primer lugar me gustaría dar las gracias a mis directores de tesis. Andreari, tesia egiteko aukera emateagatik, eta niregan konfidantza osoa edukitzeagatik. A Iñaki, por tu apoyo e interés a lo largo de estos 3 años. Ha sido un placer poder trabajar contigo.

Thank you to Prof. Celis for those interesting discussion meetings at your office. A Wilson por tu ayuda y tus conocimientos. A Ana y al resto del equipo COPROMAT por compartir sus conocimientos y por hacerme sentir una más en mis breves visitas.

También me gustaría decir eskerrik asko a mi familia y a David, por apoyarme en esta aventura que ya no sé ni el tiempo que ha durado!

Lo que sí que sé es que me ha dado la oportunidad de trabajar junto con personas que merece la pena conocer. La kuadri de los veteranos. Alaitz, con una mirada ya nos sobran las palabras. Jokin, con tantas heridas de guerra debes de tener como 200 años. Joanes, me gusta tu cerve. Elena, no te sigo. Javi, un grande. Nagore, vuelve pronto. Manex, tan reflexivo. Haritz, siempre hay una pregunta más rara. Alain, David, Kintana, Joseba, Irantzu, Miren, Ekaitz, Mikel, Aitor, Luis... mis chóferes, Chamorro, Buru, Cuesta y Torrano, huyendo juntos a diario. Gotzon, Iñaki, Larraitz, Nagore, etab. eskerrikasko zuei ere zuen lanagatik.

Leuveners. I really miss that stage because of the people I met. And beer. And chocolate. Ah! and cheese. My counselors, Manolis, Houcine and Ivan, thank you for putting up with me. Mi querida Andrea... Frodo y Enea, todo lo que sé de cervezas es gracias a vosotros. María, la misionera euskaldunizadora, su proyecto 'Móstoles' y su cobaya, Mikeltxo. Goku, Nachi, my spicy guys. Kim, the spaniard who wanted to be belgian, but failed. Simona, my little italian patissier. Maarten and his endless curiosity. Ali, so bitch. And so on.

Eskerrik asko ere bai aipatzen ez ditudanei.

HURRENGORARTE!

Contents

Contents **xvii**

1 Introduction **1**

1.1 Introduction 2

1.2 Metallic biomaterials for dental implants 4

1.3 The oral environment 6

1.3.1 Human saliva 7

1.3.2 Mastication events 9

1.4 Electrochemical behaviour of titanium dental implants 11

1.5 Tribocorrosion behaviour of titanium dental implants 15

2 Motivation and scope of the thesis **19**

2.1 Motivation and background 20

2.2 Scope of the thesis 22

3 Ti13Nb13Zr alloy generalities **25**

3.1 Material and electrolyte preparation 26

3.1.1 Materials 26

3.1.2 Electrolyte preparation 26

3.2 Surface characterisation 27

3.2.1 Microstructure 27

3.2.2 XPS 28

3.3 Chemical characterisation 30

3.4 Mechanical properties 31

3.4.1 Hardness test 31

3.4.2 Tensile test 31

4 Influence of fluoride and pH on corrosion and tribocorrosion behaviour of Ti13Nb13Zr alloy in oral environment **33**

4.1 Introduction . . . 34
4.1.1 Objectives and hypothesis . . . 34
4.2 Materials and methods . . . 34
4.2.1 Materials . . . 34
4.2.2 Electrochemical and reciprocating sliding corrosion tests . . . 34
4.3 Results and discussion . . . 36
4.3.1 Corrosion behaviour . . . 36
4.3.2 Reciprocating sliding corrosion tests . . . 39
4.3.3 Wear track characterisation . . . 44
4.4 Conclusions . . . 47

5 Repassivation kinetics of Ti13Nb13Zr alloy in oral environment 49
5.1 Introduction . . . 50
5.1.1 Experimental depassivation techniques . . . 53
5.1.2 Electrochemical techniques to measure the depassivation/repassivation events measurement . . . 54
5.1.3 Theoretical repassivation models . . . 55
5.1.4 Objectives and hypothesis . . . 56
5.2 Materials and Methods . . . 57
5.2.1 Materials . . . 57
5.2.2 Repassivation kinetics tests . . . 57
5.2.3 Reciprocating sliding corrosion tests . . . 58
5.3 Results and discussion . . . 59
5.3.1 Sliding frequency . . . 60
5.3.2 Repassivation kinetics . . . 63
5.3.3 Sliding time . . . 66
5.3.4 Intermittency . . . 68
5.4 Conclusions . . . 69

6 Effects of corrosion inhibitors added to the oral medium on the tribocorrosion behaviour of Ti13Nb13Zr 71
6.1 Introduction . . . 72
6.2 Objetives and hypothesis . . . 74
6.3 Materials and Methods . . . 74
6.3.1 Corrosion tests . . . 75
6.3.2 Repassivation kinetics tests . . . 75

6.3.3 Reciprocating sliding corrosion tests . . . 76
6.4 Results and discussion . . . 76
6.4.1 Corrosion behaviour . . . 76
6.4.2 Repassivation kinetics . . . 78
6.4.3 Reciprocating sliding corrosion tests . . . 79
6.5 Conclusions . . . 82

7 Improvement of the tribocorrosion resistance by thermal oxidation of Ti13Nb13Zr alloy 83
7.1 Introduction . . . 84
7.2 Objetives and hypothesis . . . 85
7.3 Materials and Methods . . . 86
7.3.1 Materials . . . 86
7.3.2 Electrochemical and reciprocating sliding corrosion tests . . . 87
7.4 Results and Discussion . . . 88
7.4.1 Influence of temperature on thermally oxidised Ti13Nb13Zr . . . 88
7.4.2 Influence of treatment duration on thermally oxidised Ti13Nb13Zr 94
7.4.3 Tribocorrosion behaviour of thermally oxidised Ti13Nb13Zr. . . . 99
7.5 Conclusions . . . 104

8 Conclusions and future work 105
8.1 Conclusions . . . 105
8.2 Future work . . . 106

List of Figures 109

List of Tables 115

Bibliography 117

Chapter 1

Introduction

CpTi and Ti6Al4V alloy are the most widely used materials for implant application, but the release of toxic elements (*e.g.* Al and V) and the so-called *stress-shielding* effect are still a concern. In recent years, β and near-β titanium alloys have been developed, which overcome these issues with reduced modulus of elasticity and biocompatible alloying elements. However, literature is scarce studying the tribocorrosion behaviour of these alloys for dental implantology.

In this chapter a general review of the state of the art is made.

1.1 Introduction

Dental implants are used to support one or more false teeth. They consist of a metallic screw attached to the bone replacing the root of a tooth when it fails. Four are the basic parts of a dental implant, as it can be seen in Figure 1.1: (1) Crown, (2) abutment screw, (3) abutment and (4) implant.

Figure 1.1: The dental implant is composed of (1) a crown, (2) an abutment screw, (3) an abutment and (4) an implant.

A successfully placed dental implant requires osseointegration and biocompatibility. Osseointegration is defined as the capability of the implant to remain attached to the surrounding bone tissue. In 1940, Bothe, Beaton, and Davenport were the first to observe that bone grows into titanium [1], but it was not until 1977 that 'osseointegration' concept was introduced by Bränemark [2].

Bone quality, implant surface attachment and mechanical stimulation in the surrounding bone are crucial to ensure the dental implant osseointegration. The outer wall of the bone is the cortical bone and it is a dense and solid mass with microscopic channels. Approximately 80% of the skeletal mass in the adult human skeleton is cortical bone and it is largely responsible for the supportive and protective function of the skeleton. Filling the interior of the organ, the remaining 20% of the bone mass is trabecular or cancellous bone, an open cell porous network that allows room for blood vessels and marrow. Bone density is one of the restrictions dentists have to deal with since if it is very low, it reduces bone attachment to the implant. In addition, Rubin and Lanyon highlighted that bone is 'genetically programmed to accept a particular amount and pattern of stress as normal, and its deviation from this 'optimal strain environment' would stimulate changes in the bone's remodelling balance, resulting in adaptive increase or decrease in its mass' [3]. Bone density usually also reduces with patient age. Thus, if a

lost tooth is not replaced within a reasonable period of time, bone density will be reduced hindering its replacement. Indeed, a review about the biological factors contributing to failures of dental implants, revealed that failure rates within edentulous patients were almost double those for partially dentate patients (7.6% versus 3.8%) [4].

Once the dental implant is screwed replacing a missing tooth, a proper stress transfer and surface topography are necessary to achieve the anchorage between the implant and the bone. Attending to Wolff's law [5], the internal structure of the bone adapt to mechanical request. In this way, it grows more bone tissue in the loaded areas whereas bone density decreases when no load is applied, leading to bone tissue to be resorbed by the body. Implant materials have a much higher modulus of elasticity than human bone ($E_{bone} = 13.7$ GPa [6]). Consequently, when a rigid implant is loaded due to mastication events, it may absorb the majority of mastication forces leading to insufficient stimulation to the surrounding bone. The so-called *stress-shielding effect* becomes apparent when there is a large mismatch between the mechanical properties of the dental implant and the bone [7], and it may end up in the loosening of the implant [8].

The biocompatibility contemplates the suitability of the material and alloying elements for biomedical applications and the behaviour of the implant in the oral environment. It was defined by Williams as 'the ability of a material to perform with an appropriate host response in a specific body application' [9]. However, no known surgical implant material has ever been shown to be completely free of adverse reactions in the human body. Thus, it is not only the toxicity grade of the material, but also its concentration. In this respect, corrosion is a mechanism that can lead to the release of additional ions into the body. Extensive release of ions from implant can result in adverse biological reactions, and may also lead to a mechanical failure of the device. Thus, corrosion of dental implants is closely related to its biocompatibility. Indeed, the high corrosion resistance that passive metals offer over a wide range of biological environments, it makes them reference materials for implantation. Data on corrosion resistance and biocompatibility of pure metals and representative biocompatible metallic materials are shown in Figure 1.2. Ta, Nb, Ti and Zr are the most biocompatible elements, whereas Co, Cu, Ni and V are classified as toxic.

The effect of corrosion may be visible *in vivo* when it is severe and consequently a change of surface coloration or perimplant inflammations caused by ions release can take place. Previous studies have revealed that failures in implant systems can be associated to the corrosion of titanium. Guindy *et al.* [11] analysed six implants as well as their suprastructures for surface corrosion. Extensive corrosion lesions and areas of oxidation were detected on all six of the implants and inner crown surfaces. Toxic ions were founded on the peri-implant bone, causing bone structure breakdown and

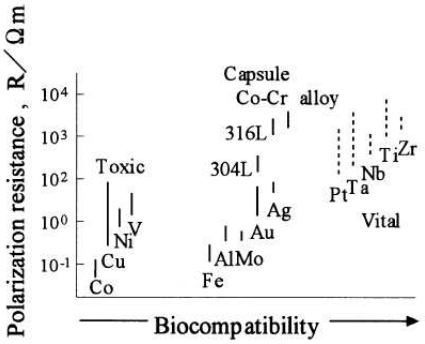

Figure 1.2: Relationship between polarization resistance and biocompatibility of pure metals and some alloys [10].

hastening osseodeintegration. Additionally, when oral fluids penetrate into microgaps between metallic components of implant system, a closed electrical circuit is established. Thus, an in vivo galvanic cell is formed and the galvanic current causes acceleration of corrosion of the less noble metal. This passes through the metal/metal junction and also through tissues, which causes pain. In addition to galvanic corrosion, crevice and pitting corrosion may occur in the marginal gap between dental implant assemblies [12].

1.2 Metallic biomaterials for dental implants

During the first half of the twentieth century, implants were designated using materials with great success in industrial applications, such as chemistry, mechanical and aerospace industry. Thus the only requirement of implant materials was to be as inert as possible in order to reduce the release of ions and particles after implantation. Stainless steel (E= 210 GPa [13]) was first used as an implant material in the surgical field. Then, CoCr and CoCrMo alloys (E= 240 GPa [13]) were also used for many years. It was not until 1969, when the field of biomaterials gained its recognition after the first meeting held on biomaterials at Clemson University, South Carolina.

The concept of biocompatibility was introduced in order to evaluate the biological response of artificial materials through a set of *in vivo* and *in vitro* standardised tests. The mechanical properties started to play an important role in the selection of implant materials.

Among the materials available for implant applications, the natural selection of titanium-based materials for implantation was due to the combination of its outstanding characteristics, such as good corrosion resistance in biological environments, good strength to weigth ratio ($E_{Ti} < 110$ GPa and $\rho_{Ti} = 4.51\ g \cdot cm^{-3}$), osseointegration and biocompatibility.

Titanium is a very reactive metal, which reacts spontaneously in the presence of air or water, forming a TiO_2 layer of few nanometers thickness. Indeed, this protective passive film is responsible for the chemical stability, good corrosion resistance and fast repassivation kinetics of the metal in a wide range of environments. However, tribocorrosion events are likely to occur when a metallic implant is inserted in the mouth. This is due to the combination of tribological processes due to mastication forces in a corrosive environment, *i.e.* saliva. This involves the degradation or even removal of the protective passive layer of titanium and thus the onset of the active dissolution of titanium takes place until it completely repassivates again. In fact, a high concentration of titanium in the body, such as ions and nano-particles, may also induce significant toxicity [14].

Nowadays, commercially pure titanium (CpTi) (E = 100 GPa [13]) is one of the most commonly used materials for dental implants. The high reactivity of titanium difficults the production of the pure metal, therefore the so-called commercially pure titanium (CpTi) is used for commercial applications. The American Society for Testing and Materials (ASTM) classifies the CpTi in four grades according to the concentration of oxygen and other elements, as it can be seen in Table 1.3. Ti6Al4V alloy (E = 110-112 GPa [13]), originally developed for aerospace applications, is also widely used for body implantation since the alloying of titanium confers an increase of the tensile strength. However, the release of vanadium and aluminium ions from the implant to the surrounding tissues have found to be associated with long-term health problems, such as Alzheimer disease, neuropathy and osteomalacia (see also Figure 1.2). In addition, vanadium is also toxic both in the elemental state and oxidated (V_2O_5) [15].

Figure 1.3: Classification and chemical composition of commercially pure titanium according to ASTM F67.

Element	Max. Composition, wt.%			
	Grade 1	Grade 2	Grade 3	Grade 4
Nitrogen	0.03	0.03	0.05	0.05
Carbon	0.08	0.08	0.08	0.08
Hydrogen	0.015	0.015	0.015	0.015
Iron	0.2	0.3	0.3	0.5
Oxygen	0.18	0.25	0.35	0.4
Titanium	balance	balance	balance	balance

In this regard, the interest to reduce the rigidity of implant materials promoted the development of a second generation of β and near-β titanium alloys with reduced

modulus of elasticity, listed in Table 1.1 together with the previous generation of titanium and its alloys. Indeed, β stabilising elements such as molybdenum (Mo), zirconium (Zr), tantalum (Ta) and niobium (Nb) used as alloying elements for titanium dental implants, have demonstrated to enhance biocompatibility and cell adherence [16, 17]; as well as a reduced Young modulus, related to the decrease of the *stress-shielding effect*.

Table 1.1: Mechanical properties of biomedical titanium alloys [13].

Material	Standard	Young Modulus (GPa)	Yield strength (MPa)	Structure
First generation of titanium based biomaterials (1950-1990)				
Cp Ti (Grade 1-4)	ASTM F67	100	240-550	α
Ti6Al4V ELI	ASTM F136	110	860-965	α+β
Ti6Al7Nb	ASTM F1295	110	900-1050	α+β
Ti5Al2.5Fe	-	110	1020	α+β
Second generation of titanium based biomaterials (1990-until date)				
Ti13Nb13Zr	ASTM F1713	79-84	973-1037	Met. β
Ti12Mo6Zr2Fe	ASTM F1813	74-85	1060-1100	β
Ti35Nb7Zr5Ta	-	55	596	β
Ti29Nb13Ta4.6Zr	-	65	911	β
Ti35Nb5Ta7Zr0.4O	-	66	1010	β
Ti15Mo	ASTM F2066	-	-	β

Ti13Nb13Zr is a near-β titanium alloy ($E = 79$ GPa). It was initially developed joint replacements [18, 19, 20, 21, 22, 23], although recently it is receiving increased attention in the field of dental implants [24, 25]. Nb addition results in the improvement of the mechanical properties of the alloy, together with the solid solution hardening effect of Zr [26].

1.3 The oral environment

When a dental implant is placed in the oral cavity to replace a missing tooth, it has to face a harsh oral environment. Human saliva is a very aggressive media which is continuously changing and may deteriorate the corrosion resistance of the implanted material. Besides the saliva, mastication events provoke microcontacts between the implant and the bone, leading to debris generation.

1.3.1 Human saliva

Natural saliva is a mixture of fluids secreted by the parotid, submaxillary and sublingual glands that have been shown to differ from each other in composition and in volume [27]. Saliva is considered to play an important role in the maintenance of the oral health of the human body, on the initial breakdown of food, on the lubrication of the oral tissue facilitating manipulation of food in the oral cavity and also on swallowing [28].

Proteins, glycoproteins and aminoacids are the main organic constituents of the saliva. Concerning the inorganic fraction, it is basically represented by ions of sodium (Na^+), chloride (Cl^-), calcium (Ca^{2+}), phosphate (PO_4^{3-}) and bicarbonate (HCO^{3-}). The organic components of the saliva have biologic functions of particular importance to oral health and glycoproteins are responsible for much of the viscosity of saliva [27, 29]. Indeed, the effect of these organic compounds on the corrosion behaviour of biomaterials in oral environment remains to be understood ([30] cited by [31]). Moreover, bicarbonate and phosphate ions act as a buffer to maintain the pH of the saliva between 6 and 7, which leads to the prevention of tooth demineralization ([32] cited by [33]).

The pH of saliva, which has a strong influence on the corrosion behaviour of Ti and its alloys [34, 35, 36, 37], is usually about 6.5 but it can temporarily fall to 3.5 due to eating habits [36]. Additionally, the composition and properties of saliva can be modified by internal factors such as salivary gland dysfunctions or due to the moment of the day. The masticatory process and the muscular movements increase the salivary flow optimizing the oral cleaning. However, the salivary flow rate decreases during sleep facilitating the increase in the number of microorganisms in the oral cavity and consequently the lowering of the pH. In fact, the increase of lactic acid-producing bacteria metabolism is a critical factor for the lowering of the pH ([38] cited by [33]). Finally, the mouth is moist and continually subjected to fluctuations in temperature which ranges from 0 °C to the temperature of a hot coffee [39].

Natural saliva is, thus, an extremely complex system with numerous constituents and variability. It is obvious that the characterisation of dental materials should be done in that media, but exact duplication is almost impossible. The unstable nature of natural saliva makes it inadequate for standardized *in vitro* studies. Then, it is necessary the use of an artificial saliva that reacts in a similar way to that of natural saliva.

Artificial saliva with inorganic components has commonly been used to study corrosion [12, 40, 41, 42, 43, 44, 45, 46] and tribocorrosion [37, 47, 48, 49, 50, 51, 52] behaviour of dental implant materials in the oral environment. In developing standard artificial saliva for electrochemical studies, very often no attempt has been made to simulate the viscosity of natural saliva, due to the practical difficulty of obtaining suitable

material. Commonly, only those inorganic components of the natural saliva which have an effect on chemical end electrochemical processes are included. If a substance has no detectable effect, the omission of that compound may be justified. However, when physical factors such as mastication forces join in the process, viscosity of saliva play a major role in tribocorrosion [53]. In the oral cavity, the viscous property of the saliva provided by glycoproteins can protect the dental surfaces against wear [54]. The usage of artificial saliva in studies related to dental implant materials can be found as early as 1931 and a complete review of the different formulations used in literature is available by Leung *et al.* and Galliano *et al.* [27, 55]. A review of nearly 60 artificial saliva solutions was carried out [27] to clarify the role of some of the compounds such as CO_2 gas, the presence of calcium ions, hydrogenocarbonates, hydrogenophosphates and thiocyanates. In fact they found that the SAGF medium had certain advantages for physicochemical studies, which could compensate for the absence in its composition of glycoproteins capable of giving it viscosity. It already enables the in vitro reproduction and the study of a large number of physicochemical phenomena, which can be developed in the mouth.

Overall, Fusayama-Meyer solution is the most common formulation to mimic human saliva for electrochemical and wear studies [33, 35, 36, 41, 43, 44, 49, 50, 51, 56, 57], since only those mineral components of the natural saliva affecting chemical and electrochemical processes were included. Indeed, a previous work where the effect of different electrolytes on the corrosion behaviour of dental implant alloys was analysed, Fusayama-Meyer solution was the only one showing consistency with the clinical experience of the materials [58]. Table 1.4 shows Fusayama-Meyer artificial saliva composition.

Figure 1.4: Composition of Fusayama-Meyer artifial saliva.

Compounds	Concentration $(g \cdot l^{-1})$
NaCl	0.4
KCl	0.4
$Na_2S \cdot H_2O$	0.005
$NaH_2PO_4 \cdot H_2O$	0.69
$CaCl_2 \cdot 2H_2O$	0.906
Urea	1

1.3.2 Mastication events

It has been widely accepted that the wear of dental implants results mainly from chewing cycles [59]. Therefore, it is important to understand the biomechanics of mastication. The most common force direction is compressive and it occurs during chewing. As a consequence of this compressive force, a lateral force component is also produced. This lateral component may cause bending moment on the system [60]. Compressive and lateral force components are shown in Figure 1.5.

Figure 1.5: Lateral force component produced from a compressive force on an oblique plane [60].

Mastication involves two stages: open and close phase. Literature shows that the shape of the occlusal force curve is similar to the positive half of a sine curve. During normal chewing the load applied to the teeth is in the range 10-20 N at the initial contact, and is increased to the range 50-150 N at the end of the chewing cycle. The magnitude of the force depends on the physical properties of food. As there is a great variety of foods, various forces can be expected. In addition, the maximum biting forces vary according to sex, age and muscle build. Typically, the maximum biting load at the incisors is about 100 N, gradually increasing as one moves posteriorly to reach around 500 N at the molars [59]. As an illustration, general chewing parameters are listed in Table 1.6.

Moving on, there is a common concern about bruxers that can cause dental implant overloading. Bruxism is defined as a repetitive jaw-muscle activity characterised by clenching or grinding of the teeth and/or by bracing or thrusting of the mandible. However, very few works addressed this issue and discard bruxism as a risk factor for biological complications around dental implants [61].

Figure 1.6: Inter-oral chewing parameters [59].

Chewing parameters		
Chewing load (N)		2-150 (max. 450)
Chewing frequency (Hz)		1-2
Sliding speed ($mm \cdot s^{-1}$)		0.25-0.50
Sliding distances (mm)		0.9-1.2
Duration (s)	Total	0.7
	Occlusion	0.1

The clinical success of an implant is largely determined by the manner in which the mechanical stresses are transferred from the implant to the surrounding bone without generating forces of a magnitude that may be detrimental for the longevity of the implant. Table 1.7 provides an overview of different finite element analysis (FEA) carried out to define maximum stress conditions in the implant at different loading conditions.

Figure 1.7: Maximum stresses present on dental implant calculated by FEA methods.

Maximum stress (MPa)	Applicated load (N)	Ref.
16.9 (non-osseointegrated) 5.5 (fully osseointegrated)	20	[62]
18	20	[63]
180	200	
532	300	[64]

Accordingly, stress distribution through the implant and to the surrounding bone also changes. However, stress values founded in literature used to characterise tribocorrosion performance of dental implants are rather higher. Table 1.8 shows some of the mechanical parameters used for those experiments and the calculated stress values.

Figure 1.8: Testing configuration and parameters used in literature for tribological characterisation of titanium dental implants. τ_H and $\tau_{H,max}$ correspond to the mean and the maximum Hertzian contact pressure, respectively.

Configuration	F_N (N)	ø (mm)	τ_H (MPa)	$\tau_{H,max}$ (MPa)	Ref.
Fretting (Ball-on-Flat)	2	10	340	510	[47, 65]
Reciprocating (Ball-on-Flat)	3	-	-	-	[66]
Reciprocating (Ball-on-Flat)	10	-	-	-	[65]
Reciprocating (Ball-on-Flat)	3	10	390	580	[33]
Fretting (Ball-on-Flat)	0.1-0.2	5	200-250	300-370	[33]
Fretting (Ball-on-Flat)	3	8	450	680	[43]

1.4 Electrochemical behaviour of titanium dental implants

When a dental implant is inserted in the oral cavity it gets exposed to the oral environment. Thus metal and oxide film dissolution are two mechanisms to introduce additional ions into the body. Extensive release of ions from implants can result in adverse biological reactions, and can lead to mechanical failure of the device. Corrosion of alloys in the mouth is the result of the presence of a number of corrosion-causing species, such as chloride ion (Cl^-), the hydrogen ion (H^+), sulfide compounds (S^{2-}), dissolved oxygen (O_2) and microorganisms [40].

Eisenbarth *et al.* [16] studied the corrosion properties and the biocompatibility of alloying elements used in beta-titanium alloys for biomedical application in physiological NaCl solution (see Figure 1.9). They founded that zirconium and molybdenum possessed a breakdown potential lower than 500 mV/$AgCl_2$ and that titanium, tantalum and niobium were the elements with the higher breakdown potential. With a breakdown potential below the value of 400-500 mV/$AgCl_2$ (body potential) the metal would show a high corrosion rate under physiological conditions and thus the release of a high amount of ions interacting with the tissue and the whole body.

In fact, the first contact between the biological environment and the titanium device will be through the oxide layer. It is, however, known that this oxide film will be modified as a consequence of chemical, biochemical and cellular activity inherent to the oral environment.

The corrosion resistance of the passive metals is closely related to the chemical composition of the oxide layer. In this regard, although most of Ti alloys form a single compact layer which contains TiO_2 with traces of other oxides, Metikos-Hucovic and co-workers [67] showed that the presence of Nb in the alloy enhanced the passivation

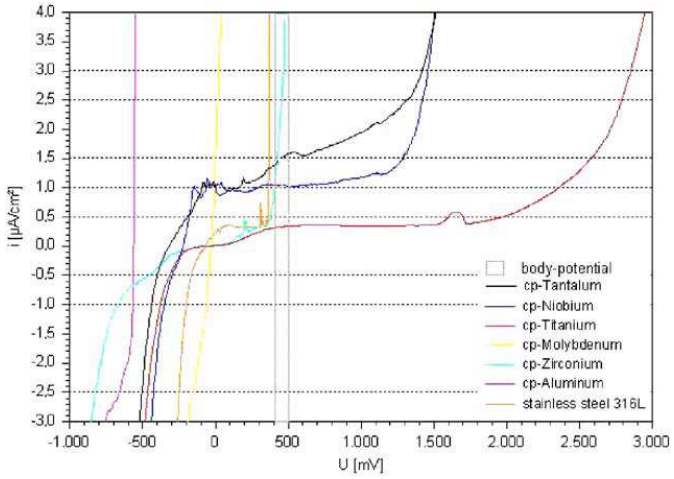

Figure 1.9: Potential-current density curve of β-stabilizing alloying elements as compared to titanium and implant steel 316 L.The reference electrode is $Ag/AgCl_2$ [16].

characteristics of the film by decreasing the concentration of the anion vacancies in the TiO_2 film.

The thermodynamic stability of oxides depends on the electrical potential of the titanium in a solution and on the pH of that solution [68]. The Pourbaix diagrams of titanium, niobium and zirconium (Figure 1.10) reveal that their oxides are stable over a wide range of potentials.

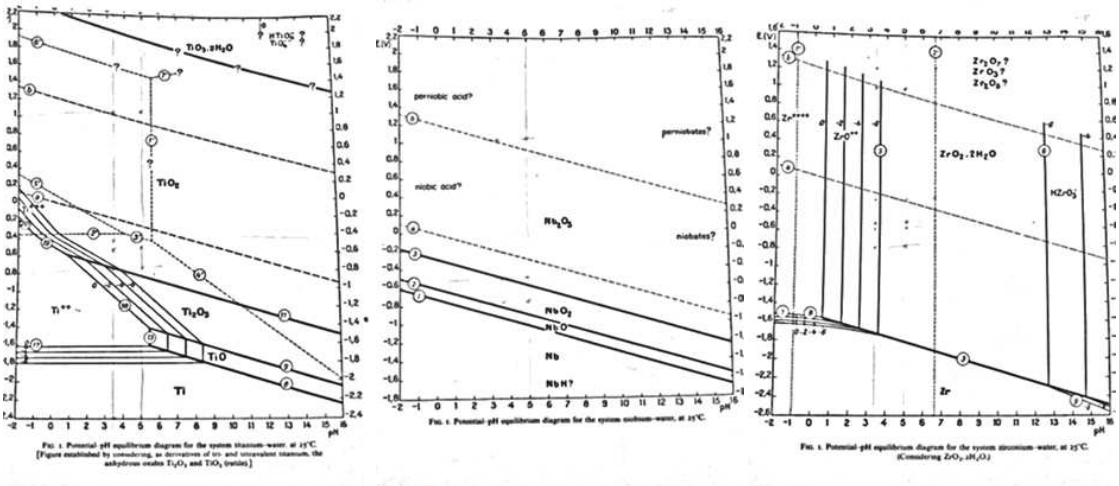

Figure 1.10: Potential- pH equilibrium diagram for the systems titanium-, niobium- and zirconium-water, at 25 °C [69].

Fluorides and other cleaning agents are successfully used in caries prevention and treatment. However, localised corrosion of titanium alloys has been detected in

solutions containing fluorides, lactic acid, hydrogen peroxide or carbamide peroxide, when associated to a lowering of the pH [70]. Tooth brushing with fluoride (F^-) containing toothpastes (1000 to 1500 ppm F^-), which is a successful anticariogenic agent [71], has been reported to negatively affect the corrosion resistance of Ti dental implants [70, 72, 73]. Indeed, a number of works have been published on this issue, Table 1.11 lists some of them. Conversely, there are some studies revealing that salivary fluoride content after tooth brushing with fluoride containing toothpastes significantly decreases after mouth rinsing with water: after a single application of fluoride-containing dentifrices (1250 ppm) salivary fluoride concentration 10-15 min after application decreases to approximately 1-3ppm [71]. Moreover, another study carried out by Watson *et al.* [74], they analysed plaque fluoride concentrations near the saliva interface after toothbrushing techniques with 1000 ppm F- solution and they measure fluoride concentrations from 13 to 227 ppm. But still this concentration might be enough to increase the corrosion rate of metallic dental implants.

Moreover, the fluoride containing solutions might be harmful to titanium devices in acid media [70, 35, 72, 77]. Thus, the corrosion behaviour of titanium depends not only on fluoride concentration but also on pH as it can be seen in Figure 1.12. The influence of fluoride content and pH in artificial saliva on dental implant corrosion has been widely studied [70, 78, 79, 46, 80]. Nakagawa *et al.* [70] analysed the influence of fluoride and pH on pure titanium and they concluded that the corrosion resistance of titanium was controlled by the HF concentration and depended on the pH value and the total fluoride concentration in the solution. Joska *et al.* [79] analysed the electrochemical behaviour of CpTi2 after short-term exposure to in acidic environment containing fluoride ions. The obtained results showed that the stabilization of titanium passive state caused by a short medical treatment may take a long time to abate, with many possible negative consequences. Milosev *et al.* [46] investigated the effect of fluoride on the corrosion behaviour of Ti6Al7Nb and Ti6Al4V alloy. They founded that fluoride was present throughout the depth of oxide layer, whose thickness increased compared to that in plain artificial saliva. However, the layer formed was less protective from that formed in fluoride-free solutions. The effect of a two-year fluoride decay protection protocol on titanium brackets was studied by Khoury *et al.* [80] for orthodontic patients being high-risk caries developers and in need of fluoride protection. Experiments showed that bracket weight loss became significant after 18 to 24 months of treatment.

Figure 1.11: Fluoride concentration values used for mechanical and chemical characterisation of dental implants in literature.

Main purpose of the study	F^- (ppm)	Ref.
· Effect of fluoride concentration and pH on corrosion behavior of titanium for dental use	90, 9050	[70]
· Influence of fluoride content and pH on the corrosion resistance of titanium and its alloys	1000	[35]
· Influence of fluoride, hydrogen peroxide and lactic acid on the corrosion resistance of commercially pure titanium	5000, 25000	[41]
· Influence of fluoride ion on the electrochemical behaviour of β-Ti alloy for dental implant application	190, 570, 1140, 9500	[75]
· Fretting corrosion behaviour of Ti6Al4V alloy in artificial saliva containing varying concentrations of fluoride ions	190, 570, 1140	[43]
· Simultaneous degradation by corrosion and wear of titanium in artificial saliva containing fluorides	20, 30, 270, 12300	[51]
· Influence of noble metals alloying additions on the corrosion behaviour of titanium in a fluoride-containing environment	910	[44]
· The Effect of Fluoride Ions on the Corrosion Behaviour of Ti metal, and Ti6-Al-7Nb and Ti-6Al-4V Alloys in Artificial Saliva	113	[46]
· Influence of pH and Fluoride Species on the Corrosion Behaviour of Ti-xNb-13Zr Alloys in RingerâĂŹs Solution	1000	[76]

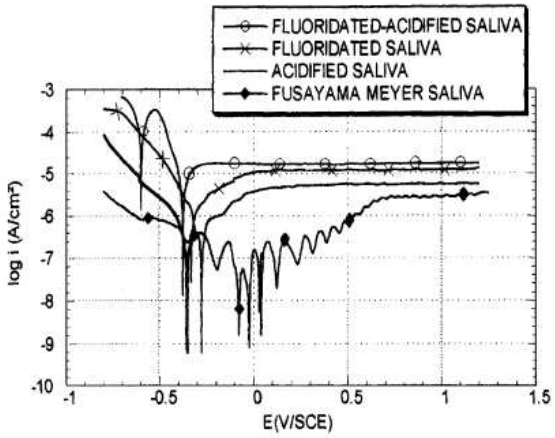

Figure 1.12: Influence of fluorides and pH of the electrolyte on polarization curves of titanium [35].

1.5 Tribocorrosion behaviour of titanium dental implants

Tribocorrosion events are likely to occur when a metallic implant is inserted in the mouth since there is a combination of tribological processes due to mastication forces with a corrosive environment, *i.e.* saliva. This involves the destruction or even removal of the protective passive layer of the titanium alloy and thus the onset of the active dissolution of the titanium until it completely repassivates again. In fact, a high concentration of titanium in the body, such as ions and nano-particles, may also induce significant toxicity [14].

The material release from the implant to the surrounding tissues due to a tribocorrosion process may occur on the basis of three main factors taking place simultaneously. Firstly, the overall exposed implant surface gets dissolved due to the contact with an aggressive environment, *i.e.* material loss due to corrosion in absence of wear. During rubbing, the material loss of the wear track might be divided into synergistic processes and pure mechanical contribution. Synergistic processes consider both corrosion accelerated by wear, *e.g.* active dissolution of the alloy after the mechanical rupture of the passive film; and wear accelerated by corrosion, *e.g.* within the wear scar an oxidised metallic particle may increase its abrasive properties and increase the mechanical wear. Pure mechanical wear is the loss of material occurred in absence of corrosive media. Some authors suggested that the later is similar to the wear reported when rubbing under potentiostatic holding at cathodic potentials. However, hydrogen embrittlement might become a problem, particularly for passive materials, due to the change of the mechanical properties of the testing material.

There have been developed several approaches to describe wear-corrosion interactions, such as, the mechanistic approach proposed by Uhlig [81] the synergistic approach, described by Watson *et al.* [82], the third body approach reported by Godet *et al.* [83], the one developed by Diomidis *et al.* [84] and the nano-chemical wear approach [85]. Most of them agree that it is necessary to identify the contribution of corrosion and wear to the total material removed by tribocorrosion. For example, if the total material loss would be controlled by wear-accelerated corrosion, then improvements in corrosion protection should be beneficial. On the other hand, materials with better mechanical performance should be used when mechanical wear determines the overall material loss rate [86].

Some of the reported studies associated with tribocorrosion in titanium based dental implants are given below.

Vieira et al. [48] studied the repassivation evolution of commercially pure titanium in artificial saliva solutions by conducting tests in different kinds of artificial saliva solutions (artificial saliva (AS), AS + citric acid, AS + anodic, cathodic or organic inhibitor). The results showed that, in some solutions, the OCP, after repassivation, was nobler than that measured before sliding. Also, the repassivation evolution appeared to be strongly affected by the electrolyte nature. The AS + citric acid solution provided a better repassivation evolution with time [87].

Ribeiro *et al.* [65] investigated the tribocorrosion behaviour of commercially pure titanium grade 2 in both fretting and reciprocating sliding conditions in contact with artificial saliva solutions. To reproduce the oral environment around the dental implant, some additives (citric acid, anodic, cathodic, and organic inhibitors) were added to simple artificial saliva constituted mainly by NaCl and KCl and with a pH between 5 and 7. It was found that titanium in artificial saliva solution with citric acid had the highest weight loss. Recently, there are many other research groups investigating the tribocorrosion behaviour of dental materials.

Souza *et al.* [33] investigated the in-vitro corrosion and tribocorrosion behaviour of commercially pure titanium in fluorinated artificial saliva solutions, and in presence of biofilms. Localized corrosion of titanium was only observed at high fluoride concentration (12300 ppm F^-) although a decrease of the corrosion resistance of titanium was noticed when the fluoride concentration increased. The presence of biofilms affected negatively the corrosion resistance of titanium probably due to acids release from the microorganisms. Finally, under wear sliding tests, biofilms generated an ultra-low friction on titanium immersed in artificial saliva solution, which can be compared to the effect of commercial lubricant agents. In dental implant systems, ultra-low friction on sliding contact areas might therefore cause a loss of the mechanical integrity ending

up in a loosening of the implant internal connections.

Licausi *et al.* [52], studied the influence of two different Ti6Al4V alloy fabrication processes in the corrosion and tribocorrosion behaviour in oral environment. The presence of fluorides increased the wear accelerated due to corrosion and sintered alloy showed a promising behaviour against cast.

Literature is scarce studying the tribocorrosion behaviour of TiNbZr alloys for dental implant application. Apart from the work carried out by Ribeiro *et al.* [25] comparing the electrochemical behaviour of Ti6Al4V, Ti35Nb5Zr and Ti35Nb10Zr in artificial saliva, there is a general lack of research in the corrosion characterisation of TiNbZr alloys for dental implant application.

Chapter 2

Motivation and scope of the thesis

At this point, the motivation and the scope of the thesis are defined.

2.1 Motivation and background

Population ageing and longevity are characteristics from developed societies and product of scientific progress from last decades. With this, new health-related challenges emerge, such as the development of dental implants as an alternative to the traditional dentures. The use of dental implants, and prosthesis as a whole, demands the co-working between medicine, engineering and science.

Huge advances have been made on the dental implant surface functionalisation in order to enhance osseointegration (implant anchorage to the bone) in the shortest time; such as topography design to promote cell adhesion. There is another complementary strategy however, to enhance implant osseointegration. Dental implant materials have higher rigidity than human bone. Consequently, the dental implant is overloaded and absorbs the majority of mastication stresses, leading to insufficient stimulation to the surrounding bone. This phenomenon is called *stress shielding* effect and is counter productive with regard to osseointegration. That is why there is a trend to develop and use implants with lower modulus of elasticity.

Biocompatibility is also an issue of great concern in implantology. Nevertheless, the biocompatibility has a lot to do not only with the toxicity of the material, but also with the release of ions and particles from the implant to the surrounding tissues due to the aggressivity of the oral environment.

In this regards, titanium is a passive metal whose protective oxide layer offers an enhanced corrosion resistance against a range of environments. Plus, the biocompatibility of titanium, together with its low modulus of elasticity, in comparison to steels, converts it in a suitable material for biological applications. Commercially pure titanium is the most widely used material for dental implant application. However, its alloying offers interesting improvements in the field of mechanical properties. Ti6Al4V alloy, a referent in aircraft industry due to its excellent mechanical and corrosion resistance properties, is also the most common titanium alloy in prosthesis application although the toxicity of Al and V has already been recognised. That is why the scientific community is working on the development of new titanium alloys with biocompatible alloying elements in addition to an even more reduced modulus of elasticity. TiNbZr, TiNbZrTa and TiMo are some of the newly developed titanium alloys with non-toxic alloying elements and reduced modulus of elasticity. Among them, Ti13Nb13Zr is an standardised alloy that fulfils expectations from a mechanical and toxicity viewpoint. There are several studies about Ti13Nb13Zr characterisation for hip and knee prosthesis application, but very few for dental implant application.

This issue leads to the former objective of this thesis, the characterisation of

ion release and particle debris generation from a Ti13Nb13Zr dental implant in oral environment, using the widely used commercially pure titanium as a benchmark.

This study requires a multidisciplinary approach to understand a system consisting of a material surface, an environment and a mechanical contact. From an engineering viewpoint, the oral environment not only refers to an aggressive media (saliva), but also to a mechanical request (mastication forces). So there is a need to integrate the knowledge from various disciplines, namely, materials science, electrochemistry, tribology and biology.

Electrochemistry is the science behind the study of the corrosion behaviour of metallic materials in aggressive environments, such as dental implants. Tribology instead, is the science in charge of studying the contact between two materials in relative motion, as the micromovements between a dental implant and the surrounding bone, originated by mastication events. In addition, the combination of a mechanical request of a metallic material in a corrosive environment involves the occurrence of tribocorrosion events. This synergy between wear and corrosion may lead to an accelerated material degradation.

The knowledge of the corrosion and tribocorrosion mechanisms establishes a criteria towards an adequate metal protection technique, in terms of corrosion enhancement or increased wear resistance.

This culminates with the second and last objective of this thesis. In view of the Ti13Nb13Zr degradation mechanisms in oral environment, two different protection techniques are explored. On the one hand, controlling the aggressivity of the artificial saliva with the addition of some corrosion inhibitors, that could be dispensed through toothpastes or mouthwash. On the other, the improvement of Ti13Nb13Zr tribocorrosion behaviour through a thermal oxidation treatment is also studied.

2.2 Scope of the thesis

In a nut shell, there are two main goals in this thesis dissertation. The former, the characterisation of an innovative titanium alloy for dental implant application, Ti13Nb13Zr, from corrosion and tribocorrosion viewpoint. In the second objective two different protection techniques are studied to improve its tribocorrosion behaviour.

Figure 2.1 shows the different steps followed to reach the objectives. First chapter contains a literature review describing implant materials and oral environment characteristics, to finish with the electrochemical and tribocorrosion behaviour of titanium alloys in the oral environment. Literature review leads to the current chapter, the motivation and the scope of the thesis, where the main objectives and the corresponding tasks/chapters are identified. Chapter 3 contains Ti13Nb13Zr alloy generalities (the surface, chemical and mechanical characterisation of Ti13Nb13Zr) in addition to the artificial saliva preparation.

The influence of fluoride and pH on corrosion and tribocorrosion behaviour of Ti13Nb13Zr alloy in oral environment is studied in Chapter 4. Repassivation kinetics of Ti13Nb13Zr and the influence of different tribological parameters on materials degradation is analysed in Chapter 5. These two chapters belong to the frame of the objective 1.

The influence of the corrosion inhibitors on the tribocorrosion resistance of Ti13Nb13Zr is studied in Chapter 6. The tribocorrosion behaviour of thermally oxidised Ti13Nb13Zr alloy is analysed in Chapter 7. These two chapters belong to the frame of objective 2.

Finally, general conclusions and future work are described in Chapter 8.

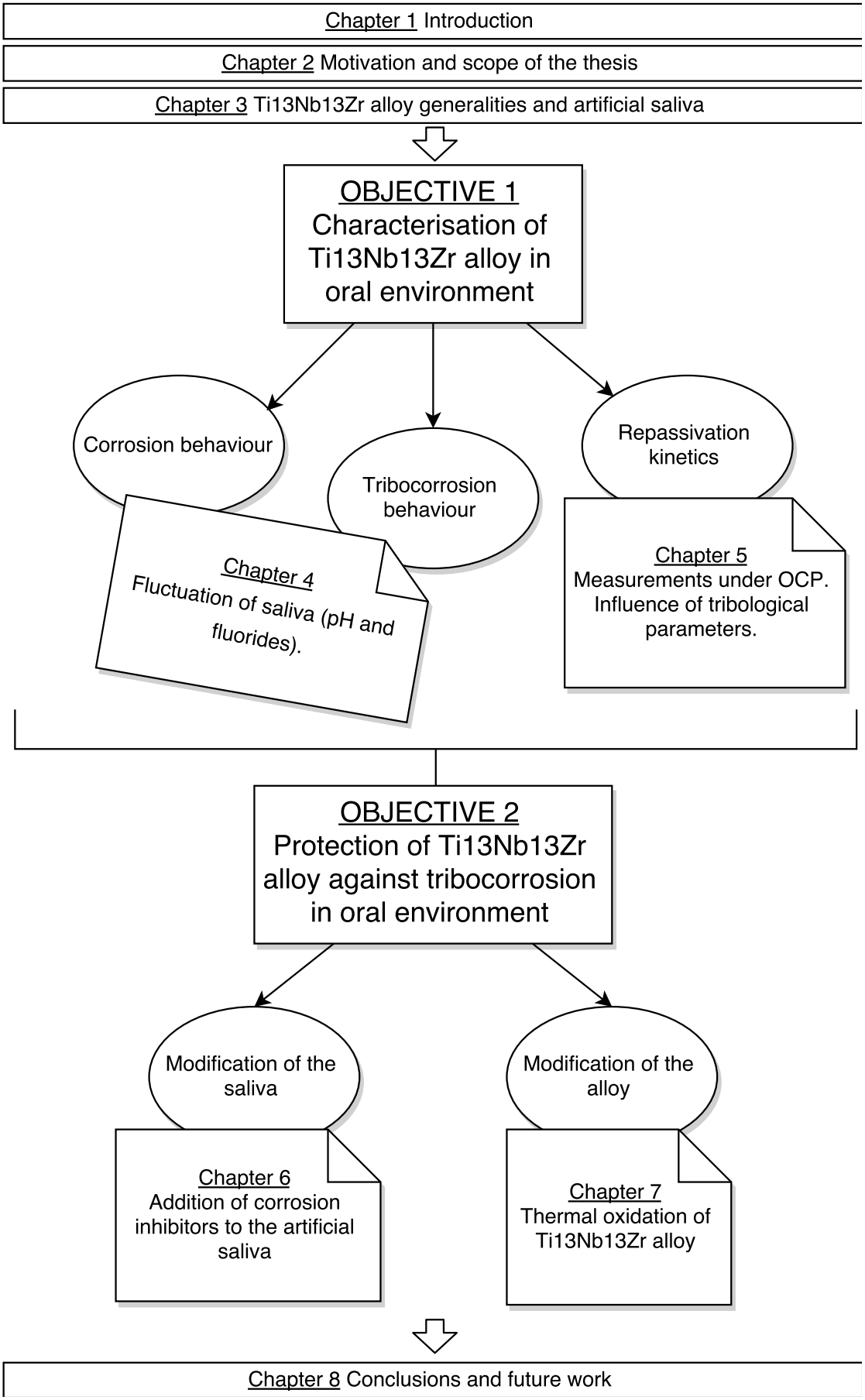

Figure 2.1: Scheme of the outline of the thesis.

Chapter 3

Ti13Nb13Zr alloy generalities

In this chapter the surface, chemical and mechanical characterisation Ti13Nb13Zr and CpTi4 is collected. This characterisation is necessary for the discussion of the following chapters. In addition the preparation of artificial saliva is also presented.

3.1 Material and electrolyte preparation

3.1.1 Materials

ASTM F67 Commercially Pure Ti grade 4 (CpTi4) (Biotechnology Institute, Spain) and ASTM F1713 Ti13Nb13Zr alloy samples (Xi'an Saite Metal Materials Development Co., China), with a 12 mm diameter and a 2 mm thickness, were cut from a bar so the exposed surface for electrochemical experiments corresponded to 113 mm^2. Nominal chemical compositions and mechanical properties of the materials are shown in Table 3.1 and Table 3.2, respectively. owing to limitations of space in Figures, the designation of the materials may appear as 'Ti4' and 'TNZ' referring to CpTi4 and Ti13Nb13Zr, respectively.

Table 3.1: Nominal chemical compositions (wt. %) of CpTi4 and Ti13Nb13Zr according to ASTM standards.

Material	C	H	N	O	Fe	Nb	Zr	Ti
CpTi4	0.08	0.015	0.05	0.4	0.5	-	-	Balance
Ti13Nb13Zr	<0.08	<0.015	<0.05	<0.15	<0.25	12.5-14	12.5-14	Balance

Table 3.2: Mechanical properties of CpTi4 [88] and Ti13Nb13Zr [89].

Material	Standard	Young modulus	Hardness
CpTi4	ASTM F67	100 GPa	200 HV
Ti13Nb13Zr	ASTM F1713	78 GPa	240 HV

3.1.2 Electrolyte preparation

Fusayama Meyer artificial saliva was used as base electrolyte, consisting of 0.4 g NaCl, 0.4 g KCl, 0.005 g $Na_2S \cdot H_2O$, 0.69 g $NaH_2PO_4 \cdot H_2O$, 0.795 g $CaCl_2 \cdot 2H_2O$ and 1 g Urea per 1 l of deionised water. This artificial saliva formulation has been used by a number of authors [35, 36, 41, 50, 57, 90], since only those mineral components of the natural saliva affecting chemical and electrochemical processes were included.

In chapter 4, in order to analyse the influence of fluoride, 0, 100 and 1000 ppm F^- solutions were prepared by adding NaF to the Fusayama Meyer artificial saliva. In addition, the effect of pH was also tested by adjusting the pH of the artificial saliva with

Table 3.3: F^- and pH values of artificial saliva tested in chapter 4.

$[F^-]$ (ppm)	0, 100, 1000
pH	3.5, 5.0

Table 3.4: Artificial saliva (SA) with the different corrosion inhibitors tested in chapter 6.

Designation	Eletrolyte
SA	SA
SA.Ca	SA + 10 mg/l $CaCO_3$
SA.Na	SA + 1000 mg/l $NaNO_3$
SA.PI	SA + 1 ml/l Povidone Iodine

lactic acid and KOH to pH 3.5 and 5.0. Table 3.3 shows the brief of the electrolytes tested in chapter 4.

In chapter 6, corrosion inhibitors were added to the artificial saliva in order to analyse its response, as shown in Figure 6.2. The pH remained constant around pH 5.0 ± 0.2.

Part of the electrochemical experiments were carried out in the KU Leuven, and thus the electrolyte preparation was done starting with the tap water of the laboratory. Flemish Brabant area is known to have very hard water, that is, water with large deposits of calcium (lime) and magnesium. Water hardness is often expressed in French degrees, in this way water in Leuven possesses 32° whereas Arrasate-Mondragon has 10-15°, which corresponds to soft water. This has direct involvement on the water treatment before its use in the chemical laboratory. After water bidestilation, in KU Leuven, water is passed through purifying filters (Direct-Q 3 UV with pump, Millipore) until it achieves a solution resistance of 18.2 MΩ · cm at 25 °C, which means that the majority of the ions have been filtrated. Thus, this fact can give rise to differences on the electrochemical measurements at Mondragon Unibertsitatea and at KU Leuven.

3.2 Surface characterisation

3.2.1 Microstructure

Sample preparation was done by progressively polishing with emery papers of up to 1200 grit, followed by fine polishing with diamond paste (6 µm and finally 1 µm). The specimens were then washed in distilled water and ultrasonically cleaned in ethanol for 5 minutes.

The surfaces were etched by immersing samples in Kroll's reagent (10% HF and 5% HNO3 (vol.) in distilled water) for 5 seconds in the case of Ti13Nb13Zr and 10 seconds in the case of Ti and then washed in distilled water and ethanol.

The microstructures were recorded using with optical microscopy, shown in Figure 3.1.

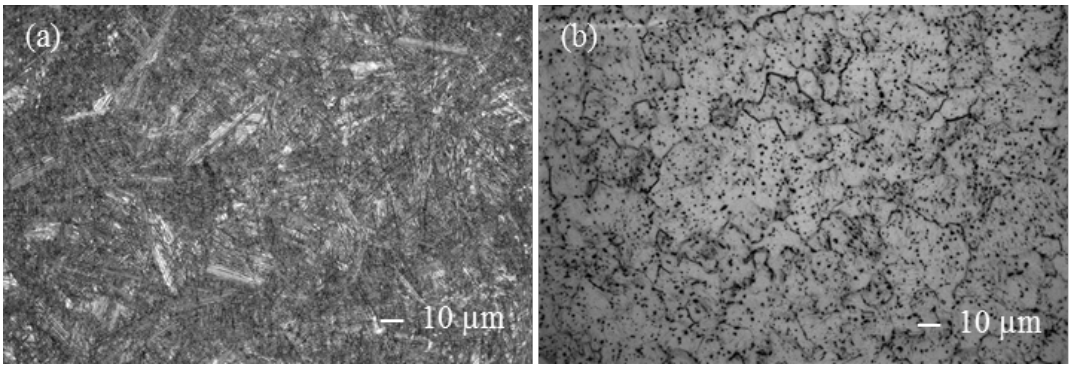

Figure 3.1: Microstructure of (a) Ti13Nb13Zr alloy and (b) CpTi4.

CpTi4 microstructure shows equiaxed alpha grains, whereas Ti13Nb13Zr exhibits martensitic microstructure, which is typical of β solution treated titanium alloys [89]. Two different types of martensitic structures could be observed in titanium alloys depending on the content of β stabilizing elements, *i.e.* hexagonal α' and orthorhombic α". Higher β alloying content favours formation of α" martensite in preference to α'. The critical composition limit of Nb in the binary Ti-Nb system for the formation of α" martensite is about 11 wt. % Nb [89]. Geetha *et al.* [89] suggested that the presence of Zr shifts the α'/α" boundary to higher Nb level, which may be between 13 and 16 wt. %. Thus an acicular martensitic α' phase, similar to that observed by Majumdar *et al.* [91], Cvijovic-Alagic *et al.* [20] and Geetha *et al.* [89] may be seen in microstructure of Figure 3.1 (a).

3.2.2 XPS

XPS measurements were performed in order to gain further insight on the chemical composition of the CpTi4 and Ti13Nb13Zr alloys, located at CENIM/CSIC. Measurements were carried out both before and after Ar ions sputtering for 0.5 min. In the case of CpTi4, the survey spectrum (not shown), taken before and after Ar ions sputtering, shows the presence of Ti, O, Ca, C, and N elements. The latter (Ca, C and N) are appended to surface contamination. Nevertheless, C and N is also a typical impurity related with the absorption of these elements from the atmosphere [92, 93]. On the other hand, Ca, may be presented due to the use of industrial detergents during industrial

processes [94, 95]. The corresponding Ti2p, and O1s core-level electronic transitions are given in Figure 3.2. Regarding Ti2p signal, the $2p_{3/2}$ and $2p_{1/2}$ symmetric peaks located at 458.1 and 463.8 eV, respectively, correspond to the TiO_2 of Ti (Δ_{oxide} = 5.7 eV). Besides, after the Ar ion sputtering a peak corresponding to the typical asymmetric peak shape for zero-valent Ti (454.1 eV) emerges. The presence of Ti metal after Ar ion sputtering is expected since the natural passive layer that typical forms on Ti metal is a few nanometers-thick and also due to the selective sputtering of the oxygen.

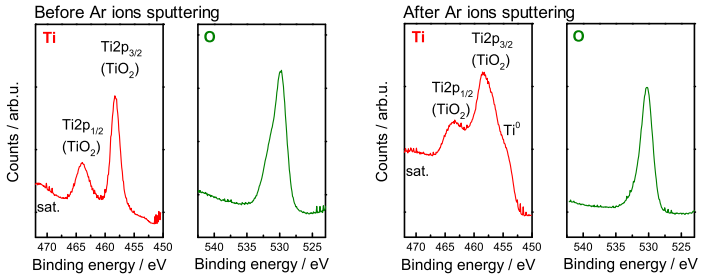

Figure 3.2: XPS spectra for CpTi4 before and after 30 s Ar ions sputteting.

On the other hand, Ti13Nb13Zr alloy was also been analized throught XPS measurements. The survey spectrum (not shown), taken before and after Ar ions sputtering, shows the presence of Ti, Zr, Nb, O, and C elements. The corresponding Ti2p, Zr3d, Nb3d and O1s core-level electronic transitions are given in Figure 3.3. Before Ar ions sputtering, Ti2p signal show the same symmetric peaks, appended to TiO_2 observed, in CpTi4, together with an small peak corresponding to the zero-valent Ti (454.1 eV). After Ar ion sputtering, the Ti metal clearly emerges together with its split spin-orbit component (Δ_{metal}=6.1eV). Concerning the Zr3d core level XPS spectrum, the position of $Zr3d_{5/2}$ peak (182.9 eV) and $Zr3d_{3/2}$ peak (185.24 eV) are characteristics of ZrO_2. The shoulder at 178.9 eV could be assigned to metallic Zr. After Ar ion sputtering the metallic Zr emerges together with different Zr3d sub-oxides, because the oxide is reduced to sub-oxides by argon ion bombardment. Although before the Ar ions sputtering, the peaks corresponding to Nb3d could not be appended, after it two peak emerges, the $Nb3d_{5/2}$ peak (202.2 eV) and $Nb3d_{3/2}$ peak (204.9 eV) that could be attributed to zero valent Nb and NbO_2, respectively. The O1s spectrum shows a peak with maxima at 530 eV, distinctive for metal oxides (M_xO_y).

Lopez *et al.* [96] analysed oxide layer composition by XPS technique and they observed a decrease of the Ti contribution at the outermost native oxide layer formed on TiNbZr alloys. This was due to element diffusion of minority alloying elements from the bulk, where Zr diffused predominantly. This fact agrees with Ellingham diagrams [97], which show that Zr oxidation is more thermodynamically favoured than Nb oxidation.

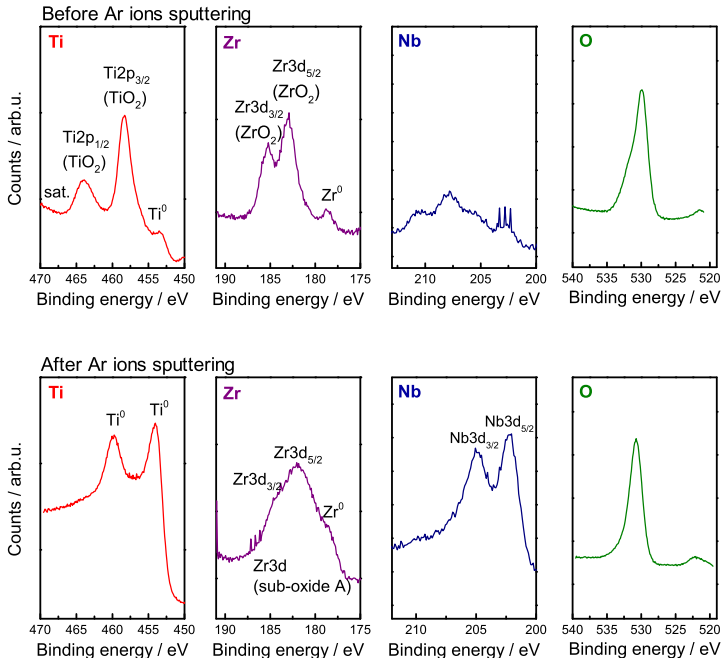

Figure 3.3: XPS spectra for Ti13Nb13Zr before and after 30 s Ar ions sputteting.

3.3 Chemical characterisation

ICP-OES is an analytical technique used for the detection of trace metals. In this thesis it was used to verify the composition of the Ti13Nb13Zr alloys (ASTM F1713). It is a multi-element analysis technique that dissociates a sample into its atoms and ions. The elements emit light of a characteristic wavelength which can then be measured and quantified. Measurements were taken with a Varian 720 ES equipment, located at the MTM department of Katholieke Universiteit Leuven and results are shown in Table 3.5. Nb content is above the maximum percentages recommended in the ASTM standard (see Table 3.1).

Table 3.5: Ti13Nb13Zr alloy composition (wt. %) obtained with ICP-OES technique.

	Fe	Nb	Zr	Ti
Ti13Nb13Zr	0.046	17.02	12.81	balance

3.4 Mechanical properties

3.4.1 Hardness test

Hardness measurements were carried out according to ASTM E92-82 standard in a Vickers hardness tester with a load of 100 N applied for 15 s. Three measurements were carried out under the same experimental conditions and the average values obtained are shown in Table 3.6. Ti13Nb13Zr alloy possesses higher hardness than CpTi4, probably due to the solid solution hardening effect of zirconium [67].

Table 3.6: Hardness values of Ti13Nb13Zr and CpTi4 obtained from Vickers test.

Material	Vickers
Ti13Nb13Zr	242 ± 9
CpTi4	202 ± 2

3.4.2 Tensile test

Tensile tests were carried out using a universal testing machine Instron 3369 tensile tester with a 50 kN load cell and the displacement were measured with an extensometer. For the purpose of complete tensile test to characterise mechanical properties of Ti13Nb13Zr, ASTM E-8M Standard test method was followed. The effective diameter of the sample was 8 mm and the applied strain rate was 10^{-3} s^{-1}. Figure 3.4 shows the stress strain curve for the tensile test of the Ti13Nb13Zr specimen.

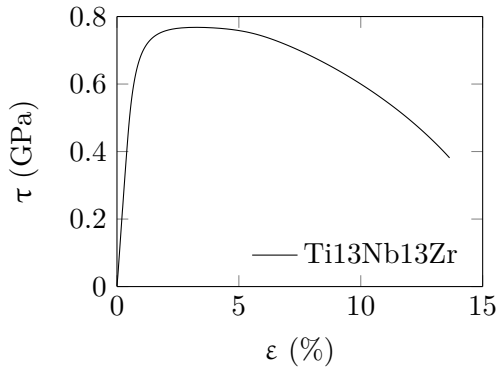

Figure 3.4: Stress-strain curve of Ti13Nb13Zr alloy.

Throughout these curve the main mechanical properties of Ti13Nb13Zr were calculated. Table 3.7 compares both supplier certificate and Ti13Nb13Zr ASTM F1713-03 standard with the obtained results from tensile tests.

Table 3.7: Comparison of mechanical properties between test, supplier and the standard of the material for Ti13Nb13Zr.

	Young Modulus (GPa)	Yield strength (MPa)	Tensile strength (MPa)	Elongation (%)
Tensile test	78.079	680	790	13-14
Supplier	-	700-715	835-845	24-25
ASTM F1713	-	550 (min.)	345 (min.)	15 (min.)

Table 3.7 showed that results are not within the supplier specifications, but above the minimum values specified by the ASTM standard of the material. The elongation is the only parameter which is below the minimum required by the standard and it may be due to the conicity of the tensile specimens.

Mechanical properties of CpTi4 have been taken from the standard ASTM F67 due to the unavailability to obtain material to carry out tensile tests. Mechanical properties of CpTi4 (Commercially pure Titanium grade 4) according to ASTM standards are shown in Table 3.8.

Table 3.8: Mechanical properties of commercially pure titanium according to ASTM F67.

Material	Young Modulus (GPa)	Tensile strength (MPa)	Yield strength (MPa)	Elongation (%)
CpTi4	100 (acc. [19])	550	483	15

Chapter 4

Influence of fluoride and pH on corrosion and tribocorrosion behaviour of Ti13Nb13Zr alloy in oral environment

The present work studies the tribocorrosion behaviour of the near-β Ti13Nb13Zr alloy in oral environment, using CpTi4 for comparison purposes. To that end, the influence of the pH and fluoride concentration in artificial saliva was analysed. Reciprocating sliding corrosion tests were carried out under open circuit potential and potentiostatic conditions. Results reveal a negative influence of the increase of fluoride concentration and the acidified artificial saliva on the material degradation. Moreover, some light has shed on the different tribocorrosion mechanisms of Ti13Nb13Zr and CpTi4 in simulated oral environment.

4.1 Introduction

Literature is scarce studying the tribocorrosion behaviour of TiNbZr alloys for dental implant application. Apart from the work carried out by Ribeiro et al. [25] comparing the electrochemical behaviour of Ti6Al4V, Ti35Nb5Zr and Ti35Nb10Zr in artificial saliva, there is a general lack of research in the corrosion characterisation of TiNbZr alloys for dental implant application.

4.1.1 Objectives and hypothesis

Following objectives are defined to characterise the corrosion and tribocorrosion behaviour of Ti13Nb13Zr alloy. For that CpTi4 is used as a benchmark.

- To study the influence of F^- concentration and pH on corrosion behaviour of Ti13Nb13Zr alloy in artificial saliva.
- To study the influence of F^- concentration and pH on tribocorrosion behaviour of Ti13Nb13Zr alloy in artificial saliva.

The hypothesis is that the degradation of Ti13Nb13Zr alloy under corrosion and tribocorrosion request is similar or lower compared to the widely used CpTi4.

4.2 Materials and methods

4.2.1 Materials

The exposed surface of CpTi4 and Ti13Nb13Zr corresponded to 113 mm^2. Sample preparation was done by progressively grinding titanium discs with emery papers until 1200 grit, followed by fine polishing with diamond paste (6 μm and finally 1 μm). Then the specimens were washed in distilled water, ultrasonically cleaned in ethanol for 5 minutes and dried with warm air. All the samples were stored in a drying chamber for 24 h before experiments.

4.2.2 Electrochemical and reciprocating sliding corrosion tests

Fusayama Meyer artificial saliva was used as base electrolyte. In order to analyse the influence of fluoride, 0, 100 and 1000 ppm F^- solutions were prepared by adding NaF to the Fusayama Meyer artificial saliva. In addition, the effect of pH was also tested by

adjusting the pH of the artificial saliva with lactic acid and KOH to pH 3.5 and 5.0, respectively.

The electrochemical behaviour of titanium samples was studied using a three electrode cell: titanium samples as a working electrode, a Saturated Calomel Electrode (SCE) as a reference electrode, and a platinum coil as a counter electrode. A Voltalab 40 potentiostat was used for the electrochemical test. All potentials were referred to the SCE (+244 mV/SHE). Samples were first immersed in electrolyte for 60 minutes under open circuit potential (OCP) for potential stabilisation. Then, potentiodynamic polarisation curves of titanium alloys were obtained from -250 mV/OCP to 1500 mV/SCE at a scan rate of 0.16 $mV \cdot s^{-1}$ and at room temperature. Several parameters were evaluated from the polarisation curves: the corrosion potential (E_{corr}) and the corrosion current density (i_{corr}), determined by the Tafel slope extrapolation; and the passive current density (i_p), obtained from the measured current within the passive domain.

Reciprocating sliding corrosion experiments were carried out at 37 $\pm$ 1 °C coupling the electrochemical cell to a tribometer (Microtest) with a ball-on-plate reciprocating sliding configuration. The reference electrode was placed no more than 10 mm away from the wear track. A 6 mm diameter alumina ball was used as a counter part. A normal force of 1 N was applied, which resulted in an initial contact pressure of 320 and 360 MPa for CpTi4 and Ti13Nb13Zr, respectively, a sliding speed of 1 Hz and a stroke of 2 mm was imposed. Tribological parameters were chosen based on inter-oral chewing parameters [59] and maximum stress conditions present on a dental implant calculated by Finite Element Analysis [62, 64, 63]. During each sliding cycle, friction coefficient was measured. Only the steady values were used to compute an average coefficient of friction for each cycle. In addition, in order to avoid the running-in period, the average coefficient of friction of the complete sliding test was calculated by averaging the values concerning the last two-thirds of the test. Sliding tests were carried out at open circuit potential and at an applied potential of 750 mV/SCE, corresponding to the current *plateau*. The experimental sequence was:

- Allowing the system to stabilize at OCP during 60 min and then, in the case of potentiostatic tests, applying a potential step of 750 mV/SCE for 15 minutes.
- Starting of the sliding for 60 min while either the OCP was measured or the polarisation step of 750 mV/SCE was applied.
- Removing the load once sliding finished and continuing recording OCP or current for potentiostatic test for 20 min.

At the end of the wear tests titanium samples were ultrasonically cleaned with

ethanol, dried with warm air and examined using a JEOL JSM 5600 LV scanning electron microscope (SEM). The volumetric wear was measured by confocal laser profilometry, Sensofar PLu 2300, and calculated by averaging the cross sectional area determined at three locations along the track, multiplied by the wear track length. Objectives from 10 to 100x (EPI) were used depending on the depth and the slope of the scar.

All electrochemical and tribocorrosion tests were repeated at least three times to confirm reproducibility of the measurements. Legends comply with the following designation: *material.pH.[F^-]* (TNZ for Ti13Nb13Zr and Ti4 for CpTi4; 35 for pH 3.5 and 50 for pH 5.0 and 0, 100 or 1000 for fluoride concentration, respectively). For example, 'Ti4.35.100' refers to CpTi4 inmersed in artificial saliva with pH 3.5 and 100 ppm F^-.

4.3 Results and discussion

4.3.1 Corrosion behaviour

During the initial stabilisation period of 60 min after the immersion, similar trends were observed on both materials. Figure 4.1 shows the evolution of the OCP for CpTi4 and Ti13Nb13Zr immersed in artificial saliva at pH 3.5 with different fluoride concentrations. Both materials immersed in acidic solutions containing up to 100 ppm F^- exhibited a constant OCP during the stabilization stage, showing a similar thermodynamic trend to oxidize. In contrast, a cathodic shift was observed on samples immersed in solutions containing 1000 ppm F^- due to the growth of a less stable oxide with lower protective properties.

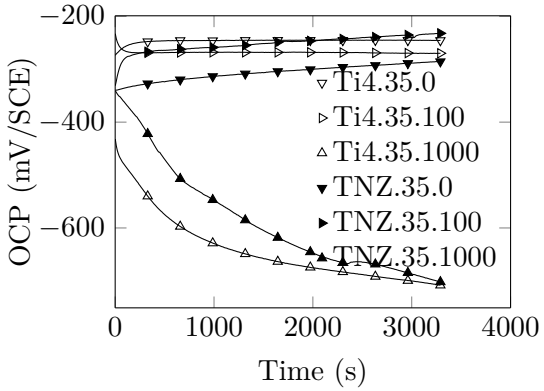

Figure 4.1: OCP evolution for CpTi4 and Ti13Nb13Zr immersed in artificial saliva with different fluoride concentrations (0, 100 and 1000 ppm F-) at pH 3.5.

Polarisation curves representing the most and the least aggressive conditions (pH

3.5, 1000 ppm F^- and pH 5.0, 0 ppm F^-, respectively) are shown in Figure 4.2. As expected, the least aggressive condition leaded to lower corrosion rates. In fact, the high current values obtained in artificial saliva with pH 3.5 and 1000 ppm F^- at the anodic branch ($10^{-4}A \cdot cm^{-2}$), discloses that in these conditions the material cannot be consider as in a truly passive state. Moreover, a less stable oxide layer with more defects might be expected at these pH and [F^-] conditions. This film may promote a competitive mechanism between the formation of hydroxylated species and the release of ions into the solution, leading to an equilibrium current that would not represent a real passivation state.

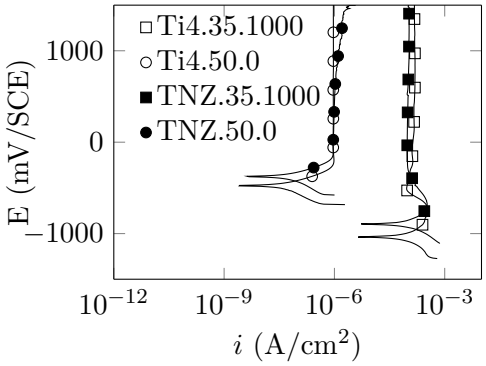

Figure 4.2: Polarisation curves of CpTi4 and Ti13Nb13Zr in artificial saliva with the most (pH 3.5, 1000 ppm F-) and the least (pH 5.0, 0 ppm F-) aggressive conditions.

Table 4.1 summarizes the average OCP values measured during the initial stabilisation and the main corrosion parameters calculated from polarisation curves; *i.e.* E_{corr}, i_{corr} and i_p.

OCP and E_{corr} had similar values and trends in all the evaluated solutions, so Figure 4.3 can serve as a reference for both parameters. Higher fluoride concentrations shifted E_{corr} towards more cathodic values in both materials.

The corrosion current density, i_{corr}, showed in Figure 4.4, was not significantly affected by the fluoride content up to 100 ppm F^-. Conversely, at the highest F^- contentration evaluated the increase of the i_{corr} was strongly dependent on the pH. At acidic pH, the i_{corr} increased about three orders of magnitude.

The influence of the electrolyte on i_p showed in Figure 4.5, followed the same trend as the i_{corr}. In solutions with 1000 ppm F^- and pH 3.5, the high value of the i_p showed that the oxide film growth in this condition was less stable and protective leading to values about $10^{-4}A \cdot cm^{-2}$. Such high values appeared to be more related to kinetics restriction resulting from competition established between the formation of hydroxylated titanium species and the flow of titanium into the solution. These results are in agreement with

Table 4.1: Electrochemical parameters of CpTi4 and Ti13Nb13Zr alloys in the studied solutions.

Material	pH	[F^-] (ppm)	OCP* (mV/SCE)	E_{corr} (mV/SCE)	i_{corr} ($\mu A/cm^2$)	i_p ($\mu A/cm^2$)
CpTi4	3.5	0	-265 ± 10	-260 ± 5	0.09 ± 0.04	3 ± 0.7
		100	-445 ± 75	-450 ± 85	0.06 ± 0.01	1.1 ± 0.2
		1000	-1065 ± 5	-1055 ± 25	115 ± 35	140 ± 4
	5.0	0	-480 ± 15	-475 ± 5	0.034 ± 0.002	1 ± 0.2
		100	-270 ± 35	-285 ± 55	0.05 ± 0.02	1.1 ± 0.1
		1000	-455 ± 160	-495 ± 140	0.3 ± 0.2	9 ± 8.5
Ti13Nb13Zr	3.5	0	-215 ± 95	-240 ± 70	0.1 ± 0.06	3.2 ± 2
		100	-460 ± 50	-440 ± 15	0.09 ± 0.09	1.4 ± 0.2
		1000	-915 ± 40	-895 ± 30	140 ± 20	100 ± 10
	5.0	0	-245 ± 200	-245 ± 185	0.17 ± 0.15	1.7 ± 0.6
		100	-400 ± 5	-390 ± 15	0.06 ± 0.03	1.7 ± 0.6
		1000	-630 ± 30	-680 ± 20	1.3 ± 0.1	6 ± 0.5

* OCP values correspond to the average value of the last two-thirds of 60 min of measurements under open circuit potential just after immersion.

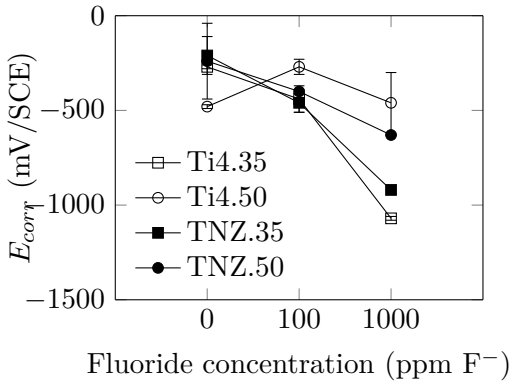

Figure 4.3: Corrosion potential of CpTi4 and Ti13Nb13Zr in artificial saliva solutions.

those reported by Sakairi *et al.* [77]. They observed that the anodic current of CpTi4 in presence of F^- only changed when the solution was acidic. Similar results were obtained by Nakagawa *et al.* [70], who studied the limit values of F^- concentration and pH in artificial saliva at which the corrosion behaviour of CpTi2 changed from non-corrosive to corrosive state. Results obtained by anodic polarization and immersion tests in the present work, show that artificial saliva with 1000 ppm F^- and pH 3.5 is the only solution tested that clearly exceed the limit proposed by Nakagawa for the destruction of the Ti passive film.

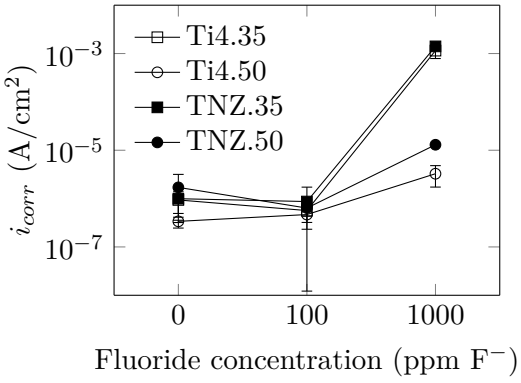

Figure 4.4: Corrosion current density of CpTi4 and Ti13Nb13Zr in artificial saliva solutions.

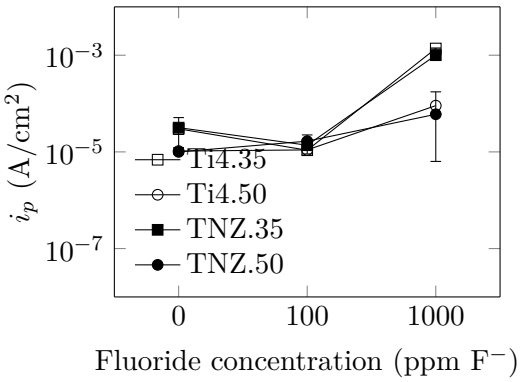

Figure 4.5: i_p of CpTi4 and Ti13Nb13Zr in artificial saliva solutions.

4.3.2 Reciprocating sliding corrosion tests

Open circuit potential conditions. Reciprocating sliding corrosion tests at OCP were carried out to analyse the tribocorrosion behaviour and mechanisms of CpTi4 and Ti13Nb13Zr in artificial saliva with different pH and F^- concentrations. The average coefficient of friction (COF) registered on rubbing experiments at OCP was around 0.45 and was not influenced by material, pH or fluoride changes in the analysed ranges. The value of 0.45 has was in literature for tribological pairs with CpTi [51]. Both materials showed similar electrochemical behaviour. Therefore, for the sake of simplicity just the results corresponding to Ti13Nb13Zr are shown in Figure 4.6, which shows the evolution of the OCP during the reciprocating sliding experiments in the different test conditions.

When rubbing started a sudden potential drop towards cathodic values was observed, indicating the mechanical activation of the scratched area as a result of the oxide removal, what leaves a more active surface exposed to the electrolyte. In acidified artificial saliva (pH 3.5) with 1000 ppm F^-, both materials showed a slight decrease of the potential

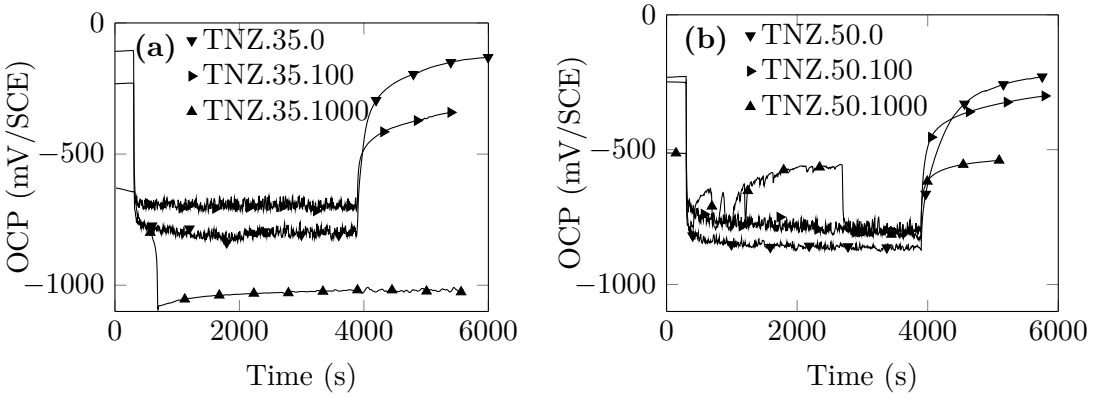

Figure 4.6: OCP evolution for Ti13Nb13Zr during sliding tribocorrosion experiments in artificial saliva with pH 3.5 (a) and pH 5.0 (b).

at the beginning of the rubbing, reaching the lowest value several minutes latter with a sudden potential drop. This fact together with the OCP values recorded before rubbing, revealed that the potential drop might not only be related to mechanical depassivation but also to the enhance of the active corrosion of the exposed surface. Indeed, the more negative values recorded for the OCP during rubbing in most of the experiments indicated that metal dissolution and oxide layer formation may not have been the only reactions taking place on the Ti surfaces. According to Pourbaix diagrams [34], at such cathodic values, water may be out of equilibrium, so hydrogen evolution can also contribute to the potential fluctuations.

With respect to the electrolytes containing lower fluoride concentrations, potential oscillations were recorded during rubbing due to the dynamic equilibrium between depassivation and repassivation events. The fact that no oscillation occurred in acidified saliva with 1000 ppm F^- and the very negative OCP supports that repassivation was not taking place and that the surface was actively dissolving. This occurred since the low pH as well as the high fluoride concentration hindered the formation of a good passive film on the metal surface [52].

After some sliding time, the potentials achieved a steady value that remained stable during the sliding test. These average OCP values are gathered in Figure 4.7.

Potentiostatic conditions. Tribocorrosion tests at an applied passive potential were performed in order to study the behaviour of the passive films under controlled electrochemical conditions (Figure 4.8).

Current evolution in the most aggressive condition (Figure 4.8 (a)) showed a constant current value of about 10^{-3}A/cm^2 that did not change when rubbing was applied. The

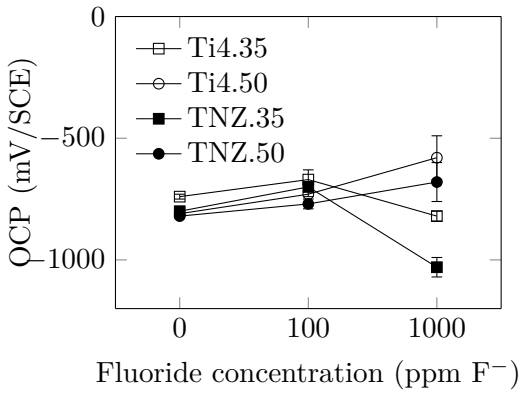

Figure 4.7: Average value of the OCP during reciprocating sliding test.

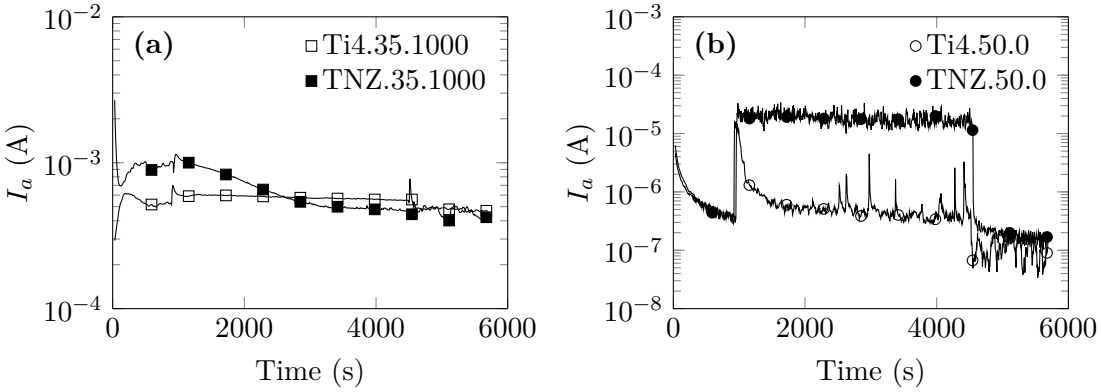

Figure 4.8: Current evolution of CpTi4 and Ti13Nb13Zr during rubbing at an applied passive potential (+750 mV/SCE) in artificial saliva with (a) pH 3.5 and 1000 ppm F^- (b) pH 5.0 and 0 ppm F^-.

shape of current evolution in the least aggressive condition (Figure 4.8 (b)) is applicable to the other testing conditions. At the beginning of the experiment, when an anodic potential was applied, a current decay was observed as a result of a thickening of the passive layer. When rubbing started, a sudden increase of the current occurred due to the mechanical removal of the oxide layer and the anodic dissolution of the surface active sites. A dynamic equilibrium was reached between the mechanical removal and the anodically grown oxide. After rubbing, the current abruptly dropped since the mechanical removal effect was suppressed allowing the anodic coarsening of the oxide layer at the worn area.

During sliding, different current evolution was recorded on each material. CpTi4 specimens showed an initial current peak but then the current gradually decreased over time, indicating an ability to withstand the rubbing process at the applied passive potential and contact pressure. Indeed, large spikes were observed during rubbing due

to local depassivation processes and the consequent fast repassivation.

This repassivation ability was also reported by Diomidis *et al.* [98] in fretting experiments in Ti-29Nb-13Ta-4.6Zr alloy against an alumina ball at passive applied potential. Conversely, Ti13Nb13Zr exhibited an initial current increase that remained constant during the whole rubbing test. The same behaviour was observed by Licausi *et al.* [52] on a sliding corrosion test of Ti6Al4V against an alumina ball. Such a high current values indicated a severe anodic dissolution of the wear track as a consequence of rubbing, suggesting the higher relevance of the corrosion accelerated by wear process on the tribocorrosion mechanisms of Ti13Nb13Zr compared to CpTi4.

The wear volume due to anodic dissolution under passive applied potential conditions, V, can be estimated from the measured current transients [99] using Faraday's law (4.1):

$$V = \frac{QM}{n\mathrm{F}\rho} \tag{4.1}$$

where M is the atomic weight, ρ the density of the metal, F is the Faraday constant (96500 $\mathrm{C} \cdot \mathrm{mol}^{-1}$) and n is the charge number (number of electrons transferred in the oxidation reaction). Assuming that M of Ti is 48 $\mathrm{g} \cdot \mathrm{mol}^{-1}$, n=4 ($\mathrm{Ti} + \mathrm{O} \rightarrow \mathrm{TiO_2}$) and ρ=4.51 $\mathrm{g} \cdot \mathrm{cm}^{-3}$, for both materials.

As shown in Figure 4.9, the charge in the unworn area (Q_{unworn}) corresponds to the anodic dissolution of surface surrounding the wear scar and is determined by the area below the estimated current sliding, I_{unworn} (interpolation of the current values prior and after rubbing with a third degree polynomial equation). The charge from the worn area (Q_{worn}) corresponds to the anodic dissolution of titanium mechanically activated and it was calculated by the area between the measured current during rubbing and I_{unworn} [99].

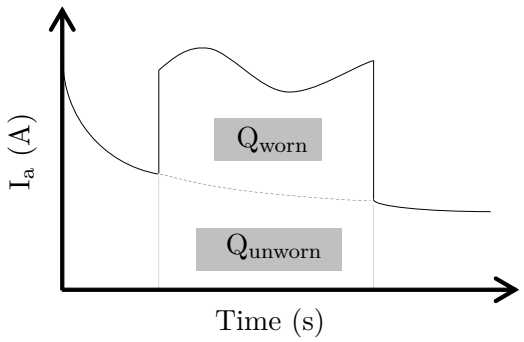

Figure 4.9: Schematic diagram of the charge (Q) corresponding to worn and unworn areas.

As material dissolution occurs either at the wear scar or at the surrounding exposed area, assuming that the material dissolution takes place homogeneously at the corresponding area, then, thickness of the dissolved material can be defined by $h = V/\mathrm{A}$ where A is the corresponding area. Figure 4.10 shows the thickness of the dissolved material due to passive and mechanically active dissolution.

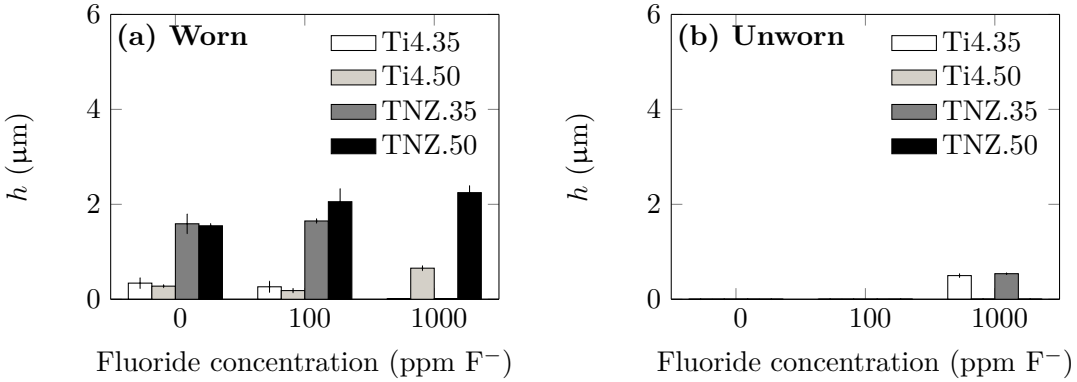

Figure 4.10: Material dissolution, h, from the (a) worn and (b) unworn areas as a result of reciprocating sliding test under anodic polarisation conditions.

Material loss, h, because of the anodic dissolution at the worn area during rubbing test revealed important differences depending on the material. The much higher h_{worn} of Ti13Nb13Zr in comparison to CpTi4 made clear that the tribocorrosion behaviour of these materials largely differ one from each other. Apart from the most aggressive condition, no significant influence of fluoride on h_{worn} was found. The h_{unworn} was significant in both materials only in the most aggressive condition, the solution with 1000 ppm F^- and pH 3.5, disclosing a higher dissolution of Ti due to its active state. This is in agreement with Figure 4.8 where no influence of rubbing on measured current density was observed in the most aggressive condition.

The average coefficient of friction (COF) recorded during reciprocating sliding tests under passive applied potential are shown in Figure 4.11.

CpTi4 displayed bigger COF values in comparison to Ti13Nb13Zr. In addition, there was a reduction of the COF as the fluoride content increased. The fluorides present in the solution may be adsorbed on the Ti modifying the tribocontact and leading to a lower COF. This behaviour was also reported by Souza *et al.* [51] for CpTi.

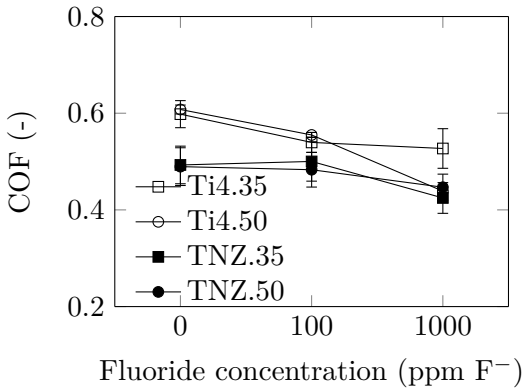

Figure 4.11: Average coefficient of friction recorded during reciprocating sliding corrosion tests under potentiostatic conditions.

4.3.3 Wear track characterisation

SEM images of wear scars belonging to tribocorrosion experiments under OCP conditions are shown in Figure 4.12. The morphologies of the specimens worn with 100 ppm F^- solution are not included because they show similar characteristics to those without fluorides. Material spalling can be observed at the contact surfaces suggesting that adhesive wear occurred at the wear scar. During sliding, contacting asperities undergo an increase of the plastic strain promoting crack nucleation below the surface of the material with lower hardness. In addition, the high reactivity of titanium results in a high bonding strength with the counterpart, facilitating crack propagation and layer detachment. Some of the detached layers get out of the wear scar, but others remain inside. Wear tracks also showed plastically deformed grooves aligned with the sliding direction. Abrasive wear or ploughing results from the indentation and scratching of particles present on the worn surface during rubbing. The hardness of these particles increases the abrasive wear, thus an oxidizing environment where particles oxidise and thus harden, is likely to promote the abrasive wear. In this regard, Figure 4.12 supports that under the most aggressive solution conditions, *i.e.* artificial saliva with pH 3.5 and 1000 ppm F^-, reduction reactions prevailed so the extent of abrasive wear became smaller or even negligible. Indeed, dark areas analysed by EDX were composed of Ti, O and F. This reveals the incorporation of fluoride into the debris or the surface resulting in a less protective film. Souza *et al.* studied the influence of fluorides on tribocorrosion behaviour of CpTi grade 2 and they also noticed no abrasive wear in the wear track of the sample under a very aggressive condition, 12300 ppm F^- and pH 6.5 [51]. In addition, the extent of plastic deformation was found to be higher in the case of Ti13Nb3Zr. The higher hardness of detached particles from Ti13Nb3Zr alloy compared to those of CpTi4, may explain the higher contribution of Ti13Nb3Zr to abrasive wear. Conversely, detailed

investigation of delaminated areas showed cracks perpendicular to the sliding direction on CpTi4 samples rubbed in artificial saliva with 1000 ppm F^-. This suggests a higher contribution to adhesive wear as the aggressiveness of the media increases.

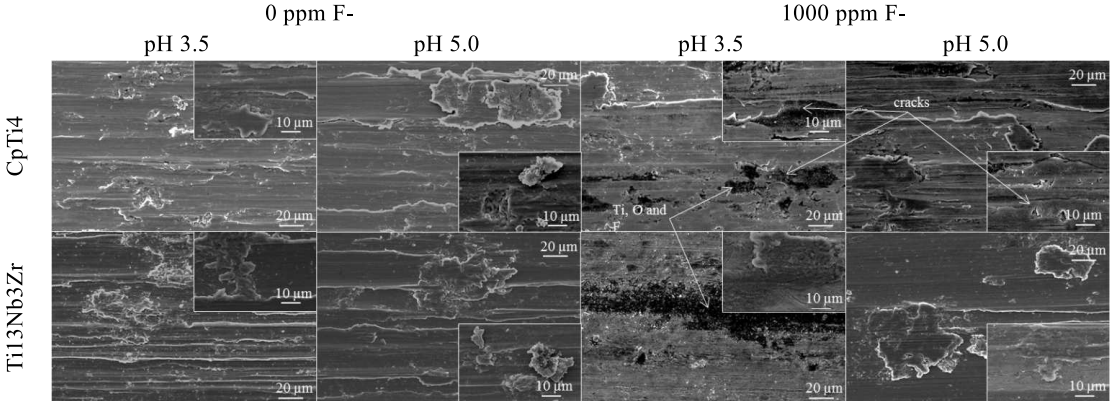

Figure 4.12: SEM images of the wear mechanisms of CpTi4 and Ti13Nb13Zr after reciprocating sliding test in pH 3.5 artificial saliva under OCP conditions.

The wear rate corresponding to the reciprocating sliding tests performed under open circuit potential and potentiostatic conditions are shown in Figure 4.13. The wear rate measured by profilometry (Figure 4.13) is not only given by (i) the material dissolution in the worn area due to mechanical interaction (Figure 4.10a). It is also given by (ii) material loss due to mechanical interaction and (iii) mechanical wear accelerated by corrosion. Thus, wear rate results obtained by profilometry should not be compared to the material losses calculated through Faraday's law from potentiostatic tests (Figure 4.10). This is because the latter serves to qualitatively identify the contribution of corrosion accelerated by wear, whereas the measurements carried out by profilometry estimate the total volume loss at the wear scar after rubbing in different media.

It also should be noted that the wear measurements by profilometry do not take into account the recess of the surface surrounding the wear scar due to dissolution processes. Material dissolution promoted by the aggressiveness of the medium may reduce the depth of the wear scar. This is observed in Figure 4.10b, under potentiostatic conditions, in the most aggressive condition, where material dissolution at the surrounding area of the wear track corresponds to 0.5 µm. Thus, the wear rate measured under these conditions (at Figure 4.13) may be underestimated. This fact might also explain the lower wear rate obtained by Vieira *et al.* [48] after a tribocorrosion test in acidified artificial saliva. Regarding fluoride effects, besides the most aggressive condition, artificial saliva with 1000 ppm F- and pH 5.0 was the only solution that significantly reduced the wear rate on both materials. This indicates the importance of the wear accelerated by corrosion under tribocorrosion request on titanium in comparison to pure electrochemical processes.

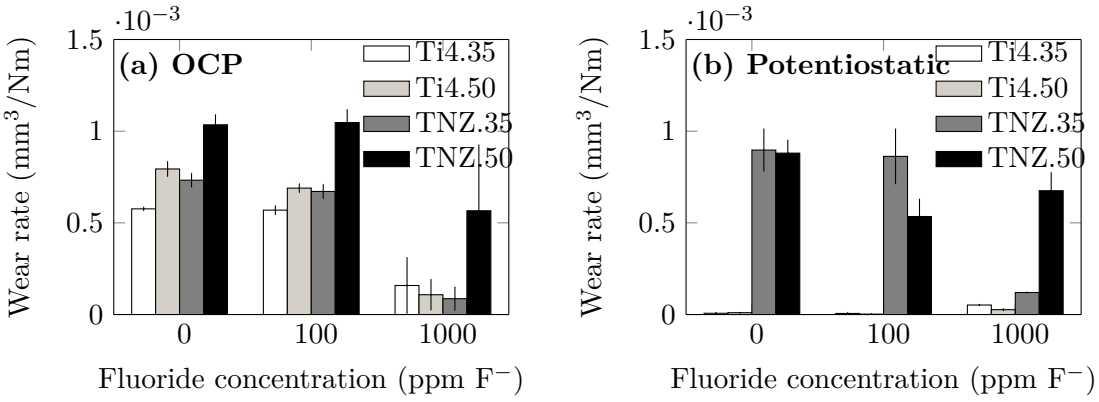

Figure 4.13: Wear rate measured by profilometry on wear scars made on reciprocating sliding test under A) OCP and B) Potentiostatic conditions.

Under open circuit potential, the lower wear rate of CpTi4 compared to Ti13Nb13Zr revealed that the latter possessed a higher contribution to the corrosion-accelerated by wear. In effect, the fact that almost no wear rate was measured on CpTi4 under potentiostatic conditions by profilometry revealed that its high repassivation capability (see Figure 4.8) was not at the expense of repassivated oxide layer breakdown and consumption. Thus, the high repassivation rate of CpTi4 did not increase the wear rate through wear accelerated by corrosion mechanisms. Indeed, while at pH 3.5 wear rate of Ti13Nb13Zr at OCP is similar to CpTi4, at pH 5.0 the wear rate increases. A weakly oxidizing environment, such as a low pH, may hinder the spontaneous repassivation of titanium. Similar trend was observed by Mathew *et al.* [36] and Vieira *et al.* [48], who studied the influence of pH on tribocorrosion behaviour of CpTi in oral environment. In this regard, the wear rate of Ti13Nb13Zr increases in oxidizing environments due to its dissolution during rubbing and the breakdown and consumption of the protective layer. This also supports the higher contribution of Ti13Nb13Zr to the corrosion accelerated by wear. Moreover, the chemical composition of the oxide layer determines its mechanical properties. This may explain the tribocorrosion mechanisms of each material. The native oxide layer on CpTi4 is composed mainly by TiO_2 [100], whereas ZrO_2 and Nb_2O_5 are also present on Ti13Nb13Zr [101]. The presence of different oxides at the protective layer induces defects which may reduce its cohesive and adhesive properties facilitating its degradation in the case of a rubbing request. Moreover, once the oxide layer has been removed, the thermodynamics of the oxidation of the bulk material condition the oxide layer repassivation rate.

4.4 Conclusions

In this work, Ti13Nb13Zr alloy was proposed as a potential alternative to the commonly used CpTi4 for dental implant application, due to its better biocompatibility and strength to weight ratio. The main goal of the current study was to determine the influence of pH and fluoride concentration on corrosion and tribocorrosion response of Ti13Nb13Zr alloy. To this end, CpTi4 was used as benchmark.

- Both materials presented similar corrosion resistance in artificial saliva but Ti13Nb13Zr showed higher wear rate values after reciprocating sliding tests under OCP conditions, which appeared to be related to a lower wear resistance of the alloy. Anodically polarised reciprocating sliding tests revealed different tribocorrosion mechanisms depending on the evaluated material. Ti13Nb13Zr experienced an important material loss due to corrosion accelerated by wear. Conversely, the higher repassivation capacity of CpTi4 was not at expense of repassivated protective layer breakdown and consumption. Future research should therefore concentrate on a deeper investigation of oxides cohesive and adhesive properties and repassivation kinetics of Ti13Nb13Zr and CpTi4 in oral environment.

- Fluoride concentration had a significant influence on the corrosion behaviour of these alloys, the higher the fluoride content the lower the corrosion resistance. On the other hand, the influence of the pH on the corrosion resistance of the materials was more significant on 1000 ppm F^- solutions, wherein an acidic pH resulted detrimental for the corrosion resistance of the metals. Under reciprocating sliding conditions, as the aggressiveness of the solution increased, the wear scar depth decreased due to the recess of the surrounding area. The active state of both materials in artificial saliva with 1000 ppm F^- and pH 3.5 dominated the synergy between wear and corrosion.

Overall in this work, tribocorrosion experiments under OCP are the ones that better resemble *in vivo* conditions, since tribocorrosion experiments under potentiostatic condition are a tool to better understand the underneath tribocorrosion mechanisms. This, along with the fact that the most aggressive condition tested in the work (artificial saliva with pH 3.5 and 1000 F^-) is unlikely to take place, involves that wear rate under tribocorrosion conditions of Ti13Nb13Zr alloy is higher but still similar to the widely used CpTi4.

Chapter 5

Repassivation kinetics of Ti13Nb13Zr alloy in oral environment

In the previous chapter, a slight decrease of Ti13Nb13Zr wear resistance compared to CpTi4 against tribocorrosion was observed. Namely, Ti13Nb13Zr experienced a higher material loss due to corrosion accelerated by wear. However, potentiostatic techniques provide limited information about wear-corrosion mechanisms at *in vivo* conditions.

Thus, in this chapter, the difference between Ti13Nb13Zr and CpTi4 wear-corrosion mechanisms under free corroding conditions will be elucidated. To that end, repassivation kinetics of both materials will be measured under open circuit potential using electrochemical noise technique. In addition, the analysis of the influence of different tribological parameters on the wear rate of the materials will reveal the underlying tribocorrosion mechanisms.

The work of this chapter was partially carried out in KU Leuven, under the supervision of Prof. J-P Celis.

5.1 Introduction

The passive oxide film formation kinetics play an important role in the release of metals from metallic biomaterials in living organisms, making a fuller understanding of the repassivation kinetics and details of the oxide film structure of great importance.

In tribocorrosion processes of passive materials, repassivation kinetics are key since after a depassivation event, they involve the time the material is actively dissolving in an aggressive medium, until it completely repassivates again. In dental implants, mastication events cause mechanical removal of the protective layer of titanium alloys. Such is the importance of repassivation kinetics that it has been extensively studied in literature [77, 102, 103, 104, 105, 106].

Different depassivation methods have been used, such as, abrasion [107], breaking electrode [102], etc.; where electrochemical reactions due to repassivation events were commonly measured under potentiostatic control. Table 1 shows the main parameters of depassivation-repassivation experiments from several authors in addition to the corresponding time constant deduced from graphic data. The time constant, τ, is defined as the time elapsed to get a current reduction of 66.3 % from the initial hop. Overal, repassivation kinetics under potentiostatic control show to be fast compared to the chewing frequency, which is around 1-2 Hz [59]. This means that by the time the following depassivation event occurred, the already depassivated area is repassivated again.

Table 5.1: Main parameters of depassivation and repassivation experiments in literature (E_{app} is the applied potential (potentiostatic control) and τ is the time constant).

Reference	Material	Solution	E_{app} (V/SCE)	Depassivation technique	τ (s)
Sakairi *et al.* [108]	CpTi	PBS	1.46	Laser beam irradiation	0.00078
Hanawa *et al.* [102]	CpTi2	Hanks	1.5	Electrode fast-fracture	0.0015
Kolman *et al.* [109]	CpTi	0.6 M NaCl	0	Manual scratch	0.000034
Kolman *et al.* [103]	CpTi2	0.6 M NaCl	0	Scratch test	0.000046
Gilbert *et al.* [104]	Ti6Al4V	PBS	-0.04	Scratch test	0.0007
Beck *et al.* [110]	CpTi	3M HCl	-0.36	Electrode fast-fracture	0.00165
Jemmely *et al.* [106]	AISI 430	H2SO4	0.13	Potential step method	0.02
Jemmely *et al.* [106]	AISI 430	H2SO4	0.13	Tribocorrosion	0.001

There are some important features one must be aware of when measuring repassivation kinetics of a passive metal immersed in an electrolyte. Whatever the experimental technique, the measured current is not only related to the bare metal repassivation, but also to the effect of ohmic potential drop, the charging of the adjacent double layer; and the ratio between the activated and passive surface, if any.

The ohmic drop effect. The finite value of the conductivity of the electrolyte causes an ohmic drop between the working electrode and the reference electrode. Thus, in presence of an ohmic drop, (IR_Ω), the apparent impedance (Z_{app}) is measured, instead of double layer impedance (Z):

$$Z_{app} = Z + R_\Omega \tag{5.1}$$

The ohmic drop also depends on the current and in the case of the growth of a surface oxide film, its value changes over time, leading to different ohmic drop values along the measurement [111]. A technique such as galvanostatic methods with current interruption may be used to experimentally determine R_Ω. When the current is switched off, the ohmic contribution of the measured potential instantaneously disappears, whereas the potential across the double layer slowly decays, analogous to a discharging capacitor. The applied current is the sum of the capacitive current (I_C) and the faradaic current (I_F) described by the Butler-Volmer equation:

$$I = I_F + I_C \tag{5.2}$$

where

$$I_C = \mathrm{C}\frac{dE}{dt} \tag{5.3}$$

The disappearance of the ohmic contribution when the current is cut, however, is a rather idealised behaviour. In fact, the complexity of the system makes this drop to be less sharp [111].

Charging of the Double Layer. When part of a passivated surface is activated, most of the initial current would be delivered to the filmed surface (approximately in proportion to its surface area), basically in charging the double layer [112]. So at the very beginning of the repassivation, the Faradaic current is zero because the double layer must be charged first.

$$I(t = 0) = I_C \tag{5.4}$$

As the potential across the double layer increases, the faradaic current increases, while the capacitive current becomes less important. The steady state is reached when the capacitive current becomes zero. According to 5.3 and 5.4, the derivative of the potential with respect to time at t = 0 provides the double layer capacity.

Galvanic effects. The existence of a galvanic effect between the wear scar and the non-damaged (passive) surface is frequently mentioned in reports of tribocorrosion [86, 113]. The metal with the more negative potential, *i.e.* the depassivated wear scar, is the anode; and the one with the more positive potential, *i.e.* the surrounding passive

area, is the cathode. As both are coupled, additional corrosion can take place in the anode owing to the galvanic coupling condition. Apart from thermodynamics, galvanic corrosion kinetics depend on the electrolyte, the electrochemical properties of the anode and the cathode; and the geometry of the system. A complete description of the potential distribution on the surfaces of a galvanic couple can be obtained by solving Laplace's equation with suitable boundary conditions

$$\nabla^2 \Phi = 0 \tag{5.5}$$

where ∇^2 is Laplace operator and Φ is a scalar function. This equation is derived from Ohm's law, which states that, at any point in the electrolyte, the current density is proportional to the potential gradient:

$$I = -\nabla \Phi \tag{5.6}$$

The repassivation process is a transient step during which the effect of the interaction between two elementary circuits (passive impedance and localized corrosion site impedance) cannot be neglected [113]. Oltra *el al.* [113] analysed the effect of electrical transient coupling phenomena on the initiation of pits by a pulsed laser method on 304 stainless steel. They proposed an equivalent electric circuit to model passive metal activation and repassivation under free corroding potential conditions considering the interaction between the two elementary circuits: passive impedance and localized corrosion site impedance, shown in Figure 5.1.

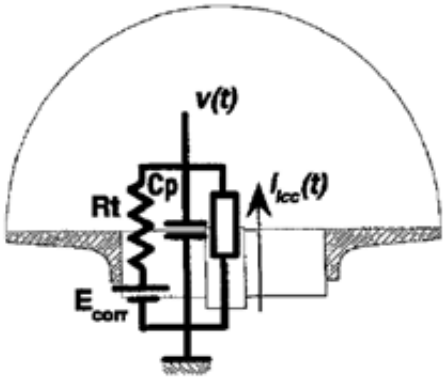

Figure 5.1: An equivalent electrical circuit for describing a localized corrosion situation under free corroding conditions [113].

They concluded that the growth of a 'birth and death' pitting event at the pitting potential is under control of electrode area, which is in accordance with other authors

[114, 115].

5.1.1 Experimental depassivation techniques

Different occurrences such as mastication forces or a sudden worsening of the aggressiveness of the media in the oral environment, may locally cause the local loss of the protective oxide layer on a dental implant. In order to resemble this process at laboratory scale, a number of depassivation techniques have been developed. Due to the fast repassivation kinetics of passive metals, the fast depassivation rate is been a requirement. A general overview of these mechanical and electrochemical depassivation techniques can thus be found down below.

Guillotined surfaces. The stationary guillotined electrode was designed to produce potential transients from a freshly generated specimen surface of a known surface area using a single and rapid pass of the cutter through the whole surface [105, 110, 116]. It consists in a fast mechanical interaction so it provides measurements of the repassivation kinetics from the first millisecond of the life of the new metal surface. However, the introduction of metallic devices on the electrochemical cell (*i.e.* the guillotine) may alter the following electrochemical measurements. In addition, in a real system, a repassivation event is inextricably linked to interactions with the surrounding passive surface area.

Breaking-electrode A masked working electrode with band geometry and small section is cantilevered into a plexiglass cell through a slot in the side and secured at the notches with a plexiglass clamp. Then, an impact on the free part inside the cell breaks the electrode and the bare metal gets exposed to the electrolyte [117]. This technique is also a fast repassivation technique but the interactions with the surrounding area are also restricted.

Laser. The laser depassivation technique, a laser impact on the passive metal which is able to provide a complete depassivation during a short time, similarly to the so called 'birth and death' pitting events [113]. The pulsed laser beam is able to strip oxide film at extremely high rates and with no contamination from the film removing tools, such as mechanical depassivation techniques. In addition, as the spot size can be adjusted, the activated area to passive area ratio is easy to obtain. However, the rapid solidification following the laser beam irradiation leads to the modification of the microstructure of the material at the laser beam irradiated area, which may lead to inaccurate measurements.

Scratch tests. This technique consist of generating a scratch on the passive surface of the material with an insulating tip (made of diamond or alumina), thus it allows the study of the influence of the surrounding passive area on the repassivation kinetics

[118, 119]. However, this technique is not as fast as others and by the time the end of the scratch has being created, the beginning of the scar might have already experienced a significant repassivation, which results in mixed activation/repassivation. In this regard, Bosch *et al.* [118] made a convolution calculation to overcome this problem.

Micro-indentation. Through this technique, a micro indentation is made on the material to fracture the passive film so it allows to simultaneously measure the load-depth curve of the substrate and the electrochemical response. However, the film-ruptured area depends on the hardness of the material. Like in the scratch test, this technique is not as fast as others.

Potencial pulse test. The electrochemical depassivation of a passive film is made with a cathodic polarisation that completely removes the oxide film [120, 121]. Although this is a fast depassivation method, ambiguities exist related to the extent of reduction of pre-existing oxide films achieved, the simultaneous reduction of water in aqueous electrolytes, and variation in the surface composition of alloys after reduction. For example, the removal of titanium oxide surface film in aqueous solutions by cathodic reduction renders difficult because of the preferential reaction of hydrogen evolution [102].

5.1.2 Electrochemical techniques to measure the depassivation/repassivation events measurement

Open circuit potential is the electrochemical technique that better resembles corrosion events occurring at material-electrolyte interface. No information about the current fluctuation and thus the reaction rate can be obtained however. Thus, potentiostatic holding is actually the most used one. Below, the potentiostatic-galvanostatic technique and an alternative electrochemical noise techniques are reviewed.

Potentiostatic-galvanostatic methods. Potentiostatic holding has been the most widely used technique to measure depassivation and repassivation kinetics and the passive/transpassive behaviour of passive metals [103, 104, 105, 106]. However, *in vivo* conditions at the oral environment are better represented under free corroding conditions, that is, at open circuit potential. In fact, depassivation experiments in literature under open circuit potential revealed a much more steeper potential recovery of titanium in Hanks solution, in the order of tens of second [122]. Although potential recovery is slower than current decay due to the capacitive behaviour of the passive metals, this still contrasts with the fast kinetics observed under potentiostatic conditions (See Table 5.1). Hence, electrochemical conditions would make the difference analysing repassivation kinetics, which may change from faster to slower, compared to the depassivation rate to which the material is subjected. As a consequence, the prevailing damage mechanisms

and wear rates can be misleading. Hanawa *et al.* [122] measured the open circuit potential evolution towards anodic values after a depassivation event. With this technique they obtained slower repassivation kinetics of the potential of titanium in simulated bioliquids, compared to those listed in Table 5.1.

Electrochemical noise technique. The electrochemical noise technique uses a Zero Resistance Amperimeter (ZRA), which is an active device that generates a current source equal to the one which is being measured. In this way, current can be measured under free corroding conditions. This technique has been widelly used for localised corrosion [114, 123] and for tribocorrosion measurements [124, 125].

There are several ways to measure potential and current noise in an electrochemical system. The two identical working electrode connected through a ZRA measure the stochastic corrosion events occurring on both electrodes (*e.g.* pitting corrosion). In addition, if one of the areas is depassivated, potential and current differences between the two electrodes can also be measured [123]. However, the galvanic coupling between the two electrodes originated due to the wear of one of them, may accelerate the corrosion process. The use of Pt microelectrode instead of a second WE, coupled through the ZRA may overcome this problem.

To authors knowledge, no research has been carried out to measure repassivation kinetics of titanium alloys with electrochemical noise technique.

5.1.3 Theoretical repassivation models

The theoretical modelling of the shape of the current or potential transient allows one to obtain details about repassivation kinetics. Some of the developed models are then reviewed down below.

Surface coverage model. This model assumes that after the passive film is removed, metal oxidation exclusively occurs on the bare metal surface leading to lateral growth of an oxide in principle of monolayer thickness. In presence of ohmic drop in the electrolyte between reference electrode and working electrode, the value of the actual anode potential may differ from that of the applied potential [106]. In all cases, the current density stays constant up to the formation of an oxide monolayer. Then, the current drops when the oxide covers the entire surface. As there is not such an abrupt current drop in repassivation currents, this model is only valid for the very initial stage of the oxide formation.

High field conduction theory. The high field conduction model is based on Cabrera-Mott theory [126]. It is assumed that an anodic oxide grows uniformly on the surface, the growth rate being determined by high field conduction. This model is not

expected to be physically realistic in the very first moments of repassivation. Cabrera and Mott proposed an oxidation theory for intermediate thickness (around few nm). They proposed that injection of ions into the oxide film is rate-determining, with a near-logaritmic growth law, since electrons can easily overcome the energy barrier at the metal-oxide interface. In their model, injection was controlled mainly by the electric field across the oxide by adsorbed charges at the oxide surface and taken to have the expression

$$E = V/x \tag{5.7}$$

with x the thickness and V the difference between the metal work function and the electron affinity to the adsorbed species. A comparison of the calculated and experimental transients carried out by Jemmely *et al.* [106] indicated that the model is correct qualitatively describing the influence of the different variables, although a quantitative prediction of the current was not achieved. This was explained by the fact that all the current does not go into film formation, because selective dissolution of bare material can occur during film growth [127].

Active wear track. A critical load is required to delaminate a passive film and a stress distribution exists in every contact point under elastic loading conditions. Therefore, part of the real contact area can be subjected to a pressure below that critical load, and is thus not activated mechanically in corrosion-wear tests. The active wear track area in corrosion-wear can be determined from electrochemical measurements [120]. The current, I, flowing through an electrode of total area A subjected to sliding wear, is the sum of two components. The first component is the product of the active wear track area, A_a, and the repassivation current density, $i_a(t)$, and the second component is the product of the passive area, (A - A_a), and the passive current density, $i_p(t)$. The repassivation current density, $i_a(t)$, at a given anodic potential usually decreases with time due to the re-growth of the passive film. The $i_p(t)$ corresponds to the anodic current density for passive material polarized at that given anodic potential. It can be measured by conventional polarization techniques.

5.1.4 Objectives and hypothesis

The aim of this chapter is to analyse the repassivation kinetics of Ti13Nb13Zr and CpTi4 in oral environment. This work also attempts to put some light on the validity of potentiostatic holding for the evaluation of repassivation kinetics by analysing current repassivation kinetics of CpTi4 in artificial saliva under open circuit potential using electrochemical noise (EN) technique. To that end, following objectives are defined:

- To obtain the repassivation kinetics after a mechanical depassivation (scratch test)

of the materials under free corroding conditions.

- To analyse the influence of the surrounding area on the current evolution of an scratched area in free corroding conditions.
- To clarify the differences between the tribocorrosion mechanisms of Ti13Nb13Zr in comparison to CpTi4 in free corroding conditions.

These are the raised hypothesis in this Chapter:

- Conventional potentiostatic holding for repassivation kinetics studies do not represent accurately the real situation.
- There is a relation between the surrounding passive area and the repasivation kinetics due to the galvanic coupling.

5.2 Materials and Methods

5.2.1 Materials

CpTi4 and Ti13Nb13Zr sample preparation was done by progressively grinding titanium discs until 1200 grit and then polishing with 0.1 μm colloidal silica. Then the specimens were washed in distilled water, ultrasonically cleaned in ethanol for 5 min and dried with warm air. All the samples were stored in a drying chamber for 24 h before experiments. Influence of surrounding area on repassivation kinetics was tested by covering the WE with lacquer and leaving different areas exposed to the electrolyte: 1, 50 and 100 mm^2.

The electrolyte was Fusayama-Meyer artificial saliva at pH 5.0 and at room temperature.

5.2.2 Repassivation kinetics tests

Alumina balls (diameter 0.25 mm) were used as counterbody material due to their hardness, electric insulating, and chemical inertness properties. A 5 mm length scratch was made in the middle of the sample at a normal force of 3 N and at 1 mm/s. The bidirectional sliding/fretting test equipment used for higher accuracy is described elsewhere [128].

The electrochemical measurements were done using a three electrode cell containing a Ag/AgCl (3 M KCl) reference electrode (RE), and the titanium working electrode coupled to a Pt microelectrode (with a diameter of 0.25 mm and a length of 1 mm) through a ZRA. A potentiostat (Solartron electrochemical interface model 1287) was

used for the electrochemical noise measurements, which allows voltage and current measurements at a resolution of 1 μV and 1 pA, respectively. Potential values in Figures are given with respect to SCE. The tribometer and the potentiostat were grounded and coaxial cables were used wherever possible in order to reduce noise contamination. Data acquisition of potential and current was done at a sampling rate of 8 Hz.

The experimental sequence was:

- Allowing the system to stabilize at OCP during 60 min.
- Starting of the scratch test while the current and potential under free corroding conditions were measured.
- Removing the load once current and potential have recovered their initial values.

Curve fitting is a common but complex procedure to determine representative parameters of the repassivation kinetics which may lead to inaccurate results. In this work, a straightforward but robust process was applied to obtain characteristic parameters.

5.2.3 Reciprocating sliding corrosion tests

The electrochemical measurements were done using a three electrode cell containing a SCE reference electrode (RE), and a Pt coil as a counter electrode (CE). Reciprocating sliding corrosion experiments were carried out in Mondragon Unibertsitatea coupling the electrochemical cell to a tribometer (Microtest) with a ball-on-plate reciprocating sliding configuration. The reference electrode was placed no more than 10 mm away from the wear track. A 6 mm diameter alumina ball was used as a counter part. A normal force of 1 N was applied, which resulted in an initial contact pressure of 320 and 360 MPa for CpTi4 and Ti13Nb13Zr, respectively, sliding frequency and time varied with the experiments. During each sliding cycle, friction coefficient was measured. Only the steady values were used to compute an average coefficient of friction for each cycle. In addition, in order to avoid the running-in period, the average coefficient of friction of the complete sliding test was calculated by averaging the values concerning the last two-thirds of the test. Sliding tests were carried out at open circuit potential. The experimental sequence was

- Allowing the system to stabilize at OCP during 60 min.
- Starting of the sliding test while the OCP was measured.
- Removing the load once sliding finished and continuing recording OCP.

5.3 Results and discussion

The evolution of current recorded during a scratch test at open circuit potential (under free corroding conditions) is shown in Figure 5.2. It can be stated at first glance that the repassivation kinetics of titanium in an oral environment is much slower compared to experiments under potentiostatic control reviewed in literature. Under open circuit potential, chemical and electrochemical reactions take place at their natural rate, whereas under potentiostatic conditions they are forced and accelerated to happen.

This finding disagrees with the statement that repassivation kinetics of titanium alloys in agressive environments are fast (Table 5.1). In fact, it takes an order of tens of seconds to the oxide layer to regrowth again. This might be misleading on the understanding of degradation mechanisms of passive materials. Depending on the time elapsed between two contacts during a continuous sliding test, t_{elaps}, one can find a link between mastication frequency and the synergy between wear and corrosion: (i) if $t_{elaps} << \tau_I$, where τ_I is the constant time, once the oxide layer has been removed, the material remains active during rubbing and no repassivation takes place, thus there might be no increase of wear due to the oxidation of the worn surface; (ii) if $t_{elaps} \geqslant \tau_I$, repassivation events occur between two consecutive contacts and thus the oxidation of the worn surface may increase the wear. In the case of a dental implant, the mastication frequency approximately corresponds to 1 Hz, suggesting that t_{elaps} is much smaller that the repassivation time, thus the oxidation of the worn track might have less importance in the degradation mechanisms.

The current passing between the WE and the CE establishes a potential gradient in the electrolyte. The so-called ohmic drop effect escalates as the measured current increases or when the ohmic resistance through the electrolyte is large. The initial current augmentation due to the scratch may lead to the increase of the ohmic drop, distorting the initial potential jump and its evolution. Figure 5.3 shows the influence of the ohmic effect ($R_{ohm} = 500$ ohm/cm^2 in Fusayama-Meyer solution [45]) on the measured potential. In this case, however, the ohmic effect results negligible due to the small current values.

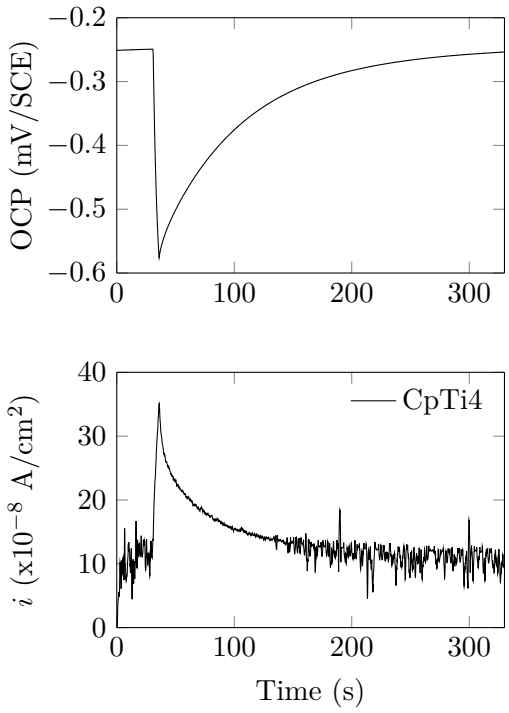

Figure 5.2: Potential and current evolution after a scratch experiment on CpTi4 immersed in artificial saliva.

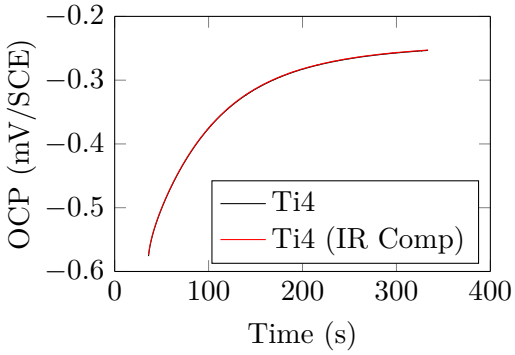

Figure 5.3: Potential evolution before and after a scratch experiment on CpTi4 immersed in artificial saliva with and without ohmic drop compensation.

5.3.1 Sliding frequency

Titanium and its alloys are passive materials, so as soon as their protective oxide is removed as a consequence of a mechanical interaction, it will start to regrow again. Hence, in a reciprocating sliding test, the time elapsed between two successive contacts influences the wear mechanism. Figure 5.4 shows the influence of the sliding frequency on the wear rate. Mastication frequency is usually around 1 Hz [59], so values from

0.5 to 2 Hz have been used to analyse its effect on the wear rate after a reciprocating sliding during 300 s. No changes on the wear rate, however, were observed at different sliding velocities. This might be associated with the slow repassivation kinetics observed in Figure 5.2. The oxide regrowth velocity is so slow that the studied sliding frequency range hindered the repassivation of the wear track during rubbing. When the wear scar gets oxidised, the adhesive strength between the detached particles and the first body diminishes, reducing the smear and attachment of debris particles to the wear scar and thus increasing wear [129]. Results showed that the sliding velocity range from 0.5 to 2 Hz has no influence on the wear rate, so it can be stated that the wear scar is in active state during the rubbing test. In addition, no statistically significant differences in terms of wear rate were observed between both materials.

In this regard, Barril *et al.* [130] studied the effect of sliding frequency on the fretting corrosion behaviour of Ti6Al4V in 0.9 % NaCl solution. To this end, they measured the wear scar volumes after experiments performed under applied potential of -1 and +0.5 V (Ag/AgCl) and under an oscillation frequency of 0.5, 1 and 2 Hz with a displacement amplitude of 100 μm. Test duration was 3600 s, so the number of strokes increased as the sliding frequency increased. Under the anodically polarised conditions, they observed a decrease of the wear volume per stroke as the sliding frequency increased. This was attributed to the variation of the time allowed to the metal to oxidise during a stroke. Although at the potential of -1 V the current is dominated by the cathodic reduction of oxygen, the same trend in wear rate evolution with frequency was observed. The repassivation kinetics under potentiostatic conditions might be minimised up to the order of sliding frequency, so a small variation of it would increase the contribution to corrosive wear and the total material loss. In that case, tribocorrosion mechanisms were different to those found in present work. If the protective film reached a certain thickness by the time the following contact occurred, it would have probably got removed due to its poor mechanical properties compared to the substrate. This increases the material loss by the breaking of the oxide film once a critical thickness was reached. This theory is based on Quinn's oxidative model [131] where the high temperature promotes the thermal oxidation of the substrate. In this case, instead of high temperature, the driving force accelerating the oxide growth was the polarisation of the system.

The average coefficient of friction measured during reciprocating sliding test at different sliding frequencies is presented in Figure 5.5. The COF decreased as the sliding frequency increased and it was smaller for Ti13Nb13Zb alloy compared to CpTi4.

In this regard, open circuit potential was measured during rubbing test. Potential oscillations during sliding have been previously reported [131] and they commonly have been attributed to mechanical and electrochemical events. The frequency domain

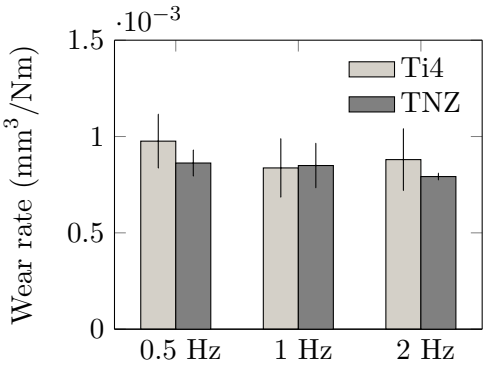

Figure 5.4: Wear rate of CpTi4 and Ti13Nb13Zr after tribocorrosion test at different sliding frequencies.

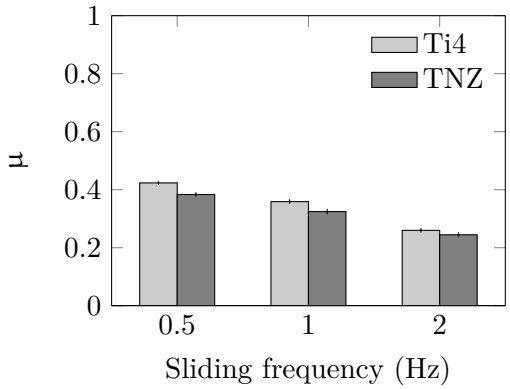

Figure 5.5: Average coefficient of friction of CpTi4 and Ti13Nb13Zr during rubbing at different sliding frequencies.

analysis enables a deeper analysis of the origin of these oscillations. Figure 5.6 shows Fast Fourier Transform (FFT) of the OCP values of CpTi4 and Ti13Nb13Zr during rubbing at different sliding frequencies. Both materials presented a similar frequency domain, although the one of Ti13Nb13Zr was more pronounced. Interestingly, the value of the big peak is double of the sliding frequency. Harmonics are the smaller peaks after the fundamental frequency. If one studies the pin movement in a reciprocating sliding test, within a cycle, the pin passes twice through each point of the wear track. This means that OCP oscillation during rubbing may only belong to a mechanical request. This supports the idea that under these conditions there was no influence of sliding frequency on the wear rate and tribocorrosion mechanisms. Repassivation of the wear track was hindered because the kinetics were much lower than the sliding frequency, so no electrochemical events could be observed at the OCP signal.

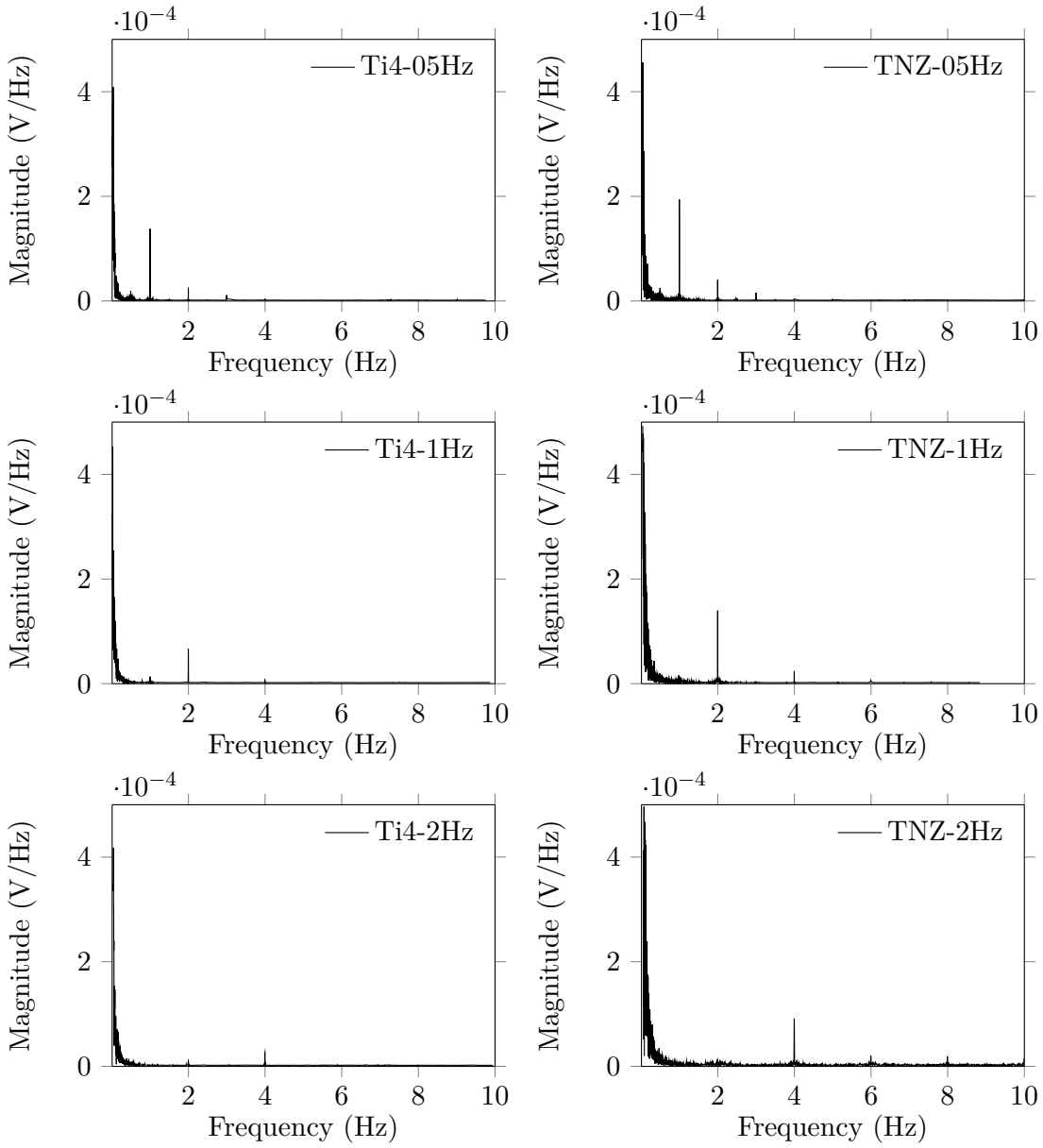

Figure 5.6: FFT of the OCP values of CpTi4 and Ti13Nb13Zr during rubbing at different sliding frequencies.

5.3.2 Repassivation kinetics

Once a scratch is made on a passive metal, the passive layer is removed and a galvanic coupling is generated between the activated area, A_{act}, and the surrounding passive area, A_{pas}. The A_{pas}/A_{act} ratio is a key fact conditioning the repassivation event, thus, in this section, the influence of A_{pas}/A_{act} ratio on the repassivation kinetics was analysed. For that, titanium samples were masked in order to obtain the A_{pas} and the corresponding A_{pas}/A_{act} ratios listed in Table 5.2.

Table 5.2: The A_{pas}/A_{act} ratio of the masked CpTi4 and Ti13Nb13Zr samples to study the influence of the galvanic coupling.

Ratio	A_{pass} (mm^2)		
	1	50	100
A_{act}/A_{pass}	3.00E-04	6.00E-06	3.00E-06
A_{pas}/A_{act}	3.33E+03	1.67E+05	3.33E+05

Several characteristics of the current and potential evolution during and after the scratch test allows one to analyse the repassivation kinetics of the system. The initial current peak, I_{peak}, is defined as the highest current value recorded when the activated area reached its maximum value. The time constant, τ, is defined as the time needed by the system to reduce the current down to 66.3 % of the initial hop. Similar procedure can be followed with potential evolution data. Figure 5.7 shows three parameters for the description of current decay, I_{peak} and τ_I, after scratching according to the passive area. Similarly, Figure 5.8 represents two parameters for the description of the potential evolution, namely E_{peak} and τ_E, after scratching on different sizes of passive area.

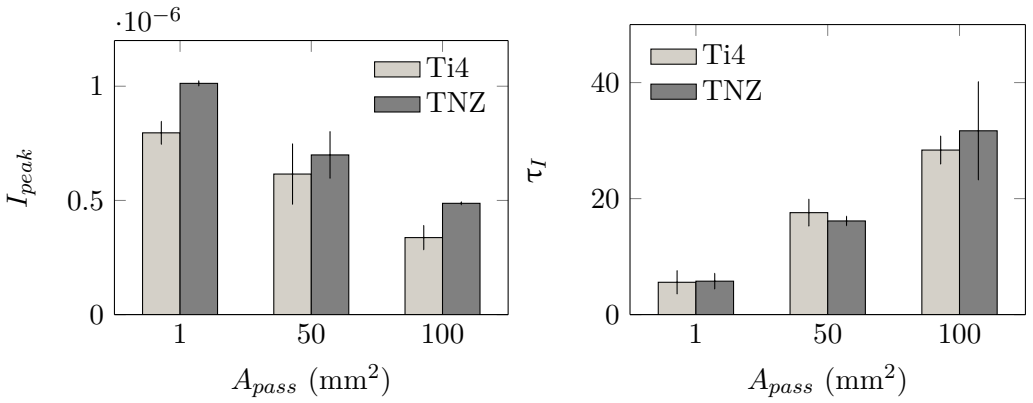

Figure 5.7: I_{peak} and τ_I, representing repassivation kinetics of CpTi4 and Ti13Nb13Zr alloy with different active to passive area immersed in artificial saliva.

Both materials showed same trend regarding the influence of the surrounding area. Figure 5.7 shows that even at the very initial stage of the repassivation process, the surrounding area played an important role, I_{peak} increased with the A_{pas}/A_{act} ratio and it showed to be higher for Ti13Nb13Zr alloy. Thus, initially, material dissolution was higher when it was surrounded by a smaller passive area. Conversely, τ_I decreased as the A_{pas}/A_{act} ratio increased, *i.e.* the repassivation kinetics were higher with a larger surrounding passive area. In this way, titanium dental implants inserted in the jaw bone form a number of micro cells, as they are osseointegrating. These small sites formed on the surface of the implant and surrounded by bone tissue may suffer localised

depassivation due to mechanical requests or because of the aggressiveness of the media. Thus, it seems that *in vivo* case is better represented with a small A_{pas}/A_{act} ratio.

In Figure 5.8, E_{peak} increased towards more cathodic values at the beginning of the repassivation as the surrounding area decreased. Potential values measured under OCP, are the result of the mixed potential between the activated titanium (cathode) and the surrounding passive area (anode). When A_{pas}/A_{act} ratio is higher the potential of the surrounding passive area gains more influence on the resulting mixed potential according to Evans diagrams, that is why E_{peak} decreases. τ_E indicated that the lower the A_{pas}/A_{act} ratio the faster the repassivation kinetics were.

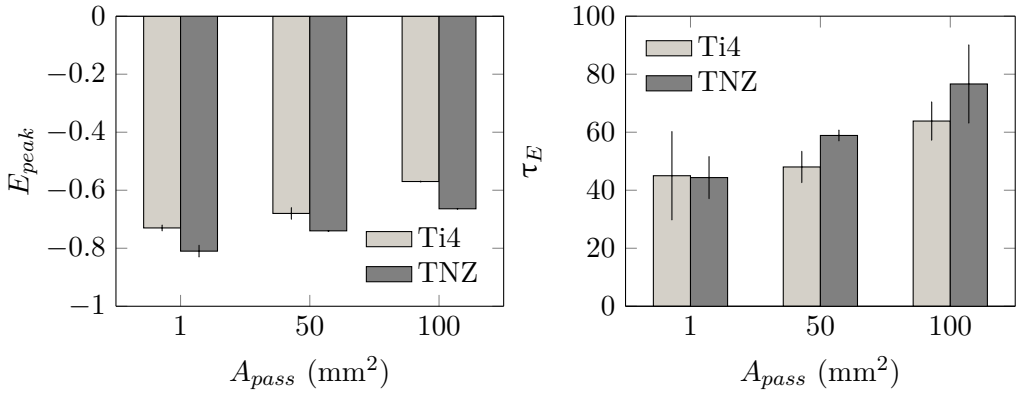

Figure 5.8: E_{peak} and τ_E, representing repassivation kinetics of CpTi4 and Ti13Nb13Zr alloy with different active to passive area immersed in artificial saliva.

Oltra *et al.* [113] studied pit initialization under free corroding conditions and they also analysed the influence of the capacitance of the passive area of an electrode on the repassivation kinetics. In the present work, a similar electric circuit has been used to explain the influence of the surrounding passive surface on repassivation first stage and kinetics of mechanically activated titanium alloys. Mechanical depassivation of a titanium surface under free corroding conditions in oxidizing environment can also be modelled as an 'input-output' system, characterized by its impulse response $h(t)$.

$$s(t) = h(t) + in(t) \tag{5.8}$$

where $s(t)$ is the output signal, $h(t)$ the impulse response, and $in(t)$ the input signal. According to the equivalent electric circuit proposed for activation under open circuit potential, Figure 5.1, the impulse response is defined by:

$$h(t) = -R_{ct}(1/\xi, exp(-t/\xi)) \tag{5.9}$$

where

$$\xi = R_{ct} \cdot C_{dl} \tag{5.10}$$

with ξ the time constant, R_{ct} the charge transfer resistance, and C_{dl} the capacitance of the double layer. Hence, ξ increases with the surface area of the passive specimen ($\mathrm{C_{dl}} = \varepsilon_0 \varepsilon_\mathrm{r} \frac{\mathrm{A}}{\mathrm{d}}$). Figure 5.9 shows the influence of the A_{pas}/A_{act} ratio on the impulse response.

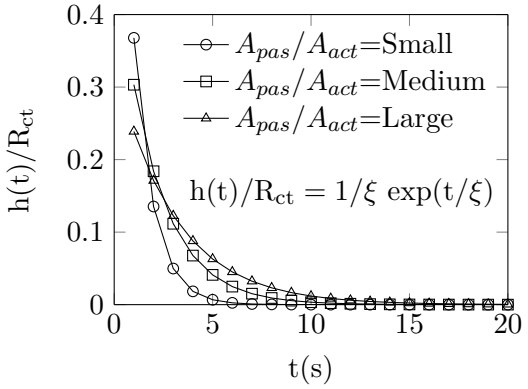

Figure 5.9: Influence of ξ on the initial $\mathrm{h(t)/R_t}$ hop after the activation of a small surface.

That E_{peak} increases when anode to cathode area is higher, could also be explained by the effect of the capacitive properties of the surrounding passive surface, which supplies the repassivation process (they are short-circuited). Consequently, for the same depassivated area, its discharge induces a more important potential drop if passive area is smaller, the capacitance being lower. Moreover, it may be of interest to note that the time constant of $\mathrm{h(t)/R_{ct}}$ increases when the surface area is bigger (increasing the value of $\mathrm{C_{dl}}$).

5.3.3 Sliding time

Sliding time is sometimes a parameter chosen without any specific criteria for the tribological characterisation of different implant systems. It can be, however, of great importance on the study of materials which wear mechanisms evolve with time. In particular, at systems where corrosion and wear simultaneously take place, such as a dental implant in oral environment, the modification of the wear mechanisms are expected to occur.

Figure 5.10 shows the wear rate dependence of CpTi4 and Ti13Nb13Zr alloy in artificial saliva on the sliding time, from 5 to 75 min. An increase of the wear rate with

the sliding time was observed, whose values were similar for both materials. After 45 min of sliding, however, the wear rate decreased for CpTi4. Meanwhile, the wear rate of Ti13Nb13Zr continued increasing with time until 60 min of sliding, when it started decreasing. Thus, wear rate differences between both materials become evident from the moment the wear rate of CpTi4 started decreasing.

The wear rate usually decreases with time. The smearing of the asperities and the enlargement of the wear scar as the time goes on, leads to a decrease of the contact pressure between the ball and the plate. However, the decrease of the wear rate does not take place well until after 45 min for CpTi4 and even later for Ti13Nb13Zr. There are a number of material degradation mechanisms when a passive material experiences tribocorrosion requests under free corroding conditions, which contribution to the total wear evolves with time. Pure mechanical wear mechanism obeys Archard's law and thus its wear rate remains constant over time. Material dissolution is also proportional to the test duration: both at the unworn area, passive dissolution, and at the wear scar during rubbing, known as corrosion accelerated by wear, as it follows Faraday's law. Thus none of these tribocorrosion mechanisms explain the increase of wear rate with time. The increase of mechanical wear due to the buildup and oxidation of wear debris on the scar is known as wear accelerated by corrosion. The oxide formation may increase the hardness of the debris leading to an increase of abrasive wear. With knowledge that both materials repassivation kinetics are similar, this fact might be related to the increase of wear due to a higher accumulation of debris in the wear track. Even its higher hardness, the poorer mechanical properties of the oxide layer of Ti13Nb13Zr may lead to its breaking and increase of abrasion.

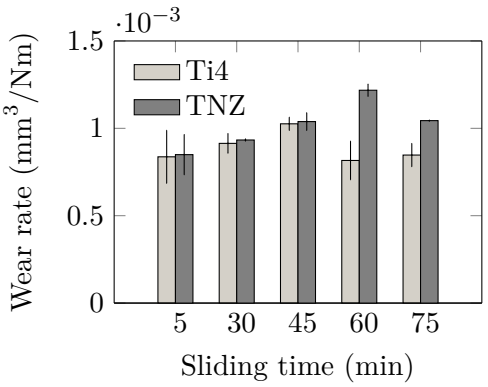

Figure 5.10: Influence of sliding time on the wear rate of CpTi4 and Ti13Nb13Zr in artificial saliva. Wear rate was measured after 5, 30 and 60 min of sliding.

5.3.4 Intermittency

Sliding intermittent tests allow one to estimate the effect of the oxide layer breaking on the wear rate. The total sliding time was 30 min for all the intermittency experiments, but two different intermittent times where studied, named 1 and 5 min sliding with a time off of 5 min, and they were compared with continuous sliding results. The time off was selected in accordance to the repassivation kinetics of both materials; Figure 5.2 shows that after 5 min, current had already achieved an asymptotic value similar to the one before the mechanical depassivation. This means that the bare metal has already reacted with the electrolyte and that the oxide layer has grown on the depassivated scar. Figure 5.11 shows the wear rate of both materials according to test intermittency. In contrast to the influence of sliding frequency (see Figure 5.4), the wear rate increased with sliding intermittency on both materials. The intermittency in the sliding corrosion test with a time-off sufficient to let the oxide layer regrowth again, an oxide layer that would be remarkably delaminated, increased the contribution of the synergy between wear and corrosion to the total wear rate.

The wear rate increase due to the intermittency was more pronounced on Ti13Nb13Zr. In this regard, Table 5.3 shows the increase of the wear rate due to the intermittency with percentage values and that the increase was softer for CpTi. These results suggest that the cohesive and adhesive properties of the oxide layer are expected to be worse on the alloy, compared to CpTi4.

Regarding the intermittency timing, a significant difference was observed between the two intermittencies tested. At the intermittency of 5 min sliding and 5 min stopped, the wear rate increased up to 25 and 8 %, for Ti13Nb13Zr and CpTi4, respectively. At the intermittency of 1 min sliding and 5 min stopped, the wear rate increased up to 14 % for Ti13Nb13Zr but the increase was negligible for CpTi4, with respect to the continuous sliding. The decrease of the wear rate when increasing the sliding cycles may be because when sliding during short times (*i.e.* 1 min) the oxide layer at the wear scar is not completely removed. In this way, intermittency tests with sliding during short times do not show to promote an additional wear in comparison to continuous sliding.

Table 5.3: The increase of the wear rate of CpTi4 and Ti13Nb13Zr in oral environment after intermittency experiments (%, compared to continuous conditions).

Material	5 min ON- 5 min OFF	1 min ON- 5 min OFF
CpTi4	8 ± 2 %	-3 ± 2 %
Ti13Nb13Zr	25 ± 2 %	14 ± 2 %

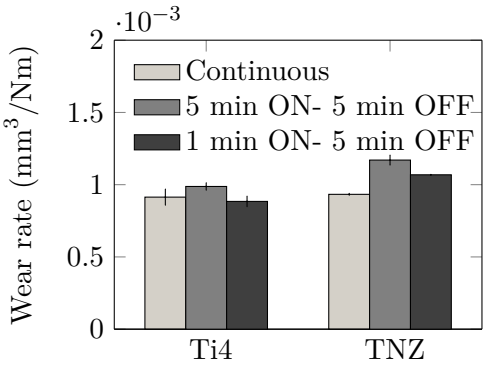

Figure 5.11: Influence of sliding intermittency on the wear rate of CpTi4 and Ti13Nb13Zr in oral environment. Total sliding time was 30 min.

5.4 Conclusions

This study was set out to determine the repassivation kinetics of Ti13Nb13Zr and CpTi4 in oral environment and clarify the main difference on their degradation mechanisms. For that, different experimental techniques have been addressed, such as scratch tests together with electrochemical noise measurements to record repassivation current under free corroding conditions. As a complement to this study, the effect of the surrounding passive area on the repassivation kinetics and the influence of tribological parameters (sliding frequency, time and intermittency) on the wear rate of both materials have also been examined.

- This study has shown that the repassivation kinetics of titanium alloy under free corroding conditions are not instantaneous, but in the order of tens of seconds. Thus, the occurrence of tribocorrosion mechanisms during sliding tests would depend on the value of the time elapsed between two successive contacts.
- The similar wear rate measured at different sliding frequencies in the range of common mastication processes (0.5 to 2 Hz), confirmed that the repassivation kinetics are too slow to have any influence of different sliding frequencies on the wear rate.
- Repassivation kinetics of Ti13Nb13Zr and CpTi4 have shown to be similar and also to be equally influenced by the extension of the surrounding passive area. Both of them showed larger I_{peak} and E_{peak} and lower τ_I and τ_E as the surrounding passive area decreased.
- The wear rate increased with the sliding time during 45-60 min, then it decreased due to the smearing of the scar. Overall, the wear rate decrease was steeper for CpTi4.

- The wear rate increased with the intermittency of sliding corrosion tests.

In general therefore, it seems that both Ti13Nb13Zr and CpTi4 alloys have similar repassivation kinetics but dissimilar tribocorrosion mechanisms. The higher wear rate showed by Ti13Nb13Zr with sliding time and intermittency, demonstrated that the mechanical properties of the oxide film naturally formed on Ti13Nb13Zr are worse compared to CpTi4. Considering the outstanding mechanical and biological compatibility of Ti13Nb13Zr alloy, the increase of the surface hardness at the step of surface treatment application would be advantageous for its performance in the oral environment.

Chapter 6

Effects of corrosion inhibitors added to the oral medium on the tribocorrosion behaviour of Ti13Nb13Zr

Previous chapters have accomplished with the first objective of this thesis dissertation, the characterisation of Ti13Nb13Zr alloy in the oral environment. This chapter and the next one propose two different ways to enhance tribocorrosion properties of Ti13Nb13Zr alloy.

With respect to this chapter, a way to reduce damage from corrosion and tribocorrosion events is studied by introducing corrosion inhibitors in oral environment. These corrosion inhibitors might be included in oral products prescribed by the dentists.

Up to date, few works have been published in the dental field and none with Ti13Nb13Zr alloy. Thus, this chapter explores an innovative protective way of dental implant materials.

The work of this chapter was carried out in KU Leuven, under the supervision of Prof. J-P Celis.

6.1 Introduction

An interesting way to control or reduce the corrosion and tribocorrosion processes taking place on titanium dental implants is by introducing corrosion inhibitors in the artificial saliva. A corrosion inhibitor is a chemical compound that is added to the environment in order to reduce the rate of metal corrosion [111] and they have been widely used for industrial applications to reduce the general corrosion of different devices

A way to reduce the rate of corrosion is by affecting the rate of partial electrochemical reactions involved (see Figure 6.1). A cathodic inhibitor lowers the cathodic partial current density and shifts the corrosion potential in the negative direction. For example, an inhibitor that, by formation of a porous film, blocks part of the surface and reduces the access of oxygen to the metal surface is a cathodic inhibitor.

On the other hand, an anodic inhibitor reduces the anodic partial current density and shifts the corrosion potential in the positive direction. For instance, an inhibitor that reduces the rate of corrosion of a metal by promoting its passivation of the metal. Buffer agents that maintain a high pH at the metal surface also favour the passive state. Other inhibitors lead to the formation of surface films by precipitation of mineral salts or weakly soluble organic complexes [111]. A mixed inhibitor reduces the rate of both partial reactions, but has a little effect on the corrosion potential. More information about the machanisms of the corrosion inhibitors can be founded in the book published by Landolt et al. [111].

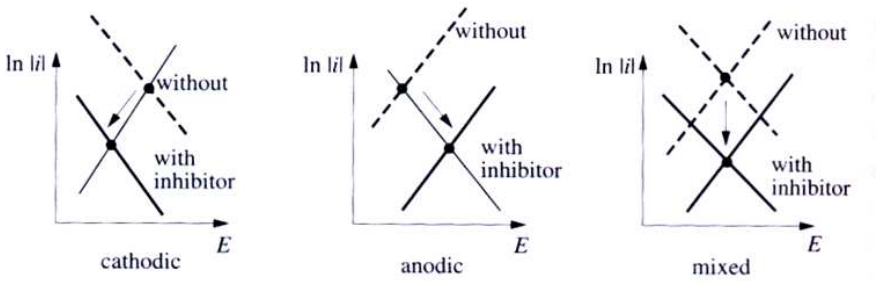

Figure 6.1: Evans diagrams showing the shift of the corrosion potential due to the presence of an anodic, cathodic or mixed inhibitor [111].

The corrosion inhibition of titanium is commonly linked with attempts to improve the passivity of the metals. Surprisingly, being the mouth an easy-access environment and the physicochemical degradation of dental implants one of the main causes of failure, very few attempt has been made to control implant corrosion through corrosion inhibitors [65, 132]. Thus the addition of corrosion inhibitors in cleaning agents could be an interesting way to reduce the damage due to corrosion in oral implants. Indeed, patient

habits have a strong influence on the corrosion behaviour of its dental implant. The curcumin ingestion for example, very common in Asian countries such as India, was recently linked to an augmentation of bacterial adhesion to implant titanium surfaces [133]. Accordingly, dentists could prescribe oral products with corrosion inhibitors to those patients with higher risks.

Table 6.1: Chemical composition of some corrosion inhibitors for titanium alloys found in literature.

Chemical compound	Concentration (mg l^{-1})	Ref.
Sodium nitrate ($NaNO_3$)	0.16	
Calcium carbonate ($CaCO_3$)	0.5	[48]
Benzotriazole ($C_6H_5N_3$)	1.5	
	0.1	
Povidone Iodine	0.2	[132]
	1	

Up to authors knowledge, the few corrosion inhibitors studied for titanium and its alloys as dental implants found in literature are listed on Table 6.1. Bhola et al. [132], studied the bactericidal agent povidone-iodine (PI) as a corrosion inhibitor towards a low modulus beta Ti45Nb implant alloy in a simulated body fluid. They found that as the concentration of PI is increased, the corrosion rate decreased, suggested by the decrease of the polarization resistance (R_p) values. This finding indicated that in addition to imparting a bactericidal effect, PI addition also could help in preventing active corrosion of the Ti45Nb implanted in the oral cavity. There is however no characterisation of Povidone Iodine effect on tribocorrosion behaviour of titanium alloys.

The influence of pH variations and the action of some corrosion inhibitors were studied by Vieira et al. [48]. Fretting-corrosion experiments in CpTi2 in contact with artificial saliva solutions were performed. Citric acid and corrosion inhibitors were added to artificial saliva to investigate their influence on the tribocorrosion behaviour of titanium. The addition of citric acid or anodic inhibitor ($NaNO_3$) to artificial saliva resulted in a slight improvement of the tribocorrosion behaviour of Ti. The addition of a cathodic ($CaCO_3$) or an organic corrosion inhibitor ($C_6H_5N_3$) to artificial saliva had a hazardous effect on the fretting-corrosion behaviour of titanium.

In summary, few are the papers published about the addition of corrosion inhibitors to enhance corrosion or tribocorrosion behaviour of titanium and its alloys, and none regarding the Ti13Nb13Zr alloy.

6.2 Objetives and hypothesis

In view of the little literature about the application of corrosion inhibitors on titanium dental implant materials and the complete absence in the case of Ti13Nb13Zr, the purpose of this chapter is to study the influence of the addition of $CaCO_3$, $NaNO_3$ and Povidone Iodine on the tribocorrosion behaviour of Ti13Nb13Zr alloy in artificial saliva.

- To analyse the influence of the addition of corrosion inhibitors to the artificial saliva on the corrosion behaviour of Ti13Nb13Zr and CpTi4.
- To analyse the influence of the addition of corrosion inhibitors to the artificial saliva on the repassivation kinetics of Ti13Nb13Zr and CpTi4.
- To analyse the influence of the addition of corrosion inhibitors to the artificial saliva on the tribocorrosion behaviour of Ti13Nb13Zr and CpTi4.

The hypothesis is that the tribocorrosion behaviour of Ti13Nb13Zr is enhanced with the addition of some of these corrosion inhibitors to the artificial saliva.

6.3 Materials and Methods

Commercially pure titanium grade 4 (CpTi4) discs, with diameter 12 x 2 mm thickness, were used as working electrode (WE). Nominal chemical composition of CpTi4 is C 0.08 wt.%, H 0.015 wt.%, N 0.05 wt.%, O 0.4 wt.%, Fe 0.5 wt.% and Ti balance. Sample preparation was done by progressively grinding Ti discs until 1200 grit and then polishing with 0.1 μm colloidal silica. Then the specimens were washed in distilled water, ultrasonically cleaned in ethanol for 5 min and dried with warm air. All the samples were stored in a drying chamber for 24 h before experiments.

The electrolyte was Fusayama-Meyer artificial saliva (0.4 g NaCl, 0.4 g KCl, 0.005 g $Na_2S \cdot H_2O$, 0.69 g $NaH_2PO_4 \cdot H_2O$, 0.795 g $CaCl_2 \cdot 2H_2O$ and 1 g Urea per 1 l of deionised water) at pH 5.0 and at room temperature.

Corrosion inhibitors were added to the artificial saliva in order to analyse its response, as shown in Figure 6.2. Maximum concentration found in literature was used to study as a go/ no go filter. The pH remained constant around pH 5.0 ± 0.2.

Table 6.2: My caption

Designation	Eletrolyte
SA	SA
SA.Ca	SA + 10 mg/l $CaCO_3$
SA.Na	SA + 1000 mg/l $NaNO_3$
SA.PI	SA + 1 ml/l Povidone Iodine

6.3.1 Corrosion tests

The electrochemical behaviour was studied using a three electrode cell: Ti samples as a working electrode, a Ag/AgCl (3 M KCl) as a reference electrode, and a platinum coil as a counter electrode. A Solartron 1287 potentiostat was used for the electrochemical test. All potentials were referred to the SCE (+244 mV/SHE). Samples were first immersed in electrolyte for 60 minutes under open circuit potential (OCP) for potential stabilisation. Then, potentiodynamic polarisation curves of Ti alloys were obtained from -250 mV/OCP to 1500 mV/SCE at a scan rate of 0.16 $mV \cdot s^{-1}$ and at room temperature. Several parameters were evaluated from the polarisation curves: the corrosion potential (E_{corr}) and the corrosion current density (i_{corr}), determined by the Tafel slope extrapolation.

6.3.2 Repassivation kinetics tests

Alumina balls (diameter 0.25 mm) were used as counterbody material due to their hardness, electric insulating, and chemical inertness properties. A 5 mm length scratch was made in the middle of the sample at a normal force of 3 N and at 1 mm/s. The bidirectional sliding/fretting test equipment used for higher accuracy is described elsewhere [128].

The electrochemical measurements were done using a three electrode cell containing a Ag/AgCl (3 M KCl) reference electrode (RE), and a Pt wire with a diameter of 0.25 mm and a length of 1 mm as a counter electrode (CE). A potentiostat (Solartron electrochemical interface model 1287) was used for the electrochemical noise measurements. The tribometer and the potentiostat were grounded and coaxial cables were used wherever possible in order to reduce noise contamination. Data acquisition of potential and current was done at a sampling rate of 8 Hz. The experimental sequence was:

- Allowing the system to stabilize at OCP during 60 min.
- Starting of the scratch test while the current and potential were measured under

free corroding conditions.

- Removing the load once current and potential had recovered their initial values.

6.3.3 Reciprocating sliding corrosion tests

Reciprocating sliding corrosion experiments were carried out coupling the electrochemical cell to the home-made tribometer [128] with a ball-on-plate reciprocating sliding configuration. The reference electrode was placed no more than 10 mm away from the wear track. A 5 mm diameter alumina ball was used as a counter part. A normal force of 3 N was applied. Sliding tests were carried out at open circuit potential and electrochemical noise technique was used. The experimental sequence was:

- Allowing the system to stabilize at OCP during 60 min.
- Starting of the sliding test while the OCP and current fluctuation was measured.
- Removing the load once sliding finished and continuing recording OCP and current fluctuation.

6.4 Results and discussion

6.4.1 Corrosion behaviour

Polarisation curves of CpTi4 and Ti13Nb13Zr immersed in artificial saliva with different corrosion inhibitors are shown in Figure 6.2. All the curves show a passive behaviour, with an increase of the anodic current from the corrosion potential until it achieves the passive plateau, that is, the potential range at which the current remains constant.

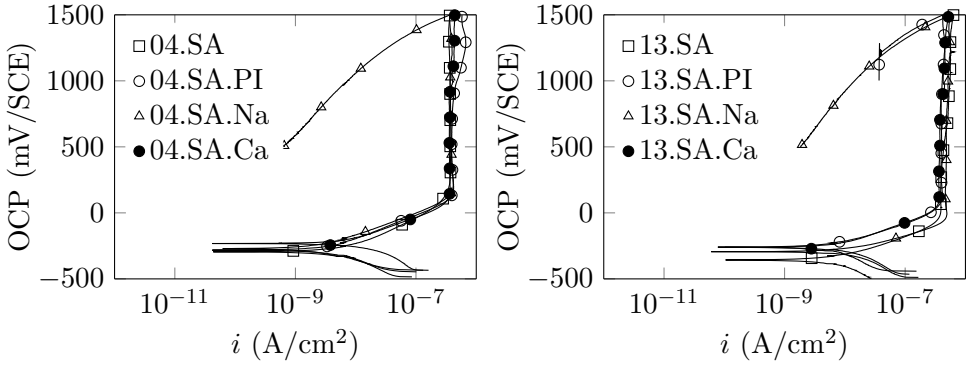

Figure 6.2: Polarisation curves of CpTi4 and Ti13Nb13Zr in artificial saliva with the addition of the corrosion inhibitors.

Table 6.3: Electrochemical parameters obtained from polarisation curves of CpTi4 and Ti13Nb13Zr in artificial saliva with the addition of the corrosion inhibitors.

Material	Electrolyte	OCP (mV)	E_{corr} (mV)	i_{corr} ($\mu A/cm^2$)	i_p ($\mu A/cm^2$)
CpTi4	SA	-345 ± 5	-339 ± 31	0.0078 ± 0.0034	0.39 ± 0.01
	SA.Ca	-236 ± 23	-232 ± 51	0.0112 ± 0.0005	0.36 ± 0.01
	SA.Na	-271 ± 12	-267 ± 6	0.0019 ± 0.0011	0.38 ± 0.02
	SA.PI	-308 ± 31	-311 ± 42	0.0029 ± 0.0013	0.39 ± 0.01
Ti13Nb13Zr	SA	-367 ± 24	-361 ± 5	0.0082 ± 0.0031	0.38 ± 0.03
	SA.Ca	-334 ± 53	-339 ± 51	0.0086 ± 0.0038	0.37 ± 0.06
	SA.Na	-363 ± 58	-360 ± 55	0.0084 ± 0.0026	0.44 ± 0.03
	SA.PI	-302 ± 46	-298 ± 53	0.0089 ± 0.0006	0.39 ± 0.01

Table 6.1 summarises the average OCP values measured during the initial stabilisation and the main corrosion parameters calculated from polarisation curves, i.e. E_{corr}, i_{corr} and i_p.

The average OCP values during the initial stabilization, and the main corrosion parameters, *i.e.* E_{corr}, i_{corr} and i_p. OCP and E_{corr} had similar values and trends, so Figure 6.3 (a) can serve as a reference for both parameters. The addition of the corrosion inhibitors seems not to modify the thermodynamic preference to anodic dissolution of CpTi4 and Ti13Nb13Zr.

The corrosion current density, i_{corr}, obtained with Tafel extrapolation from the anodic and cathodic brunch near the E_{corr}, is shown in Figure 6.3 (b). Interestingly, the i_{corr} of CpTi4 is drastically reduced in presence of the $NaNO_3$ and Povidone Iodine corrosion inhibitors in the artificial saliva. The addition of $CaCO_3$ to the artificial saliva, however, results in a slightly increase of the i_{corr}. Conversely, Ti13Nb13Zr shows to be no influenced by the corrosion inhibitors on the i_{corr}.

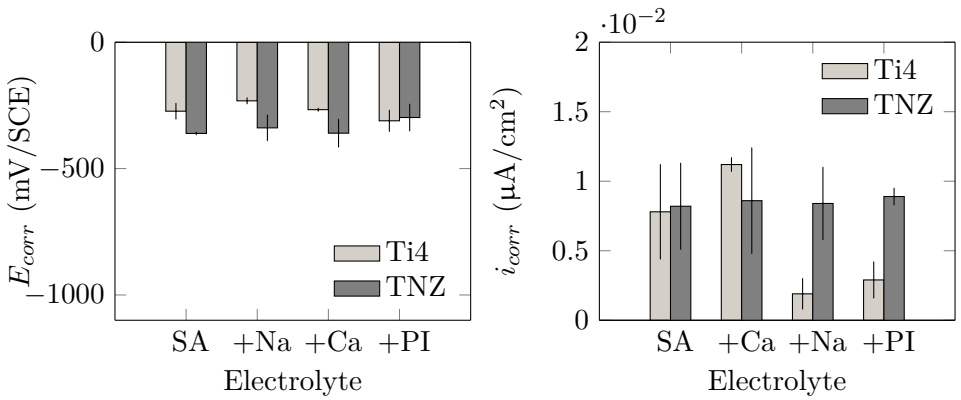

Figure 6.3: E_{corr} and i_{corr} values of CpTi4 and Ti13Nb13Zr in artificial saliva with the addition of the corrosion inhibitors.

6.4.2 Repassivation kinetics

I_{peak} and τ_I are the variables that define the anodic current evolution after a scratch made on the titanium surface (for more information, see chapter 5). Figure 6.4 represent I_{peak} and τ_I, respectively. τ_I shows to be influenced by the addition of corrosion inhibitors. τ_I considerably decreases on both materials with the addition of $CaCO_3$ or $NaNO_3$, being in the case of Ti13Nb13Zr reduced to a greater scale. But the addition of Povidone Iodine increased τ_I for CpTi4. This reveals the capacity of $CaCO_3$ and $NaNO_3$ to reduce the time necessary on both materials to reform the protective layer after the scratch test.

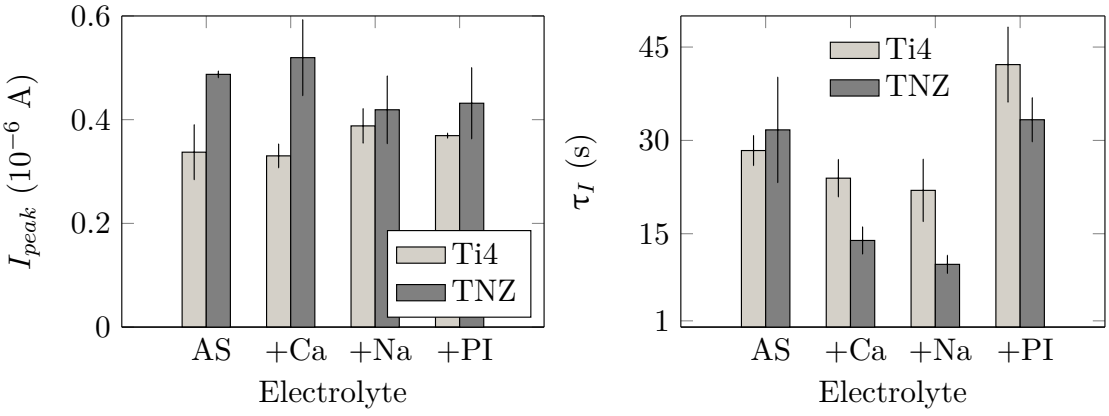

Figure 6.4: I_{peak} and τ_I, representing repassivation kinetics of CpTi4 and Ti13Nb13Zr alloy with different corrosion inhibitors added into the artificial saliva.

E_{peak} and τ_E are shown in Figure 6.5 and they display similar tendencies compared to current parameters. τ_E also shows a reduction of its value with the addition of $CaCO_3$

or $NaNO_3$ although it is only significant on Ti13Nb13Zr.

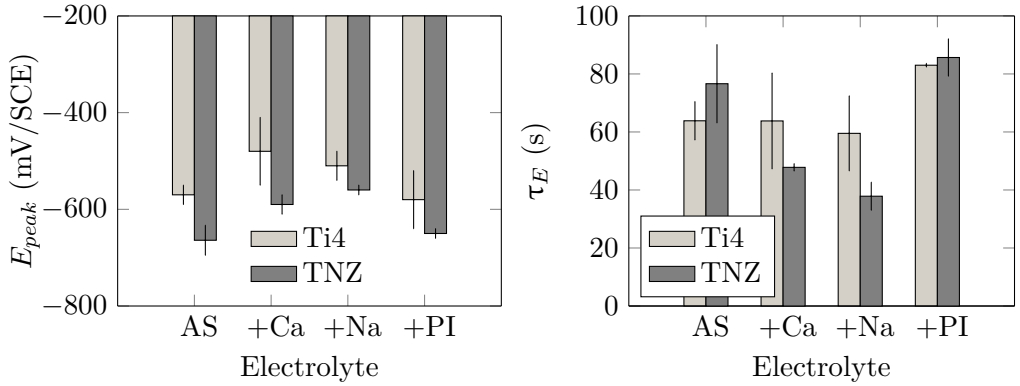

Figure 6.5: E_{peak} and τ_E, representing repassivation kinetics of CpTi4 and Ti13Nb13Zr alloy with different corrosion inhibitors added into the artificial saliva.

These results demonstrate that the repassivation kinetics of both materials, but especially of Ti13Nb13Zr, can be significantly reduced by means of the time that the material needs to regrow a protective layer on the scratched area (in the case of Ti13Nb13Zr, up to less than a half)

6.4.3 Reciprocating sliding corrosion tests

Reciprocating sliding corrosion tests were made with electrochemical noise technique under open circuit conditions, so both corrosion current and potential fluctuations were recorded. Figure 6.6 shows the potential and current evolution of Ti13Nb13Zr in artificial saliva before, during and after the rubbing test.

The average current during rubbing, $i_{rubbing}$, is shown in Figure 6.7. $NaNO_3$ is the only inhibitor that shows a slight reduction of the average current on CpTi4. The average current, of Ti13Nb13Zr remains constant or even increase with the addition of corrosion inhibitors. Accordingly, the corresponding dissolved volume rate (mm^3/Nm), V_{diss}, shown in Figure 6.8 calculated through Faraday in the same way than in chapter 4, shows similar trends. Understandably, the dissolved volume rate is proportional to the measured average current during rubbing, so the shape of the graphical bar is similar.

The average current density during the rubbing test is higher than the I_{peak} measured in the scratch test. This is because the activated area on the rubbing test is much higher than in the scratch test, thus the measured absolute current increase.

The wear rate corresponding to the reciprocating sliding test under OCP conditions is shown in Figure 6.9. The addition of corrosion inhibitors to the artificial saliva resulted detrimental for Ti13Nb13Zr, as the wear rate sharply increased, even doubling its value

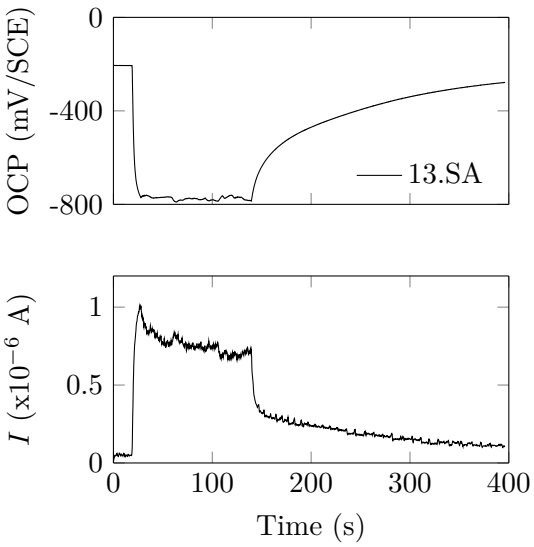

Figure 6.6: Potential and current evolution of Ti13Nb13Zr immersed in artificial saliva before, during and after the rubbing test.

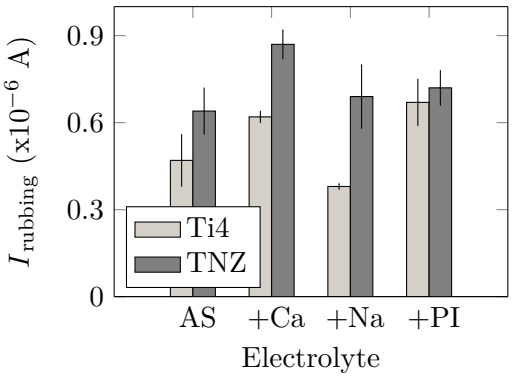

Figure 6.7: Average current measured during rubbing tests of CpTi4 and Ti13Nb13Zr alloy immersed in artificial saliva with different corrosion inhibitors.

comparing to the results obtained with artificial saliva. CpTi4 showed however a notable wear rate reduction with the addition of $CaCO_3$ and Povidone Iodine. The addition of $NaNO_3$, also increased the wear rate of CpTi4.

The wear rate measured by profilometry, has no similarities regarding tendencies with the dissolved volume rate calculated by Faraday. This is not unusual, since the later possess values three orders of magnitude lesser compared to the former (10^{-5} to 10^{-3}). This fact also reveals that most of the volume loss after a tribocorrosion event is not due to ion release but because of particle debris generation.

These results reveal that repassivation kinetics and sliding corrosion events are very

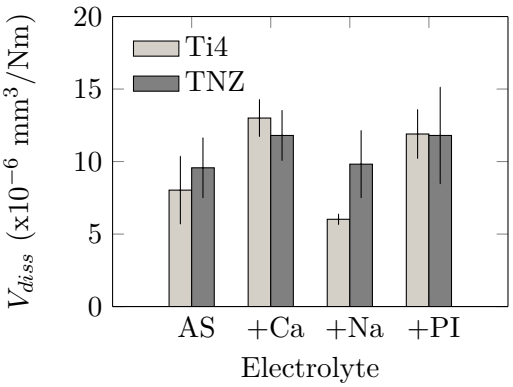

Figure 6.8: Dissolved material rate during rubbing tests, calculated through Faraday, of CpTi4 and Ti13Nb13Zr alloy immersed in artificial saliva with different corrosion inhibitors.

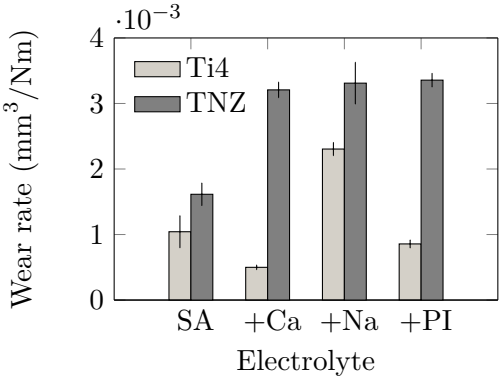

Figure 6.9: Wear rate measured by profilometry on wear scars made on CpTi4 and Ti13Nb13Zr alloy immersed in artificial saliva with different corrosion inhibitors.

different on each material. Whereas the repassivation time was considerably reduced on Ti13Nb13Zr alloy by the addition of corrosion inhibitors, its wear resistance showed to be diminished. And the other way around for CpTi4.

It is at this point that one realizes that the addition of these corrosion inhibitors does not enhance the tribocorrosion resistance of Ti13Nb13Zr, but it weakens. Although the addition of $CaCO_3$ to the artificial saliva decreased the wear rate of CpTi4, the objective of this chapter was to enhance the tribocorrosion behaviour of Ti13Nb13Zr. Thus, the research about the introduction of corrosion inhibitors to enhance the tribocorrosion behaviour concludes here.

6.5 Conclusions

In this Chapter the influence of the addition of corrosion inhibitors on the tribocorrosion response of Ti13Nb13Zr was analysed in comparison to the widely used CpTi4. The main conclusions obtained after the analysis and discussion of the results are listed hereafter:

- Both materials behave similarly from a corrosion viewpoint, although a reduction of the corrosion current density was only observed on CpTi4 in presence of $NaNO_3$ and Povidone Iodine.
- A reduction of the repassivation time was found on CpTi4 and Ti13Nb13Zr with the addition of $NaNO_3$ and $CaCO_3$. Importantly, this reduction was considerably higher on Ti13Nb13Zr.
- After a reciprocating sliding corrosion test, the dissolved wear volume only showed an ion release reduction in the case of CpTi4 with $NaNO_3$. The wear rate showed a reduction of almost 50 % on CpTi4 with the addition of $CaCO_3$. Contrarily, Ti13Nb13Zr showed an increase of the wear rate with all the corrosion inhibitors.
- Comparing the magnitude of the dissolved volume during the rubbing test with the profilometry measurements, it was clear that the wear debris generation had much greater importance (in comparison to ion release) on the tribocorrosion behaviour of titanium alloys.

To sum up, the corrosion inhibitors tested on this work, *i.e.* $CaCO_3$, $NaNO_3$ and Povidone Iodine rejected the main hypothesis of this chapter as they did not show an enhance of the tribocorrosion behaviour of Ti13Nb13Zr. Corrosion inhibitors only showed an increase of the tribocorrosion response on CpTi4.

Chapter 7

Improvement of the tribocorrosion resistance by thermal oxidation of Ti13Nb13Zr alloy

Despite the better mechanical and biological compatibility of Ti13Nb13Zr, compared to the widely used α and $\alpha - \beta$ titanium alloys, previous chapters have shown its slightly lower tribocorrosion resistance in oral environment when compared to CpTi4. Indeed, the addition of corrosion inhibitors to the artificial saliva has only showed to improve the tribocorrosion resistance of CpTi4.

In the light of the potential of this near-β titanium alloy, this chapter aims to improve its tribocorrosion behaviour by applying a suitable surface modification in view of the results above. Thermal oxidation is a cost effective surface modification technique that generates a protective thick oxide layer increasing surface hardness, which improves the wear resistance. Owing to the fact that the increased corrosion accelerated by wear is the main degradation mechanism of Ti13Nb13Zr alloy, the increase of the surface hardness can be an interesting strategy.

Very few research works have been carried out on the electrochemical characterisation of thermally oxidised Ti13Nb13Zr alloy, however, none regarding tribocorrosion behaviour. In this chapter, thus, an optimisation of temperature and duration of the thermal oxidation treatment of Ti13Nb13Zr was performed, from the tribocorrosion point of view.

7.1 Introduction

Wear debris and metal ions released from the metallic implant due to mastication events may cause adverse tissue reactions and can even result in the loosening and eventual failure of the implant [134]. These problems can be overcome modifying the metallic surface to improve wear resistance characteristics of dental materials. These techniques include physical vapor deposition [135, 136], chemical vapor deposition [137, 138], plasma spray coating [139, 140], nitriding [141, 142], anodisation [143, 144], ion implantation [145, 146] and thermal oxidation [147, 148, 149].

Thermal oxidation of titanium and its alloys is a cost effective surface treatment which improves hardness and wear resistance in addition to corrosion resistance, which results in an attractive choice for implant application. Indeed, this thermal treatment has already been investigated on titanium alloys for implant applications [96, 149, 150, 151]. Oxidation of titanium, particularly at a temperature above 200 °C, promotes the development of a crystalline oxide film on the surface.

Titanium dioxide exists in two main polymorphs, as a stable rutile and metastable anatase. These polymorphs exhibit different properties. Anatase transforms irreversibly to rutile at elevated temperatures, but the transformation temperature is not unique. The achievement of rutile oxide layer results interesting because it is inert to bacterial attack, has a higher hardness, is chemically inert and the wear resistance is improved in comparison to other oxide structures such as brookite and anatase [152]. Rutile and anatase have a tetragonal crystal system; this allows anatase to be transformed to rutile at high temperatures [153]. Rutile crystal formation is related to a high temperature treatment and its duration also increases the hardness and depth of the oxide layer. The cooling rate is also important, a slow cooling (such as furnace cooling) prevents from a reduction of adhesive strength between the oxide and the substrate [149]. As for the biocompatibility issue, osteoblast adhesion studies indicated that thermal oxidation treatments on Ti6Al4V did slightly affect the material biocompatibility. Moreover, the thermal oxidation at 700 °C enhanced the in vitro osteoblastic cell attachment compared to the thermal oxidation at 500 °C [151].

Thermal oxidation studies on Ti13Nb13Zr alloy have shown however the alloy to be more prone to have cracks and fissures on the thermally oxidised layer [147, 154, 155]. On the one hand, this is related to the higher oxidation rate of Ti13Nb13Zr compared to Ti6Al7V, which promotes a thicker but less homogeneous oxide layer [154]. On the other hand, the near-β Ti13Nb13Zr possesses a lower phase transformation temperature (735 °C) in comparison to other α and $\alpha - \beta$ titanium alloys [156]. Hence, thermal oxidation at similar or higher temperatures may produce a mismatch in the coefficient of thermal expansion (CTE) [155], causing spallation between oxide and substrate. Izman

et al. [155] analysed a range of temperatures for the same thermal treatment duration. 550 °C was the only temperature at which no cracks were observed on the upper surface.

The evolution in depth of the alloying elements concentration of thermally oxidised Ti13Nb13Zr was studied by Gutierrez *et al.* [147] using RBS, revealing that the low initial Nb content on the surface slowly increased with depth until bulk values were reached. Contrarily, Zr concentration in the outermost surface was zero, but just below a small peak was observed suggesting the Zr segregation at an intermediate layer (see Figure 7.1).

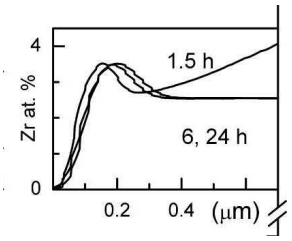

Figure 7.1: Zr concentration depth profile obtained from RBS for the thermally oxidized Ti13Nb13Zr alloy at 750 °C for different times 1.5, 6 and 24 h [147].

Nb and Zr have similar atomic number and concentration in the alloy. Thus, the higher Nb concentration detected on the surface, comparing to Zr, is in fact in agreement with the thermodynamic expectation of preferential Nb oxidation against Zr, as it can be seen in the Ellingham diagram [97]. Furthermore, Nb as a substitutional cation in the rutile lattice seems to reduce the diffusion rate of oxygen ion vacancies, thus improving oxidation resistance [147].

The formation of mechanically stable and chemically resistant oxide layers affects corrosion and wear behaviour of titanium and its alloys [154, 151]. Güleryüz *et al.* [148], thermally oxidized the Ti6Al4V alloy at 600 and 650 °C to produce corrosion and wear resistant surface layers. Corrosion wear experiments in 0.9% NaCl solution showed an increase of the wear resistance by a factor of 25.

Shi *et al.* [157], also noted that the wear resistance of UHMWPE against Ti6Al4V alloy under water lubricant condition significantly increased with thermal oxidation treatment of the alloy in addition to the ion implantation of the polymer.

7.2 Objetives and hypothesis

In this chapter, Ti13Nb13Zr was thermically oxidised at a range of temperatures to study its electrochemical behaviour in artificial saliva and a suitable temperature was chosen based on the oxide layer integrity. Then the influence of treatment duration

at that temperature was thoroughly studied by carrying out electrochemical and triboelectrochemical characterisation in a wider range of artificial saliva. Below are the specific objectives of this chapter:

- To obtain a suitable temperature at which thermally oxidised Ti13Nb13Zr has a compact and thicker oxide layer.
- To analyse corrosion and tribocorrosion properties of thermally oxidised Ti13Nb13Zr alloy at a suitable temperature in a range of treatment durations.

The hypothesis is that the material loss under tribocorrosion request is increased with the application of the thermal oxidation treatment.

7.3 Materials and Methods

7.3.1 Materials

Sample preparation was done by progressively grinding Ti13Nb13Zr discs with emery papers until 1200 grit, followed by fine polishing with 0.1 μm size colloidal silica, which provided a surface free of mechanical deformation. Then the specimens were washed in distilled water, ultrasonically cleaned in ethanol for 5 min and dried with warm air. All the samples were stored in a drying chamber for 24 h before the surface treatment. Thermal oxidation of Ti13Nb13Zr samples were done at different temperatures for 6 h, *i.e.* 400, 500, 600 and 700 °C, to analyse the influence of treatment temperature on the oxide layer properties. Then, an optimal temperature was chosen and the effect of treatment duration, *i.e.* 6h, 9h and 12h, and the electrochemical and tribocorrosion behaviour in oral environment was studied. The thermal oxidation was made in air in a furnace as follows:

- The heat rate was 10 °C/min until the required temperature was reached.
- The temperature was maintained during the scheduled time.
- The cooling was made in the furnace, known as furnace-cooling.

Surface morphology was analysed with optical microscopy. The cross section of the oxidised samples was studied by SEM (JEOL JSM 5600 LV) and the nature of the oxide film formed on thermally oxidised Ti13Nb13Zr was determined using X-ray diffraction (XRD) measurements (Bruker AXS D8) with Cu-k_α radiation.

7.3.2 Electrochemical and reciprocating sliding corrosion tests

Fusayama Meyer artificial saliva was used as base electrolyte. In order to analyse de electrochemical response of thermally oxidised Ti13Nb13Zr, different solutions were tested, *i.e.* artificial saliva with pH 5.0, with pH 3.5 and 100 ppm F^- and with pH 3.5 and 1000 ppm F^-.

The electrochemical behaviour was studied using a three electrode cell: Ti samples as a working electrode, a Saturated Calomel Electrode (SCE) as a reference electrode, and a platinum coil as a counter electrode. A Voltalab 40 potentiostat was used for the electrochemical test. All potentials were referred to the SCE (+244 mV/SHE). Samples were first immersed in electrolyte for 60 minutes under open circuit potential (OCP) for potential stabilisation. Then, EIS study was conducted by applying a sinusoidal signal of 10 mV of amplitude at the corresponding OCP value. The frequency range was from 100 kHz to 10 mHz and a recording of 20 points per decade was made. The experimental data was analysed using ZVIEW software. The quality of the fitting was ensured when $\chi^2 \leqslant 10^{-3}$. χ^2 is the square of the standard deviation between the experimental data and the calculated spectrum. Finally, potentiodynamic polarisation curves of Ti alloys were obtained from -250 mV/OCP to 1500 mV/SCE at a scan rate of 0.16 $mV \cdot s^{-1}$ and at room temperature. Several parameters were evaluated from the polarisation curves: the corrosion potential (E_{corr}) and the corrosion current density (i_{corr}), determined by the Tafel slope extrapolation.

Reciprocating sliding corrosion experiments were carried out at room temperature coupling the electrochemical cell to a tribometer (Microtest) with a ball-on-plate reciprocating sliding configuration. The reference electrode was placed no more than 10 mm away from the wear track. A 6 mm diameter alumina ball was used as a counter part. A normal force of 1 N was applied, a sliding speed of 1 Hz and a stroke of 2 mm was imposed. Sliding tests were carried out at open circuit potential . The experimental sequence was:

- Allowing the system to stabilize at OCP during 60 min.
- Starting of the sliding for 120 min while the OCP was measured.
- Removing the load once sliding had finished.

Test duration was set at 120 min due to the high wear resistance of the thermally oxidised Ti13Nb13Zr. Shorter sliding times caused problems with the profilometric measurement of the wear scar.

At the end of the wear tests Ti samples were ultrasonically cleaned with ethanol and dried with warm air. Wear scars and cross section of thermally oxidised samples

were examined using a JEOL JSM 5600 LV scanning electron microscope (SEM). The volumetric wear was measured by confocal laser profilometry, Sensofar PLu 2300, and calculated by averaging the cross sectional area determined at three locations along the track, multiplied by the wear track length.

All electrochemical and tribocorrosion tests were repeated at least three times to confirm reproducibility of the measurements. Legends comply with following designation: *TEMPERATURE.pH.[F^-]* (400, 500, 600 and 700 for temperature; 35 for pH 3.5 and 50 for pH 5.0 and 0, 100 or 1000 for fluoride concentration, respectively. For example, '400.35.100' refers to thermally oxidised Ti13Nb13Zr at 400 °C immersed in artificial saliva with pH 3.5 and 100 ppm F^-.

7.4 Results and Discussion

7.4.1 Influence of temperature on thermally oxidised Ti13Nb13Zr

The temperature is a key parameter in the thermal oxidation of metals. It is responsible of the formation for a compact, adherent and corrosion resistant oxide layer. Thus a range of temperatures from 400 to 700 °C were tested in order to chose the optimal temperature to carry out tribocorrosion characterisation of thermally oxidated (TO onwards) Ti13Nb13Zr with a range of treatment duration.

Oxide layer morphology. Different images of the oxide layer growth on Ti13Nb13Zr at different temperatures are collected in Figure 7.2. First column belongs to the top view of the oxide layer, recorded with the optical microscope. The acicular structure is common in all the temperature range, which corresponds to the martensitic microstructure with α-lamellae. These microstructures are rather similar to that of the same alloy without thermal treatment, which where showed in Figure 3.1. Colours, however, changed from lighter to darker. Gold, light blue, golden gray and bluish gray are the colours observed by optical microscope of TO Ti13Nb13Zr alloy at 400, 500, 600 and 700 °C, respectively.

SEM images of the cross section of oxidised samples are seen on the second and third column of Figure 7.2. It is clear that the adhesive properties of the oxide layer prevail until TO temperature of 500 °C. From there on, spallation and fissures separate the oxide layer from the alloy. This might be related to the closeness of the oxidation temperature to the phase transformation temperature (735 °C) and to the increase of rutile ratio with treatment temperature [155]. The large mismatch of coefficient of thermal expansion between oxide layers and substrate could also be responsible for this

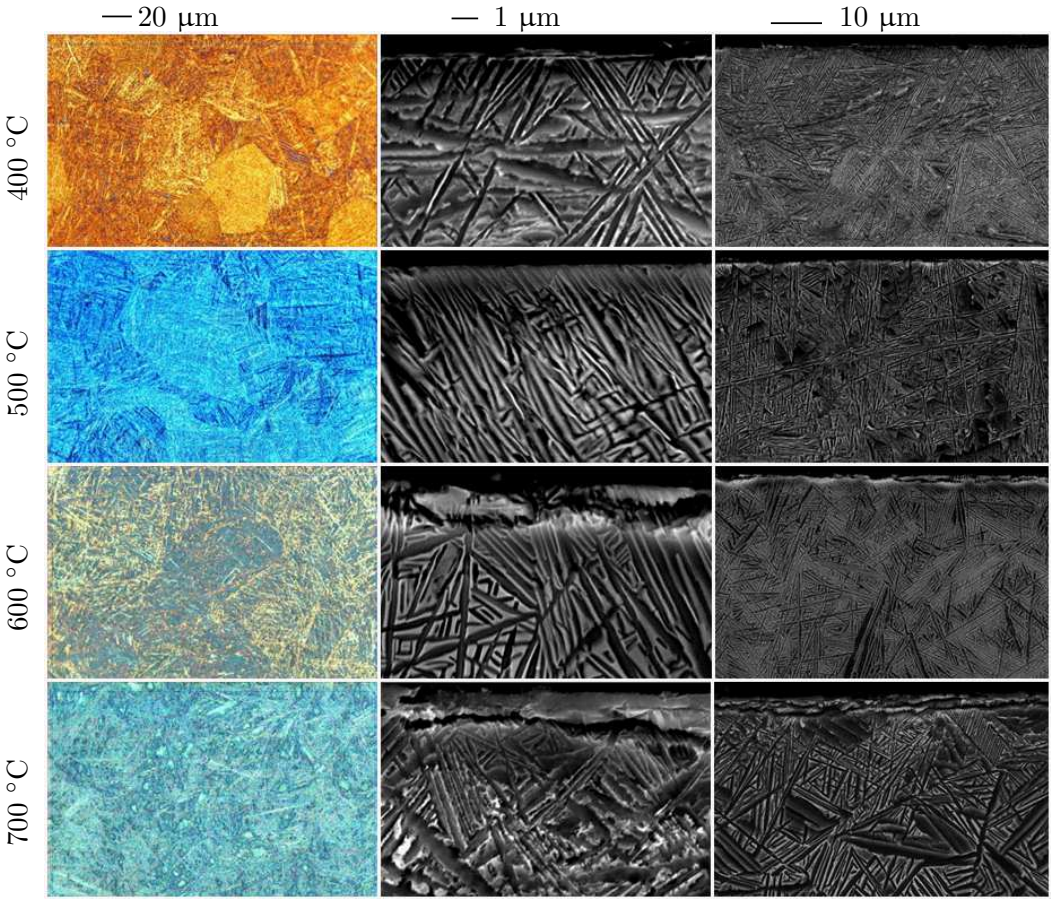

Figure 7.2: Top view (optical microscopy) and cross section (SEM) of the thermally formed oxide layer at different temperatures.

phenomenon. Lopez *et al.* [154] obtained an oxide layer with a thickness around 3 µm on Ti13Nb13Zr after a thermal oxidation treatment at 750 °C for 6 h, but the cross sectional views revealed longitudinal fissures with many pores, similar to those found at 700 °C in this work. Unlike the findings in this work, the formation of surface cracks and spallations has previously been related to the worsening of the corrosion resistance [149, 158].

Corrosion behaviour. The electrochemical stability of the TO Ti13Nb13Zr was determined by potentiodynamic polarisation curves in two different solutions, AS.50.0 and AS.35.100. Both electrolytes showed similar trends so, polarisation curves of TO Ti13Nb13Zr alloy at different temperatures in artificial saliva with pH 5.0 without fluorides are shown in Figure 7.3. The anodic brunch is not vertical, but the current density slowly increased with increasing polarisation. This reveals the pseudo-passive behaviour of TO Ti13Nb13Zr. The current values at the pseudo-passive section follows

this order, from low to high, 400>700>600>500 °C.

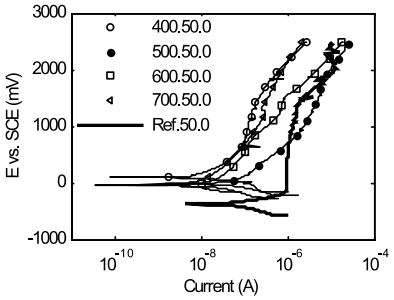

Figure 7.3: Polarisation curves of TO Ti13Nb13Zr samples at different temperatures in artificial saliva with pH 5.0 and 0 ppm F^-.

Table 7.1 summarises the average OCP values measured during the initial stabilisation and the main corrosion parameters calculated from polarisation curves, *i.e.* E_{corr} and i_{corr}.

Table 7.1: Electrochemical parameters of Ti13Nb13Zr in artificial saliva solutions. Influence of the temperature of the thermal oxidation treatment.

Temp. (°C)	Electrolyte	OCP** (mV)	E_{corr} (mV)	i_{corr} (μA/cm^2)
Ref.*	AS.50.0	-245 ± 200	-245 ± 185	0.170 ± 0.150
	AS.35.100	-460 ± 50	-440 ± 15	0.090 ± 0.090
400	AS.50.0	58.2 ± 14.6	81 ± 24	0.006 ± 0.000
	AS.35.100	-56.5 ± 0.7	-50.3 ± 31.2	0.013 ± 0.005
500	AS.50.0	-1.2 ± 18.6	-15.7 ± 32.3	0.046 ± 0.009
	AS.35.100	-30.3 ± 6.8	-42.9 ± 15.1	0.060 ± 0.008
600	AS.50.0	-38.7 ± 18.5	-50.5 ± 12.6	0.012 ± 0.005
	AS.35.100	-36.5 ± 9.2	-38.4 ± 16.1	0.004 ± 0.002
700	AS.50.0	7.7 ± 25.4	-47.2 ± 23.6	0.004 ± 0.003
	AS.35.100	12.0 ± 25.5	-13.2 ± 60.3	0.001 ± 0.001

* Ref. is related to untreated Ti13Nb13Zr.

** OCP values correspond to the average value of the last two-thirds of 60 min of measurements under open circuit potential just after immersion.

OCP and E_{corr} of TO Ti13Nb13Zr alloy have similar values so Figure 7.4 can serve as a reference for both parameters. Generally, thermal oxidation of Ti13Nb13Zr alloy involves an increase of the E_{corr} towards nobler values, regardless of the aggressiveness of the electrolyte. Indeed, no influence of the thermal oxidation temperature can be seen on the E_{corr}, except for Ti13Nb13Zr oxidised at 400 °C inmersed in AS.50.0, where it showed higher E_{corr} values.

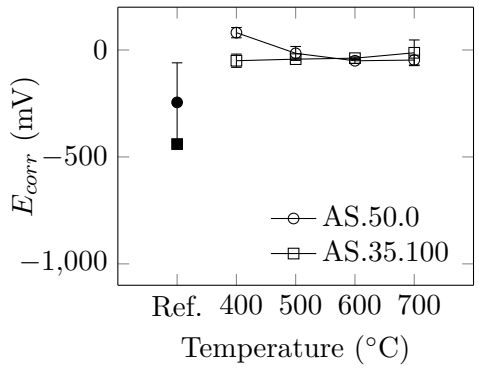

Figure 7.4: Corrosion potential of Ti13Nb13Zr in artificial saliva solutions. Influence of the temperature and electrolyte of the thermal oxidation treatment (Ref. is the E_{corr} of untreated Ti13Nb13Zr).

Figure 7.5 shows the i_{corr} values and an abrupt decrease of the TO Ti13Nb13Zr samples is seen in comparison to the non-treated ones, indicating a lower ion dissolution on the thermally oxidized samples comparing to the untreated Ti13Nb13Zr alloy. The thermally oxidised samples at 500 °C, however, showed higher i_{corr} values than at other temperatures. Indeed, TO sample at 500 °C exceeds the passive plateau of the untreated Ti13Nb13Zr with current density values up to 10 times higher.

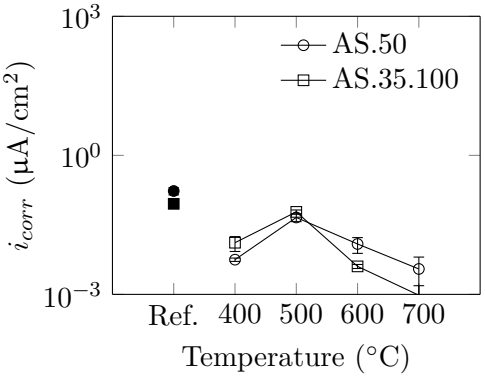

Figure 7.5: Corrosion current density of Ti13Nb13Zr in artificial saliva solutions. Influence of the temperature of the thermal oxidation treatment (Ref. is the i_{corr} of untreated Ti13Nb13Zr).

Electrochemical parameters of Ti13Nb13Zr thermally oxidised at 700 °C are rather similar to those obtained by Lopez *et al.* [154] with Ti13Nb13Zr oxidised at 750 °C immersed in Hank's solution. Overall, these results suggest that for the tested temperatures the oxidation process gives rise to the formation of an oxide layer that improves the protection against corrosion in artificial saliva.

Impedance measurements were performed on the TO Ti13Nb13Zr samples after 1 h

of immersion in artificial saliva. EIS technique was used for thermally grown oxides because it is commonly used for electrochemical characterisation of coatings since it is very sensitive to defects. The corresponding Bode diagrams are shown in Figure 7.6. The impedance spectrum of untreated and TO Ti13Nb13Zr alloy up to 500 °C is characterised by a single peak in the impedance phase angle plot, known as Randles circuit, suggesting the involvement of a single time constant. This equivalent electrical circuit is shown in Figure 7.14 (a) and it has already been used for both untreated and TO Ti alloys [149, 159]. The response can thus be modelled with an electrolyte resistance, R_Ω, in series with the parallel combination of the charge transfer resistance, R_{ct} and the double layer capacitance of the protective film, C_{dl}. However, a constant phase element, CPE, is often used replacing the C_{dl}. It represents the non-ideal conditions of the interface, such as, surface roughness, inhomogeneous reaction rates on the surface, varying thickness and composition of the coatings and non-uniform current distribution [160]. The impedance of the CPE, Z_{CPE}, is expressed using

$$Z_{CPE} = \frac{1}{Q(j\omega)^n} \tag{7.1}$$

where Q is the magnitude and n is the exponent.

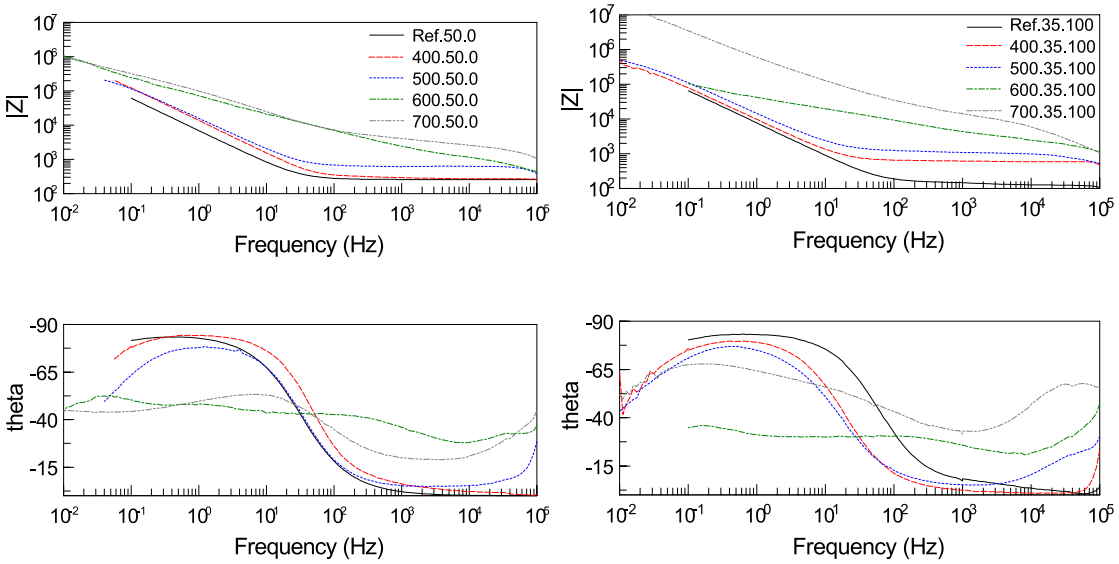

Figure 7.6: Bode impedance and phase angle plots of thermally oxidized Ti13Nb13Zr at different temperatures and in two artificial saliva solution.

The EIS spectrum of TO samples above 600 °C is characterised by two time constants. In this equivalent electrical circuit, shown in Figure 7.14 (b), R_Ω is the ohmic resistance, R_{oxide} and R_{ct} are the resistance of the oxide layer and charge transfer resistance,

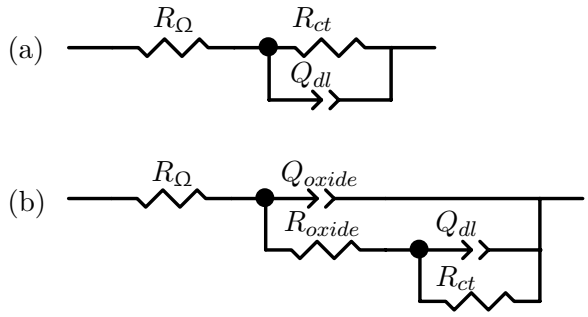

Figure 7.7: Equivalent electrical circuit of thermally oxidised Ti13Nb13Zr alloy inmmersed in artificial saliva. (a) circuit corresponds to thermally oxidised sampled at 400 and 500 °C, whereas (b) corresponds to 600 and 700 °C.

respectively; and Q_{oxide} and Q_{dl} are the capacitance of the oxide layer and double layer capacitance, respectively. James *et al.* and Zhang *et al.* had already used this two time constants equivalent circuit on TO titanium alloys [149, 159].

The EIS parameters, determined after fitting the experimental data with the proposed equivalent electrical circuits are listed in Table 7.4. Chi-square values about 10^{-3} support the good agreement between the experimental and the fitted data.

Table 7.2: Electrochemical parameters of Ti13Nb13Zr in artificial saliva solutions. Influence of the temperature of the thermal oxidation treatment.

	R_Ω (ohm·cm^2)	R_{ct} (ohm·cm^2)	Q_{dl} (Ss^n/cm^2)	n	R_{oxide} (ohm·cm^2)	Q_{oxide} (Ss^n/cm^2)	n	χ^2
No treat.50.0	2.61E+02	9.87E+05	1.40E-05	0.95				1.18E-09
No treat.35.100	1.49E+02	8.79E+05	1.18E-05	0.94				2.22E-04
400.50.0	3.03E+02	7.88E+05	8.13E-06	0.96				8.60E-04
400.35.100	5.66E+02	2.01E+06	9.16E-06	0.94				3.60E-04
500.50.0	6.08E+02	3.63E+05	4.15E-06	0.92				1.29E-03
500.35.100	1.16E+03	7.82E+05	3.07E-06	0.88				1.00E-03
600.50.0	8.72E+02	4.60E+04	5.31E-10	0.59	9.39E+06	5.39E-10	0.61	1.84E-03
600.35.100	3.36E+02	1.85E+04	3.70E-10	0.78	8.74E+06	8.95E-10	0.67	3.50E-03
700.50.0	2.44E+02	2.85E+03	7.86E-10	0.74	2.30E+06	7.86E-10	0.60	6.70E-03
700.35.100	7.62E+02	5.60E+03	4.48E-10	0.88	1.26E+07	2.25E-10	0.64	3.20E-03

Untreated and TO samples at 400 and 500 °C showed a high R_{ct} of about $10^5 - 10^6$ ohm·cm^2 indicating the formation of a protective layer that confers a high corrosion resistance to the alloy. They possess 10 times lower Q_{dl} compared to the untreated Ti13Nb13Zr and a similar R_{ct} and n value, revealing an increased protection of the protective film against charge transfer, through the control of the rate of the electrochemical processes at the oxide-electrolyte interface.

Contrarily, thermally oxidised Ti13Nb13Zr alloy above 600 °C is a more complex

system characterised by two time constants revealing two different charge transfer paths. The low R_{ct} values ($10^3 - 10^4$ ohm·cm^2) together with the low values of n coefficient indicate a defective oxide layer. Based on SEM images (Figure 7.2) of TO samples above 600 °C, the fisures and spallation at the oxide layer can be the reason for the deterioration of the corrosion protection.

Since the oxide layers have been produced to improve the tribocorrosion behaviour of Ti13Nb13Zr in oral environment, the temperature of 500 °C was chosen because it is the higher temperature at which no spalliation occurred. Even if at 400 °C the electrochemical properties showed to be better, the improvement of surface mechanical properties is related to the increase of treatment temperature [147], which promotes the formation of rutile.

7.4.2 Influence of treatment duration on thermally oxidised Ti13Nb13Zr

Oxide layer structure and morphology. Cross section of thermally oxidised Ti13Nb13Zr alloy at 500 °C with different treatment durations, are shown in Figure 7.8. The thermally grown oxide layer is compact and its thickness increases with treatment duration. Figure 7.9 shows the evolution of the oxide thickness with treatment duration. Predictably, the oxide thickness increases with treatment duration. The increase towards asymptotic values are similar to the parabolic growth rate observed by Velten *et al.* [150] with TO Ti13Nb13Zr alloy for lower oxidation times, from 5 to 160 min.

XRD patterns of the thermally oxidized samples at 500 °C for 6, 9 and 12 h are given in Figure 7.10. XRD shows the presence of crystalline phases of TiO_2 (anatase and rutile) along the expected amorphous TiO_2 layer on the oxidized surface. The rutile phase formed on the TO Ti13Nb13Zr surface at 500 °C matches that found at 750 °C [96]. As the oxidation duration increased the peaks of intensity corresponding to rutile also rised whereas the anatase peaks maintained them height, suggesting an increase of the ratio of rutile content on the oxide layer. Thus, increasing the oxidation time, involves a higher amount of rutile in the oxidised layer which increase its protective nature against a corrosive environment. As the rutile content is also related to a higher hardness, therefore, a higher wear resistance of the TO Ti13Nb13Zr alloy can be expected. Anatase is more prone to be attacked and dissolved in reducing acids whereas rutile is chemically inert [161]. The dissolution of anatase in an aggressive media can leave unprotected sites that can accelerate corrosion.

Corrosion behaviour. In order to analyse the influence of TO duration at 500 °C, a deeper study of the electrochemical properties of TO Ti13Nb13Zr alloy was made by

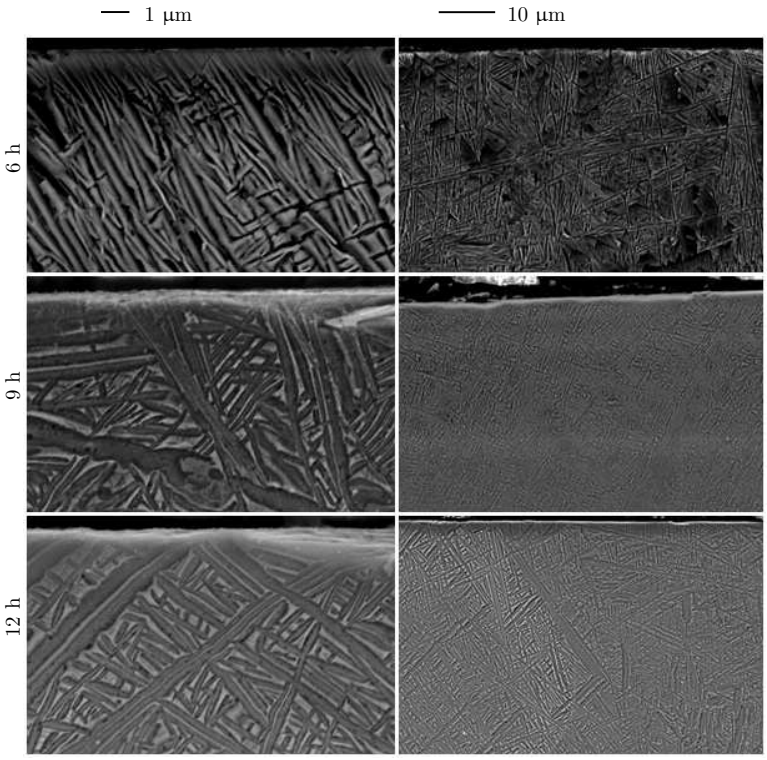

Figure 7.8: Cross section (SEM) of the thermally formed oxide layers on Ti13Nb13Zr alloy at 500 °C for different durations.

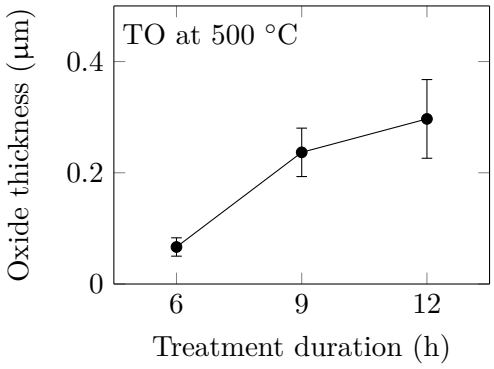

Figure 7.9: The influence of the oxidation time on the oxide thickness formed on Ti13Nb13Zr alloy at 500 °C.

introducing a more aggressive condition, *i.e.* artificial saliva with pH 3.5 and 1000 ppm F^-.

Table 7.3 summarizes the average OCP values measured during the initial stabilisation and the main corrosion parameters calculated from polarisation curves,

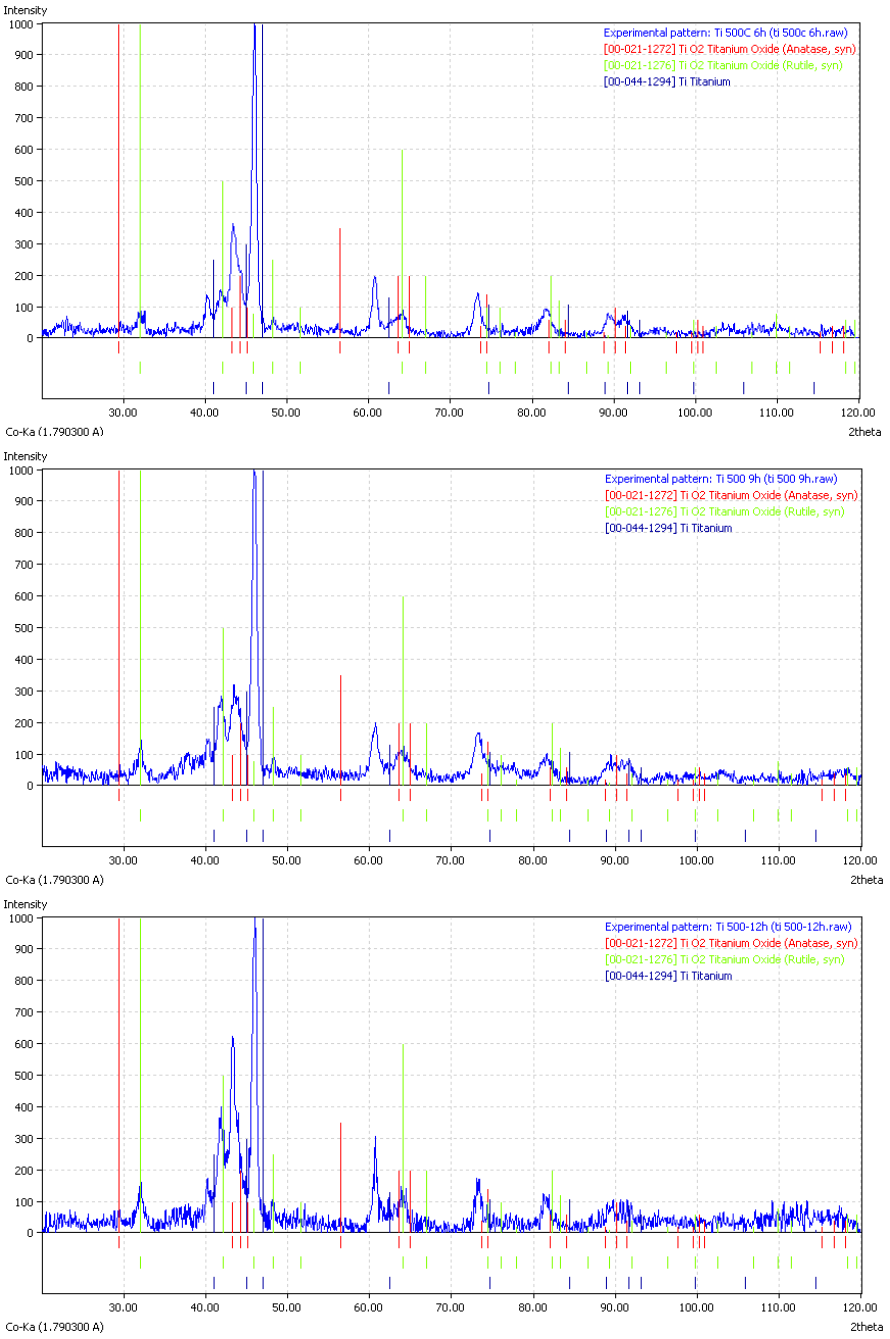

Figure 7.10: XRD patterns thermally oxidized Ti13Nb13Zr alloy for 6, 9 and 12 h, respectively.

i.e. E_{corr} and i_{corr}. OCP and E_{corr} have similar values so Figure 7.11 can serve as a reference for both parameters. E_{corr} showed nobler values in thermally oxidised samples with no influence of the treatment duration, indicating an improvement of the corrosion resistance. At the most aggressive condition, artificial saliva with pH 3.5 and 1000 ppm F^-, E_{corr} slightly increased with thermal oxidation treatment, but the difference was

remarkable on the 6 h thermally oxidised sample.

Table 7.3: Electrochemical parameters of Ti13Nb13Zr in artificial saliva solutions. Influence of the duration of the thermal oxidation treatment.

Time (h)	Electrolyte	OCP (mV)	E_{corr} (mV/SCE)	i_{corr} (μA/cm^2)
Ref.*	AS.50.0	-245.0 ± 200.0	-245.0 ± 185.0	0.170 ± 0.150
	AS.35.100	-460.0 ± 50.0	-440.0 ± 15.0	0.090 ± 0.090
	AS.35.1000	-915.0 ± 40.0	-895.0 ± 30.0	140 ± 20
6	AS.50.0	-1.2 ± 18.6	-44.3 ± 63.0	0.050 ± 0.040
	AS.35.100	-30.3 ± 6.8	-42.9 ± 7.4	0.060 ± 0.020
	AS.35.1000	-313.0 ± 10.2	-410.7 ± 12.3	0.140 ± 0.024
9	AS.50.0	-9.7 ± 17.6	-5.5 ± 24.8	0.009 ± 0.001
	AS.35.100	-40.5 ± 4.9	-35.0 ± 7.3	0.008 ± 0.006
	AS.35.1000	-412.5 ± 123.7	-615.0 ± 78.1	0.226 ± 0.063
12	AS.50.0	-81.5 ± 96.9	-82.1 ± 147.0	0.044 ± 0.039
	AS.35.100	-53.1 ± 14.2	-43.5 ± 28.9	0.007 ± 0.001
	AS.35.1000	-430.0 ± 32.1	-602.3 ± 64.2	0.100 ± 0.037

* Ref. is related to untreated Ti13Nb13Zr.

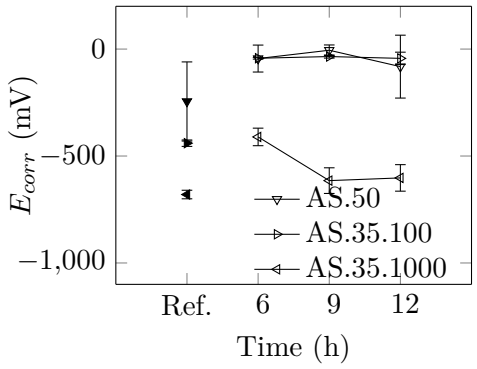

Figure 7.11: Corrosion potential of Ti13Nb13Zr in artificial saliva solutions. Influence of the duration of the thermal oxidation treatment (Ref. is the E_{corr} of untreated Ti13Nb13Zr).

The i_{corr} values are shown in Figure 7.12. A slight decrease of the i_{corr} was observed for TO samples immersed in artificial saliva with pH 5.0 and no F^- and for pH 3.5 and 100 ppm F^-. Meanwhile, in the most aggressive condition, artificial saliva with pH 3.5 and 1000 ppm F^-, i_{corr} of TO samples abruptly decreased about 3 orders of magnitude comparing with the untreated Ti13Nb13Zr. This result is relevant because it demonstrates that the thermal oxide formed on Ti13Nb13Zr provide electrochemical protection to the alloy even in the most aggressive condition, in which untreated

Ti13Nb13Zr was actively dissolving (see Chapter 4).

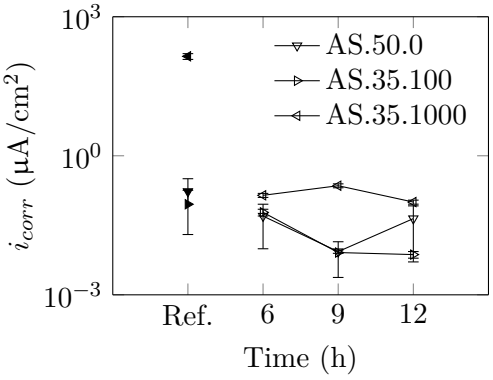

Figure 7.12: Corrosion current density of Ti13Nb13Zr in artificial saliva solutions. Influence of the duration of the thermal oxidation treatment (Ref. is the i_{corr} of untreated Ti13Nb13Zr).

Bode diagrams of thermally oxidised Ti13Nb13Zr alloy for 6, 9 and 12 h in artificial saliva are shown in Figure 7.13. The proposed equivalent electrical circuit of thermally oxidised Ti13Nb13Zr alloy in artificial saliva with pH 5.0 and no fluorides or pH 3.5 and 100 ppm F^- is a Randles circuit with a Q_{dl} replacing the C_{dl}, as the one shown in Figure 7.14 (a). The EIS parameters determined after fitting the experimental data with the proposed equivalent electrical circuits are listed in Table 7.4. Overall, samples oxidised for longer time showed a higher charge transfer resistance through a higher R_{ct} and slightly lower Q_{dl}. Thus, the compact oxide layer formed on Ti13Nb13Zr showed a more protective film as the oxidation duration increased.

Table 7.4: Electrochemical parameters of TO Ti13Nb13Zr at 500°C in artificial saliva solutions. Influence of the treatment duration.

	R_Ω (ohm·cm^2)	R_{ct} (ohm·cm^2)	C_{dl} (Ss^n/cm^2)	n	W (mho · $\sqrt[2]{s}$ · cm^2)	χ^2
500.6h	6.08E+02	3.63E+05	4.15E-06	0.92		1.29E-03
500.6h.35.100	1.16E+03	7.82E+05	3.07E-06	0.88		1.00E-03
500.6h.35.1000	9.07E+02	9.42E+04	4.95E-10	0.94	2.22E+06	7.00E-03
500.9h	5.09E+02	7.40E+05	3.86E-06	0.91		2.09E-04
500.9h.35.100	3.80E+02	1.67E+06	4.50E-06	0.90		4.82E-03
500.9h.35.1000	2.99E+03	1.55E+04	3.60E-06	0.79	2.53E+05	5.80E-03
500.12h	7.29E+02	1.36E+06	3.19E-06	0.92		3.60E-03
500.12h.100	4.81E+02	2.78E+06	3.83E-06	0.91		1.09E-03
500.12h.1000	9.88E+02	2.99E+04	1.78E-05	0.94	2.04E+05	2.30E-03

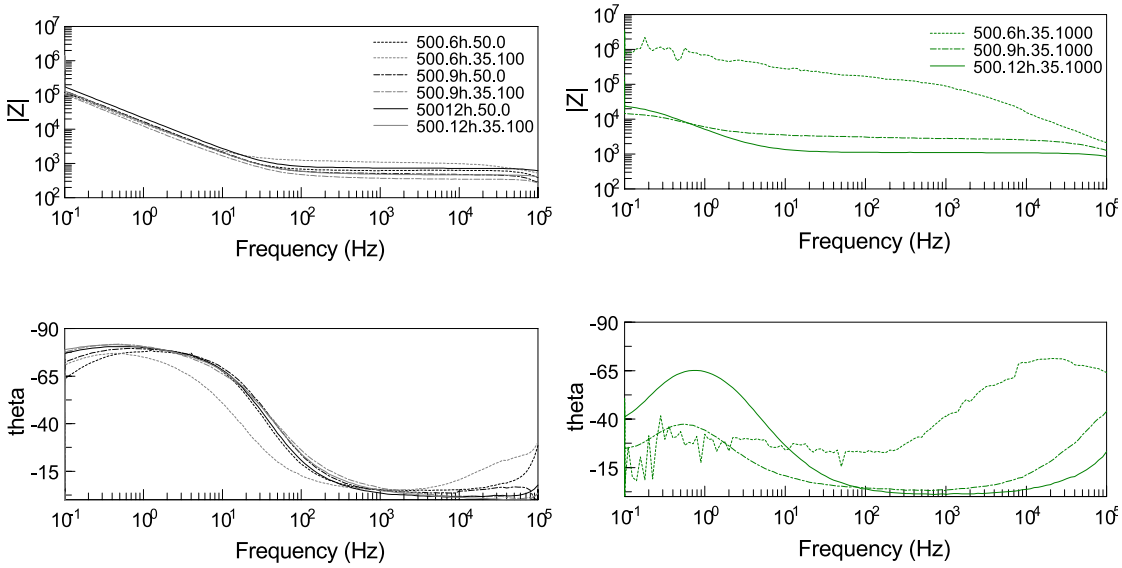

Figure 7.13: Bode impedance and phase angle plots of thermally oxidized Ti13Nb13Zr at 500 °C for different times and in three artificial saliva solutions.

The proposed equivalent electrical circuit for TO Ti13Nb13Zr samples immersed in artificial saliva with pH 3.5 and 1000 ppm F^- is a Randles circuit followed by a Warburg difussion. This equivalent electrical circuit was previously used for TO CpTi at 850 °C for 6 h [149]. The charge transfer resistance, that controls the rate of the electrochemical processes, is one or two orders of magnitude smaller than with the other solutions, revealing a loss in the corrosion protection. In addition, the Warburg element indicates an unrestricted diffusion of the electrode under this aggressive solution.

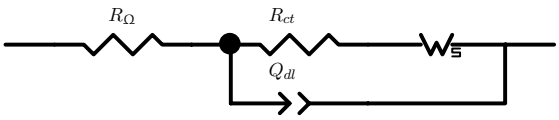

Figure 7.14: Equivalent electrical circuit of thermally oxidised Ti13Nb13Zr alloy at 500 °C inmmersed in artificial saliva with pH 3.5 and 1000 ppm F^-.

Thus, although corrosion current density values of TO Ti13Nb13Zr are not influenced by the oxidation duration, EIS results showed that the longer oxidation duration, the more hindered the charge transfer.

7.4.3 Tribocorrosion behaviour of thermally oxidised Ti13Nb13Zr.

The tribocorrosion behaviour of thermally oxidised Ti13Nb13Zr alloy at 500 °C with different treatment durations is studied hereafter.

Figure 7.15 shows the influence of the duration of the thermal oxidation on the wear rate of Ti13Nb13Zr. Overall, the thermal oxidation treatment showed to improve the wear resistance of Ti13Nb13Zr almost 3 orders of magnitude, with a wear rate from 10^{-3} (see chapter 4) to $10^{-6} - 10^{-5}$ mm^3/Nm. Thus, sliding-corrosion tests results confirmed the superiority of the thermally oxidized surface over untreated Ti13Nb13Zr alloy from tribocorrosion viewpoint.

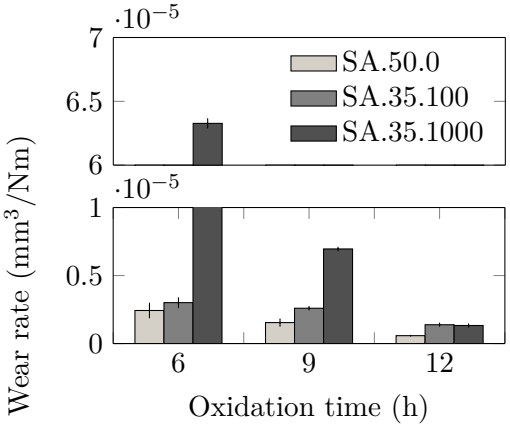

Figure 7.15: Wear rate measured by profilometry on wear scars made on TO Ti13Nb13Zr alloy reciprocating sliding test in artificial saliva.

Even though the electrochemical parameters showed a slightly higher corrosion resistance on oxidised sampled for 6 h, sliding-corrosion tests showed that the longer the thermal oxidation duration, the lower the wear rate. In addition, an increase of the wear rate was observed as the aggressiveness of the electrolyte increased.

One of the discussions in chapter 4 was that the wear track measurement after sliding-corrosion test immersed in a very aggressive solution might be a tricky matter. During sliding under free corroding conditions, the unworn area surrounding the wear scar is getting dissolved due to the oxidation reaction. The dissolved volume of a metal under open circuit potential conditions is related to the corrosion current density through Faraday's law. Thus, the higher the i_{corr}, the higher the dissolved volume or thickness. Coming back to the core of the matter, if the dissolved material is very large, the measurement of the wear scars by profilometry might not be reliable, since the unworn surface acts as a reference to calculate the worn volume.

Table 7.5 provides dissolved volume of the unworn area during the sliding corrosion test, calculated with Faraday's law from i_{corr} values, and the corresponding recession on the sample height. On TO samples, this recess is in the order of $10^{-4} - 10^{-5}$ µm. The transversal profile of the wear scars of thermally oxidised Ti13Nb13Zr immersed in artificial saliva with pH 5.0 are presented on Figure 7.16. The depth of the wear scars

Table 7.5: The dissolved volume and corresponding depth in TO Ti13Nb13Zr calculated with i_{corr} with Faraday's law.

Thermal oxidation		Electrolyte	i_{corr}	Dissolved volume	h (µm)
Temp.	Duration			(mm^3)	
		AS.50.0	0.0501	1.12E-08	9.95E-05
	6 h	AS.35.100	0.0602	1.35E-08	1.20E-04
		AS.35.1000	0.1403	3.15E-08	2.79E-04
		AS.50.0	0.0085	1.92E-09	1.70E-05
500 °C	9 h	AS.35.100	0.0081	1.83E-09	1.62E-05
		AS.35.1000	0.2260	5.07E-08	4.49E-04
		AS.50.0	0.0440	9.89E-09	8.75E-05
	12 h	AS.35.100	0.0073	1.66E-09	1.47E-05
		AS.35.1000	0.1004	2.25E-08	1.99E-04

is in the order of 10^{-1} µm, thus in this case, the recess of the unworn surface does not affect the scar measurement in any of the electrolytes. This is directly involved with higher corrosion resistance of thermally oxidised samples, compared to the untreated ones, even in the most aggressive conditions, AS.35.1000, and most especially for 12 h oxidation time.

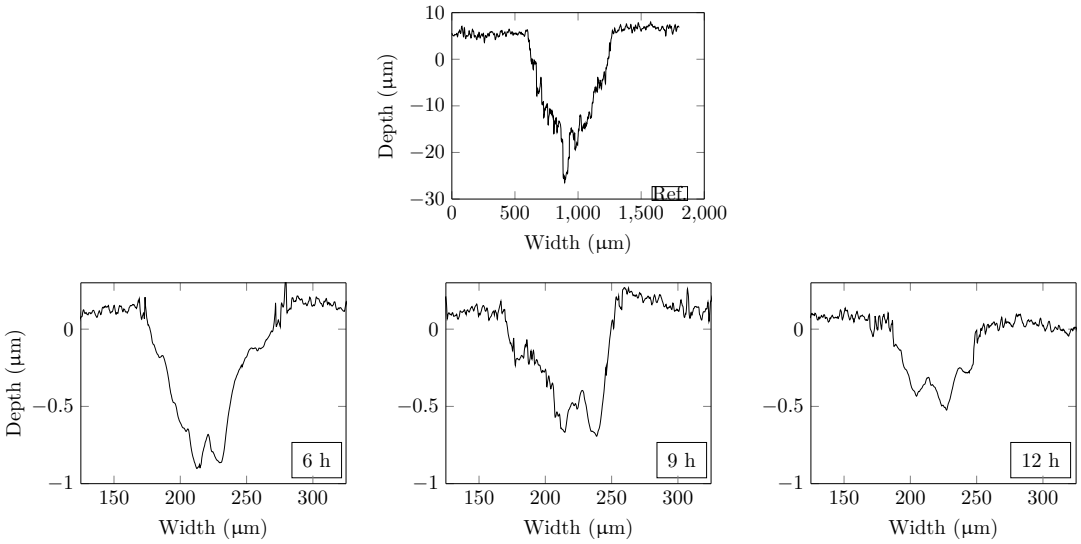

Figure 7.16: Cross section of the wear scars after sliding corrosion tests in AS.50.0 condition, obtained by profilometry. Influence of the temperature of the thermal oxidation treatment.

The depth of the wear scar decreases with the duration of the thermal oxidation treatment, going from 1 to 0.5 μm. Whichever the case, the depth of the wear scar is higher than the oxide thickness after 2 h of sliding, disclosing that the oxide layer had been broken during the sliding test in all the conditions. This means that probably the wear rate was slower when rubbing against the oxide layer, due to its better mechanical properties. Once the oxide layer was worn and the bulk material came into contact, the wear rate presumably increased. As the oxide layer thickness of TO Ti13Nb13Zr samples increased with treatment duration, it is understandable the lower wear rate for the same sliding time.

Wear morphology. The wear morphology of Ti13Nb13Zr alloy thermally oxidised with different durations is shown in Figure 7.17. Wear morphologies of samples immersed in artificial saliva with pH 5.0 and no F^- and with pH 3.5 and 100 ppm are similar. Thus, images of samples immersed in artificial saliva with pH 5.0 and no F^- can serve as a reference for both electrolytes.

In the less aggressive conditions, the wear tracks were very smooth with cracks on the detached particles showing a high abrasion resistance comparing to the untreated Ti13Nb13Zr (Figure 4.12). This would be due to the increase of the mechanical properties at the surface after the thermal oxidation treatment.

Conversely, in the most aggressive condition, thermally oxidised samples for 6h showed severe abrasion and layer detachment, whereas for 9 and 12 h the wear track showed traces of local material removal and cracks but no abrasion. Indeed, in the former column of Figure 7.17, the oxide layer of samples thermally oxidised sample for 6h seems to be completely worn in the wear track, whereas those thermally oxidised for 9 and 12 h still conserve part of the oxide layer. Thus, the absence of abrasion might be because of the higher mechanical properties of the oxide layer compared to the bulk material.

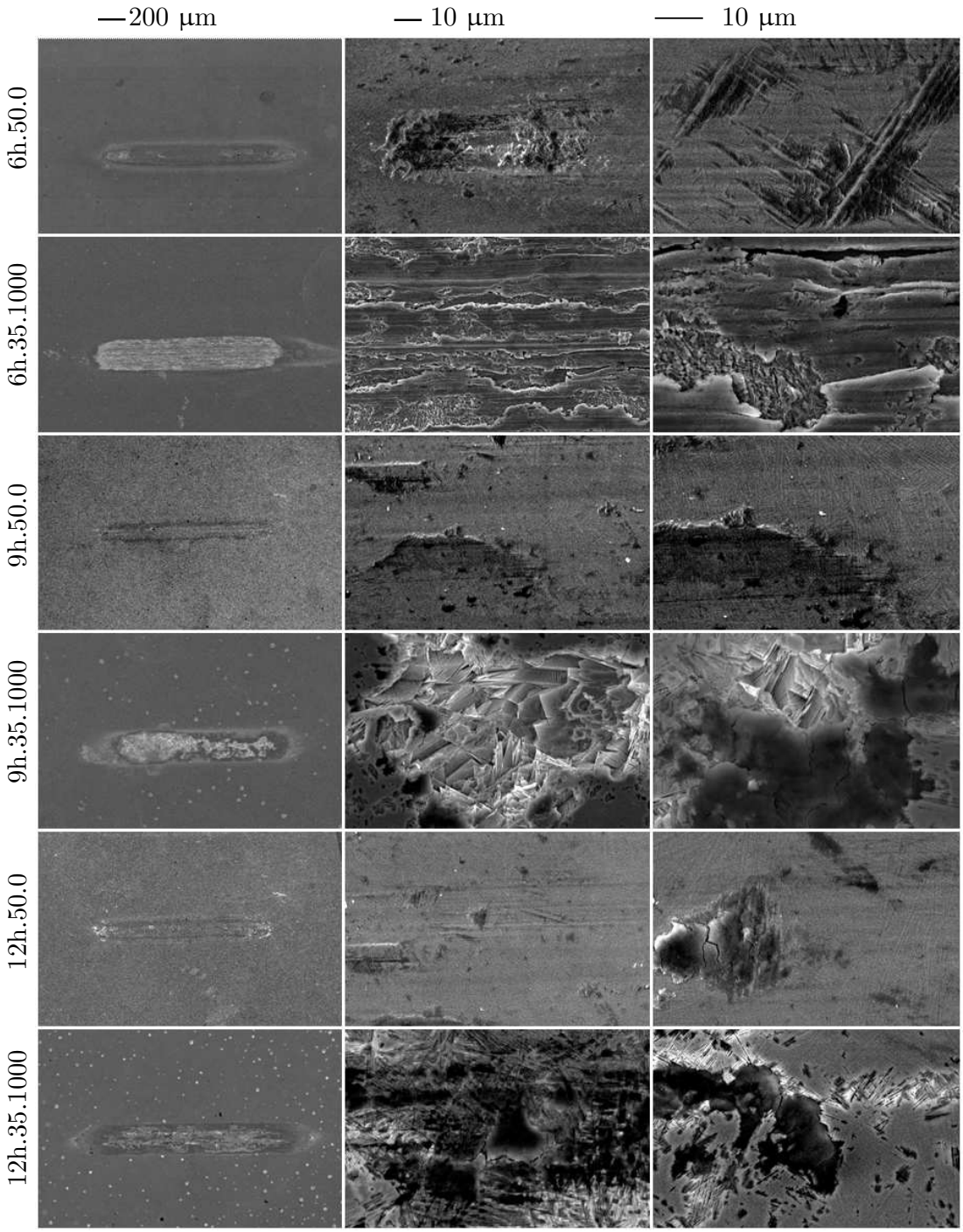

Figure 7.17: SEM images of the wear mechanisms of thermally oxidised Ti13Nb13Zr at 500 °C. Influence of the thermal oxidation duration.

7.5 Conclusions

Thermal oxidation treatment was proposed to enhance the tribocorrosion response of Ti13Nb13Zr in oral environment. To that end, a range of temperatures were studied, from 400 to 700 °C. The temperature of 500 °C was selected because it was the highest temperature at which the oxide layer showed to be compact and defect- free, even if its electrochemical properties were the less favoured. Tribocorrosion behaviour of thermally oxidised Ti13Nb13Zr alloy at 500 °C in a range of treatment durations was studied, in a following and deeper step. The oxide layer was compact and defect-free. Following are the main conclusions obtained in this chapter.

- The corrosion resistance of thermally oxidised Ti13Nb13Zr alloy increased in comparison to the untreated one due to the thermally growth oxide layer.
- The oxide layer remains compact and without defects until a treatment temperature of 500 °C, from which cracks and spallations appear.
- The treatment duration of thermally oxidised Ti13Nb13Zr at 500 °C, increases the oxide layer thickness but the corrosion resistance in artificial saliva remains unchanged.
- The wear rate due to tribocorrosion request of thermally oxidised Ti13Nb13Zr samples at 500 °C was drastically reduced with the TO treatment, about 3 orders of magnitude, because of the enhancement of the mechanucal properties of the oxide film after thermal oxidation. The larger TO treatment, 12 h, was the one with the best tribocorrosion response.
- The increased corrosion resistance of TO Ti13Nb13Zr alloys at 500 °C was remarkable under the most aggressive condition, artificial saliva with pH 3.5 and 1000 ppm F^-.

In conclusion, corrosion and tribocorrosion experiments confirmed the superiority of the thermally oxidized Ti13Nb13Zr over the untreated alloy. Thus, thermal oxidation of Ti13Nb13Zr is proposed as an alternative surface for oral implantation.

Chapter 8

Conclusions and future work

In this thesis dissertation, a promising titanium alloy in the area of oral implantology has been characterised as an alternative to widely used titanium and titanium alloys. Ti13Nb13Zr alloy has not only a much more similar mechanical properties comparing with the bone, but also biocompatible alloying elements. There are, however, few studies related to its degradation in the oral environment. Thus, the corrosion and tribocorrosion characterisation of the alloy was carried out to study the mechanical request due to mastication events in an aggressive environment such as saliva.

Two main goals were established in this research work. First, the characterisation of an innovative titanium alloy for dental implant application, Ti13Nb13Zr, from the corrosion and tribocorrosion viewpoint. The second objective, two different protection techniques are studied to improve the tribocorrosion behaviour of the alloy in the oral environment. The widely used CpTi4 was used as benchmark.

8.1 Conclusions

The former objective of this thesis dissertation was to characterise the Ti13Nb13Zr alloy for dental implant in the oral environment, from the corrosion and tribocorrosion viewpoint. In this regard, following are the most relevant conclusions.

Interestingly, the corrosion behaviour and the wear rate of Ti13Nb13Zr due to tribocorrosion request was similar to that of CpTi4, the benchmark. This finding postulates Ti13Nb13Zr as an alternative material with huge advantages such as an enhanced mechanical and biological compatibility of the alloying elements.

Regarding the tribocorrosion mechanisms, Ti13Nb13Zr experienced an important material loss due to corrosion accelerated by wear in the most aggressive conditions. An increase of material loss of Ti13Nb13Zr was also observed probably due to the worse

mechanical properties of the naturally formed oxide film on the surface, in comparison to CpTi4. This led to enhance the wear accelerated by corrosion mechanisms, which was demonstrated with the effect of sliding time and intermittency on the wear rate.

The repassivation kinetics of titanium was also tested in this work. It was shown that the repassivation kinetics under free corroding conditions are not spontaneous, but in the order of tens of seconds. Overall, Ti13Nb13Zr and CpTi4 showed similar features, with a lower repassivation times as the surrounding passive area decreased.

The second and last objective was to protect the Ti13Nb13Zr alloy against tribocorrosion in the oral environment. For that two approaches were studied, namely, the addition of corrosion inhibitors ($CaCO_3$, $NaNO_3$ and Povidone Iodine) to the artificial saliva and the application of a thermal treatment on the alloy (thermal oxidation). Hereafter are enumerated the main conclusions related to this objective.

$CaCO_3$ and $NaNO_3$ addition in the artificial saliva promoted an important reduction of the repassivation time after an scratch test, in particular on Ti13Nb13Zr. Interestingly, the wear rate of CpTi4 after the reciprocating sliding test in artificial saliva with $CaCO_3$ showed a reduction of 50%. The Ti13Nb13Zr, however, exhibited a negative effect of the corrosion inhibitors on the wear rate, rejecting the hypothesis that the tribocorrosion behaviour of Ti13Nb13Zr is enhanced with the addition of some of these corrosion inhibitors.

Thermal oxidation on Ti13Nb13Zr was applied in a range of temperatures from 400 to 700 °C for 6 h. The oxide layer was compact and corrosion resistant up to 500 °C. Thus, a range of treatment duration were analysed on thermally oxidised samples at 500 °C, as the higher the temperature, the higher the energy to promote the formation of rutile. The later oxidised samples showed an improvement in the corrosion properties, particularly in the most aggressive conditions. The wear rate under tribocorrosion request also showed an important reduction, by a factor of 100 to 1000.

8.2 Future work

This research work related to the tribocorrosion characterisation and protection of the innovative Ti13Nb13Zr alloy for oral implantology, has also given rise to interesting scenarios and starting points for new research paths. They deviated however from the main targets defined in this thesis, so they are only mentioned down below as a future labours due to the finite nature of this work.

About the tribological configuration. The real events occurring on a dental implant in the oral environment are midway between the scratch and reciprocating

sliding test carried out in this work in artificial saliva. Once known that the repassivation kinetics are so slow comparing to the mastication frequency, one can visualise the reciprocating sliding to be an accurate technique to characterize the synergy and damage caused by mastication and the aggressivity of saliva, being the mastication frequency a non determinant parameter. However, the large difference between the conclusion obtained with each method, led one to reflect on the importance of the choice of the characterisation technique.

The mastication event is in fact an oscillatory request in one direction by which food is crushed and ground by teeth. Contrarily, in reciprocating sliding configuration, the mechanical request has a bidirectional nature. However, it is the most widely used configuration, probably because the wide knowledge about it.

A more accurate technique would be through the use of a tribometer that enabled an oscillatory normal contact on the sample. In this way, the unidirectional character of the mastication would be simulated. Thus, the use of an oscillatory normal contact technique is proposed as a future work to characterize dental surfaces.

About repassivation kinetics. The relatively slow repassivation kinetics under free-corroding conditions of CpTi4 and Ti13Nb13Zr were analysed in this work. The nature of the measured current between the titanium sample and the Pt microelectrode with the electrochemical noise technique, remains however poorly understood.

The dissolution current lines from the scratched area can follow two paths. On the one hand, a galvanic coupling is established within the titanium sample between the scratched and the surrounding passive area. On the other, current lines go to the Pt microelectrode and these are the recorded current data.

Consequently, the support of a multiphysics software platform for simulating physics based problems would help to solve the concern about which is the ratio or relationship between the measured current evolution and the dissolution/repassivation events in the scratched area.

About the corrosion inhibitors. The addition of corrosion inhibitors to the saliva in the shape of mouthwash or a similar format is an interesting idea from dentists viewpoint. Although it does not work for Ti13Nb13Zr alloy in oral environment, it was seen that the effect of $CaCO_3$ on CpTi4 was very positive. Considering the current widespread use of CpTi4 on dental implantology nowadays, it would be interesting to delve into these studies.

List of Figures

1.1 The dental implant is composed of (1) a crown, (2) an abutment screw, (3) an abutment and (4) an implant. 2

1.2 Relationship between polarization resistance and biocompatibility of pure metals and some alloys [10]. 4

1.3 Classification and chemical composition of commercially pure titanium according to ASTM F67. 5

1.4 Composition of Fusayama-Meyer artifial saliva. 8

1.5 Lateral force component produced from a compressive force on an oblique plane [60]. 9

1.6 Inter-oral chewing parameters [59]. 10

1.7 Maximum stresses present on dental implant calculated by FEA methods. 10

1.8 Testing configuration and parameters used in literature for tribological characterisation of titanium dental implants. τ_H and $\tau_{H,max}$ correspond to the mean and the maximum Hertzian contact pressure, respectively. . . 11

1.9 Potential-current density curve of β-stabilizing alloying elements as compared to titanium and implant steel 316 L.The reference electrode is $Ag/AgCl_2$ [16]. 12

1.10 Potential- pH equilibrium diagram for the systems titanium-, niobium- and zirconium-water, at 25 °C [69]. 12

1.11 Fluoride concentration values used for mechanical and chemical characterisation of dental implants in literature. 14

1.12 Influence of fluorides and pH of the electrolyte on polarization curves of titanium [35]. 15

2.1 Scheme of the outline of the thesis. 23

3.1 Microstructure of (a) Ti13Nb13Zr alloy and (b) CpTi4. 28

3.2 XPS spectra for CpTi4 before and after 30 s Ar ions sputteting. 29

3.3 XPS spectra for Ti13Nb13Zr before and after 30 s Ar ions sputteting. . . 30

3.4 Stress-strain curve of Ti13Nb13Zr alloy. 31

4.1 OCP evolution for CpTi4 and Ti13Nb13Zr immersed in artificial saliva with different fluoride concentrations (0, 100 and 1000 ppm F-) at pH 3.5. 36

4.2 Polarisation curves of CpTi4 and Ti13Nb13Zr in artificial saliva with the most (pH 3.5, 1000 ppm F-) and the least (pH 5.0, 0 ppm F-) aggressive conditions. 37

4.3 Corrosion potential of CpTi4 and Ti13Nb13Zr in artificial saliva solutions. 38

4.4 Corrosion current density of CpTi4 and Ti13Nb13Zr in artificial saliva solutions. 39

4.5 i_p of CpTi4 and Ti13Nb13Zr in artificial saliva solutions. 39

4.6 OCP evolution for Ti13Nb13Zr during sliding tribocorrosion experiments in artificial saliva with pH 3.5 (a) and pH 5.0 (b). 40

4.7 Average value of the OCP during reciprocating sliding test. 41

4.8 Current evolution of CpTi4 and Ti13Nb13Zr during rubbing at an applied passive potential (+750 mV/SCE) in artificial saliva with (a) pH 3.5 and 1000 ppm F^- (b) pH 5.0 and 0 ppm F^-. 41

4.9 Schematic diagram of the charge (Q) corresponding to worn and unworn areas. 42

4.10 Material dissolution, h, from the (a) worn and (b) unworn areas as a result of reciprocating sliding test under anodic polarisation conditions. 43

4.11 Average coefficient of friction recorded during reciprocating sliding corrosion tests under potentiostatic conditions. 44

4.12 SEM images of the wear mechanisms of CpTi4 and Ti13Nb13Zr after reciprocating sliding test in pH 3.5 artificial saliva under OCP conditions. 45

4.13 Wear rate measured by profilometry on wear scars made on reciprocating sliding test under A) OCP and B) Potentiostatic conditions. 46

5.1 An equivalent electrical circuit for describing a localized corrosion situation under free corroding conditions [113]. 52

5.2 Potential and current evolution after a scratch experiment on CpTi4 immersed in artificial saliva. 60

5.3 Potential evolution before and after a scratch experiment on CpTi4 immersed in artificial saliva with and without ohmic drop compensation. . 60

5.4 Wear rate of CpTi4 and Ti13Nb13Zr after tribocorrosion test at different sliding frequencies. 62

5.5 Average coefficient of friction of CpTi4 and Ti13Nb13Zr during rubbing at different sliding frequencies. 62

5.6 FFT of the OCP values of CpTi4 and Ti13Nb13Zr during rubbing at different sliding frequencies. 63

5.7 I_{peak} and τ_I, representing repassivation kinetics of CpTi4 and Ti13Nb13Zr alloy with different active to passive area immersed in artificial saliva. . . 64

5.8 E_{peak} and τ_E, representing repassivation kinetics of CpTi4 and Ti13Nb13Zr alloy with different active to passive area immersed in artificial saliva. 65

5.9 Influence of ξ on the initial $h(t)/R_t$ hop after the activation of a small surface. 66

5.10 Influence of sliding time on the wear rate of CpTi4 and Ti13Nb13Zr in artificial saliva. Wear rate was measured after 5, 30 and 60 min of sliding. 67

5.11 Influence of sliding intermittency on the wear rate of CpTi4 and Ti13Nb13Zr in oral environment. Total sliding time was 30 min. 69

6.1 Evans diagrams showing the shift of the corrosion potential due to the presence of an anodic, cathodic or mixed inhibitor [111]. 72

6.2 Polarisation curves of CpTi4 and Ti13Nb13Zr in artificial saliva with the addition of the corrosion inhibitors. 76

6.3 E_{corr} and i_{corr} values of CpTi4 and Ti13Nb13Zr in artificial saliva with the addition of the corrosion inhibitors. 78

6.4 I_{peak} and τ_I, representing repassivation kinetics of CpTi4 and Ti13Nb13Zr alloy with different corrosion inhibitors added into the artificial saliva. . . 78

6.5 E_{peak} and τ_E, representing repassivation kinetics of CpTi4 and Ti13Nb13Zr alloy with different corrosion inhibitors added into the artificial saliva. 79

6.6 Potential and current evolution of Ti13Nb13Zr immersed in artificial saliva before, during and after the rubbing test. 80

6.7 Average current measured during rubbing tests of CpTi4 and Ti13Nb13Zr alloy immersed in artificial saliva with different corrosion inhibitors. . . . 80

6.8 Dissolved material rate during rubbing tests, calculated through Faraday, of CpTi4 and Ti13Nb13Zr alloy immersed in artificial saliva with different corrosion inhibitors. 81

6.9 Wear rate measured by profilometry on wear scars made on CpTi4 and Ti13Nb13Zr alloy immersed in artificial saliva with different corrosion inhibitors. 81

7.1 Zr concentration depth profile obtained from RBS for the thermally oxidized Ti13Nb13Zr alloy at 750 °C for different times 1.5, 6 and 24 h [147]. 85

7.2 Top view (optical microscopy) and cross section (SEM) of the thermally formed oxide layer at different temperatures. 89

7.3 Polarisation curves of TO Ti13Nb13Zr samples at different temperatures in artificial saliva with pH 5.0 and 0 ppm F^-. 90

7.4 Corrosion potential of Ti13Nb13Zr in artificial saliva solutions. Influence of the temperature and electrolyte of the thermal oxidation treatment (Ref. is the E_{corr} of untreated Ti13Nb13Zr). 91

7.5 Corrosion current density of Ti13Nb13Zr in artificial saliva solutions. Influence of the temperature of the thermal oxidation treatment (Ref. is the i_{corr} of untreated Ti13Nb13Zr). 91

7.6 Bode impedance and phase angle plots of thermally oxidized Ti13Nb13Zr at different temperatures and in two artificial saliva solution. 92

7.7 Equivalent electrical circuit of thermally oxidised Ti13Nb13Zr alloy inmmersed in artificial saliva. (a) circuit corresponds to thermally oxidised sampled at 400 and 500 °C, whereas (b) corresponds to 600 and 700 °C. 93

7.8 Cross section (SEM) of the thermally formed oxide layers on Ti13Nb13Zr alloy at 500 °C for different durations. 95

7.9 The influence of the oxidation time on the oxide thickness formed on Ti13Nb13Zr alloy at 500 °C. 95

7.10 XRD patterns thermally oxidized Ti13Nb13Zr alloy for 6, 9 and 12 h, respectively. 96

7.11 Corrosion potential of Ti13Nb13Zr in artificial saliva solutions. Influence of the duration of the thermal oxidation treatment (Ref. is the E_{corr} of untreated Ti13Nb13Zr). 97

7.12 Corrosion current density of Ti13Nb13Zr in artificial saliva solutions. Influence of the duration of the thermal oxidation treatment (Ref. is the i_{corr} of untreated Ti13Nb13Zr). 98

7.13 Bode impedance and phase angle plots of thermally oxidized Ti13Nb13Zr at 500 °C for different times and in three artificial saliva solutions. 99

7.14 Equivalent electrical circuit of thermally oxidised Ti13Nb13Zr alloy at 500 °C inmmersed in artificial saliva with pH 3.5 and 1000 ppm F^-. . . . 99

7.15 Wear rate measured by profilometry on wear scars made on TO Ti13Nb13Zr alloy reciprocating sliding test in artificial saliva. 100

7.16 Cross section of the wear scars after sliding corrosion tests in AS.50.0 condition, obtained by profilometry. Influence of the temperature of the thermal oxidation treatment. 101

7.17 SEM images of the wear mechanisms of thermally oxidised Ti13Nb13Zr at 500 °C. Influence of the thermal oxidation duration. 103

List of Tables

1.1 Mechanical properties of biomedical titanium alloys [13]. 6

3.1 Nominal chemical compositions (wt. %) of CpTi4 and Ti13Nb13Zr according to ASTM standards. 26

3.2 Mechanical properties of CpTi4 [88] and Ti13Nb13Zr [89]. 26

3.3 F^- and pH values of artificial saliva tested in chapter 4. 27

3.4 Artificial saliva (SA) with the different corrosion inhibitors tested in chapter 6. 27

3.5 Ti13Nb13Zr alloy composition (wt. %) obtained with ICP-OES technique. 30

3.6 Hardness values of Ti13Nb13Zr and CpTi4 obtained from Vickers test. . . 31

3.7 Comparison of mechanical properties between test, supplier and the standard of the material for Ti13Nb13Zr. 32

3.8 Mechanical properties of commercially pure titanium according to ASTM F67. 32

4.1 Electrochemical parameters of CpTi4 and Ti13Nb13Zr alloys in the studied solutions. 38

5.1 Main parameters of depassivation and repassivation experiments in literature (E_{app} is the applied potential (potentiostatic control) and τ is the time constant). 50

5.2 The A_{pas}/A_{act} ratio of the masked CpTi4 and Ti13Nb13Zr samples to study the influence of the galvanic coupling. 64

5.3 The increase of the wear rate of CpTi4 and Ti13Nb13Zr in oral environment after intermittency experiments (%, compared to continuous conditions). 68

6.1 Chemical composition of some corrosion inhibitors for titanium alloys found in literature. 73

6.2 My caption 75

6.3 Electrochemical parameters obtained from polarisation curves of CpTi4 and Ti13Nb13Zr in artificial saliva with the addition of the corrosion inhibitors. 77

7.1 Electrochemical parameters of Ti13Nb13Zr in artificial saliva solutions. Influence of the temperature of the thermal oxidation treatment. 90

7.2 Electrochemical parameters of Ti13Nb13Zr in artificial saliva solutions. Influence of the temperature of the thermal oxidation treatment. 93

7.3 Electrochemical parameters of Ti13Nb13Zr in artificial saliva solutions. Influence of the duration of the thermal oxidation treatment. 97

7.4 Electrochemical parameters of TO Ti13Nb13Zr at 500°C in artificial saliva solutions. Influence of the treatment duration. 98

7.5 The dissolved volume and corresponding depth in TO Ti13Nb13Zr calculated with i_{corr} with Faraday's law. 101

Bibliography

[1] R. Bothe, L. Beaton, H. Davenport, Reaction of bone to multiple metallic implants, Surg Gynecol Obstet 71 (6) (1940) 598–602.

[2] P.-I. Bränemark, Osseointegrated implants in the treatment of the edentulous jaw. experience from a 10-year period., J. Plast. Reconstr Surg 16 (1977) 1–132.

[3] C. Rubin, L. Lanyon, Osteoregulatory nature of mechanical stimuli: Function as a determinant for adaptive remodelling in bone, Journal of orthopaedic research 5 (2) (2005) 300–310. doi:10.1002/jor.1100050217.

[4] M. Esposito, J.-M. Hirsch, U. Lekholm, P. Thomsen, Biological factors contributing to failures of osseointegrated oral implants,(II). Etiopathogenesis, European journal of oral sciences 106 (3) (1998) 721–764. doi:10.1046/j.0909-8836..t01-6-.x.

[5] J. Wolff, P. Maquet, R. Furlong, The law of bone remodelling, Springer Berlin, 1986. doi:10.1007/9783642710315.

[6] D. Carter, D. Spengler, Mechanical properties and composition of cortical bone, Clinical orthopaedics and related research 135 (1978) 192.

[7] B. Story, Dental implant having a force distribution shell to reduce stress shielding, US Patent 6,193,516 (2001).

[8] T. Achour, A. Merdji, B. B. Bouiadjra, B. Serier, N. Djebbar, Stress distribution in dental implant with elastomeric stress barrier, Materials & Design 32 (1) (2011) 282 – 290. doi:10.1016/j.matdes.2010.05.053.

[9] D. Williams, Progress in biomedical engineering. definitions in biomaterials, in: Proceedings of a Consensus Conference of the European Society for Materials. Amsterdam: Elsevier, 1987.

[10] M. Niinomi, Recent metallic materials for biomedical applications, Metallurgical and Materials Transactions A 33 (2002) 477–486. doi:10.1007/s11661-002-0109-2.

[11] J. Guindy, H. Schiel, F. Schmidli, J. Wirz, Corrosion at the marginal gap of implant-supported suprastructures and implant failure, Int J Oral Maxillofac Implants 19 (6) (2004) 826–31.

[12] T. Oh, K. Kim, Electrochemical properties of suprastructures galvanically coupled to a titanium implant, Journal of Biomedical Materials Research Part B: Applied Biomaterials 70B (2) (2004) 318–331. doi:10.1002/jbm.b.30046.

[13] M. Geetha, A. Singh, R. Asokamani, A. Gogia, Ti based biomaterials, the ultimate choice for orthopaedic implants - A review, Progress in Materials Science 54 (2009) 397–425. doi:10.1016/j.pmatsci.2008.06.004.

[14] J. Soto-Alvaredo, E. Blanco, J. Bettmer, D. Hevia, R. M. Sainz, C. L. Cháves, C. Sánchez, J. Llopis, A. Sanz-Medel, M. Montes-Bayon, Evaluation of the biological effect of Ti generated debris from metal implants: Ions and nanoparticles, Metallomics 6 (2014) 1702–1708. doi:10.1039/C4MT00133H.

[15] H. Silva, S. Schneider, C. M. Neto, Study of nontoxic aluminum and vanadium-free titanium alloys for biomedical applications, Materials Science and Engineering: C 24 (2004) 679–682. doi:10.1016/j.msec.2004.08.051.

[16] E. Eisenbarth, D. Velten, M. Müller, R. Thull, J. Breme, Biocompatibility of β-stabilizing elements of titanium alloys, Biomaterials 25 (2004) 5705–5713. doi:10.1016/j.biomaterials.2004.01.021.

[17] R. Bhola, S. Bhola, B. Mishra, D. Olson, Corrosion in titanium dental implants/prostheses: A review, Trends in Biomaterials and Artificial Organs 25 (2011) 34–46.

[18] A. Choubey, B. Basu, R. Balasubramaniam, Tribological behaviour of Ti-based alloys in simulated body fluid solution at fretting contacts, Trends Biomater.Artif.Organs. 18 (2005) 141–147. doi:10.1016/j.msea.2004.02.027.

[19] S. L. Assis, S. Wolynec, I. Costa, Corrosion characterization of titanium alloys by electrochemical techniques, Electrochimica Acta 51 (2006) 1815–1819. doi:10.1016/j.electacta.2005.02.121.

[20] I. Cvijovic-Alagicï, Z. Cvijovic, S. Mitrovicï, M. Rakin, D. Veljovicï, M. Babicï, Tribological behaviour of orthopaedic Ti-13Nb-13Zr and Ti-6Al-4V alloys, Tribol Lett 40 (2010) 59–70. doi:10.1007/s11249-010-9639-8.

[21] L. Duarte, S. Biaggio, R. Rocha-Filho, N. Bocchi, Influence of hydroxyapatite on the corrosion resistance of the Ti-13Nb-13Zr alloy, Journal of Materials Science: Materials in Medicine 20 (2009) 1009–1015. doi:10.1007/s10856-008-3662-4.

[22] N. More, N. Diomidis, S. Paul, M. Roy, S. Mischler, Tribocorrosion behavior of β titanium alloys in physiological solutions containing synovial components, Materials Science and Engineering: C 31 (2010) 400–408. doi:10.1016/j.msec.2010.10.021.

[23] N. Diomidis, S. Mischler, N. More, M. Roy, S. Paul, Fretting-corrosion behavior of β titanium alloys in simulated synovial fluid, Wear 271 (2011) 1093Ű1102. doi:10.1016/j.wear.2011.05.010.

[24] F. A. Müller, M. C. Bottino, L. Müller, V. A. Henriques, U. Lohbauer, A. H. A. Bressiani, J. C. Bressiani, *In vitro* apatite formation on chemically treated (P/M) Ti–13Nb–13Zr, Dental Materials 24 (2008) 50–56. doi:10.1016/j.dental.2007.02.005.

[25] A. L. R. Ribeiro, P. Hammer, L. G. Vaz, L. A. Rocha, Are new TiNbZr alloys potential substitutes of the Ti6Al4V alloy for dental applications? An electrochemical corrosion study, Biomedical Materials 8 (2013) 065005. doi:10.1088/1748-6041/8/6/065005.

[26] E. Robare, C. Bugle, J. Davidson, Development of processing methods for Ti-13Nb-13Zr, Advances in the Science and Technology of Titanium Alloy Processing. The Minerals, Metals and Materials Society (1996) 283–291.

[27] J. Gal, Y. Fovet, M. Adib-Yadzi, About a synthetic saliva for in vitro studies, Talanta 53 (6) (2001) 1103 – 1115. doi:10.1016/S0039-9140(00)00618-4.

[28] K. De Brabandere, T. Loix, K. Engelen, B. Bolsens, J. Van den Keybus, J. Driesen, R. Belmans, Design and operation of a phase-locked loop with kalman estimator-based filter for single-phase applications, in: IEEE Industrial Electronics, IECON 2006-32nd Annual Conference on, IEEE, 2006, pp. 525–530. doi:10.1109/IECON.2006.348099.

[29] M. Dodds, D. Johnson, C. Yeh, Health benefits of saliva: a review, Journal of Dentistry 33 (3) (2005) 223–233. doi:10.1016/j.jdent.2004.10.009.

[30] R. Singh, N. Dahotre, Corrosion degradation and prevention by surface modification of biometallic materials, Journal of Materials Science: Materials in Medicine 18 (2007) 725–751. doi:10.1007/s10856-006-0016-y.

[31] M. Geetha, D. Durgalakshmi, R. Asokamani, Biomedical implants: Corrosion and its prevention- A review, Recent Patents on Corrosion Science 2 (2010) 40–54. doi:10.2174/1877610801002010040.

[32] A. Bardow, D. Moe, B. Nyvad, B. Nauntofte, The buffer capacity and buffer systems of human whole saliva measured without loss of CO2, Arch Oral Biol 45(1) (2000) 1–12. doi:10.1016/S0003-9969(99)00119-3.

[33] J. C. M. Souza, Biotribocorrosion behavior of titanium in simulated oral environments, Ph.D. thesis, Universidade do Minho (2009).
URL http://hdl.handle.net/1822/10439

[34] M. Pourbaix, J. Burbank, Atlas d'equilibres electrochimiques, Journal of The Electrochemical Society 111 (1) (1964) 14C–15C. doi:10.1149/1.2426051.

[35] N. Schiff, B. Grosgogeat, M. Lissac, F. Dalard, Influence of fluoride content and pH on the corrosion resistance of titanium and its alloys, Biomaterials 23 (2002) 1995–2002. doi:10.1016/S0142-9612(01)00328-3.

[36] M. Mathew, S. Abbey, N. Hallab, D. Hall, C. Sukotjo, M. Wimmer, Influence of pH on the tribocorrosion behavior of CpTi in the oral environment: Synergistic interactions of wear and corrosion, Journal of Biomedical Materials Research Part B: Applied Biomaterials 100 (2012) 1662–1671. doi:10.1002/jbm.b.32735.

[37] M. Licausi, A. Igual Muñoz, V. Borrás, Tribocorrosion mechanisms of Ti6Al4V biomedical alloys in artificial saliva with different pHs, Journal of Physics D: Applied Physics 46 (2013) 404003. doi:10.1088/0022-3727/46/40/404003.

[38] P. Marsh, M. Martin, M. Lewis, Oral Microbiology, 2009. doi:9780443101441.

[39] G. Novikova, Introduction to corrosion of bioimplants, Protection of Metals and Physical Chemistry of Surfaces 47 (3) (2011) 372–380. doi:10.1134/S2070205111030105.

[40] C. Marino, L. Mascaro, EIS characterization of a Ti-dental implant in artificial saliva media: Dissolution process of the oxide barrier, Journal of Electroanalytical Chemistry 568 (0) (2004) 115 – 120. doi:10.1016/j.jelechem.2004.01.011.

[41] G. Mabilleau, S. Bourdon, M. Joly-Guillou, R. Filmon, M. Baslé, D. Chappard, Influence of fluoride, hydrogen peroxide and lactic acid on the corrosion resistance of commercially pure titanium, Acta Biomaterialia 2 (2006) 121–129. doi:10.1016/j.actbio.2005.09.004.

[42] J. C. Souza, R. M. Nascimento, A. E. Martinelli, Characterization of dental metal-ceramic interfaces immersed in artificial saliva after substructural mechanical metallization with titanium, Surface and Coatings Technology 205 (3) (2010) 787 – 792. doi:10.1016/j.surfcoat.2010.07.116.

[43] B. Sivakumar, S. Kumar, T. Narayanan, Fretting corrosion behaviour of Ti-6Al-4V alloy in artificial saliva containing varying concentrations of fluoride ions, Wear 270 (3) (2011) 317–324. doi:10.1016/j.wear.2010.09.008.

[44] F. Rosalbino, S. Delsante, G. Borzone, G. Scavino, Influence of noble metals alloying additions on the corrosion behaviour of titanium in a fluoride-containing environment, Journal of Materials Science: Materials in Medicine (2012) 1–9doi:10.1007/s10856-012-4591-9.

[45] M. Dilea, A. Mazare, D. Ionita, I. Demetrescu, Comparison between corrosion behaviour of implant alloys Ti6Al7Nb and Ti6Al4Zr in artificial saliva, Materials and Corrosion 64 (6) (2013) 493–499. doi:10.1002/maco.201206526.

[46] I. Milošev, B. Kapun, V. S. Šelih, The effect of fluoride ions on the corrosion behaviour of Ti metal, and Ti6-Al-7Nb and Ti-6Al-4V alloys in artificial saliva, Acta Chimica Slovenica 60 (3) (2013) 543–555. doi:01/2013;60(3):543-55.

[47] A. Vieira, A. Ribeiro, L. Rocha, J. Celis, Tribocorrosion behaviour of titanium in artificial saliva solutions, EUROCORR 2004, Nice.

[48] A. Vieira, A. Ribeiro, L. Rocha, J. Celis, Influence of pH and corrosion inhibitors on the tribocorrosion of titanium in artificial saliva, Wear 261 (2006) 994–1001. doi:10.1016/j.wear.2006.03.031.

[49] J. Souza, S. Barbosa, M. Henriques, R. Oliveira, L. Rocha, J. Celis, Tribocorrosion of commercially pure titanium in artificial saliva containing fluoride, 8th World Biomaterials Congress 2008, Amsterdam.

[50] E. Mardare, L. Benea, J. Celis, Importance of applied normal loads on the tribocorrosion behaviour of Ti-6Al-4V alloy in bio-simulated environment, Optoelectronics and advanced materials 6 (2012) 474–478. doi:10.1155/2009/250986.

[51] J. Souza, S. Barbosa, E. Ariza, J. Celis, L. Rocha, Simultaneous degradation by corrosion and wear of titanium in artificial saliva containing fluorides, Wear 292-293 (2012) 82–88. doi:10.1016/j.wear.2012.05.030.

[52] M. Licausi, A. Igual Muñoz, V. Borrás, Influence of the fabrication process and fluoride content on the tribocorrosion behaviour of Ti6Al4V biomedical alloy in artificial saliva, Journal of the Mechanical Behavior of Biomedical Materials 20 (2013) 137–148. doi:10.1016/j.jmbbm.2013.01.019.

[53] M. Mathew, P. Srinivasa Pai, R. Pourzal, A. Fischer, M. Wimmer, Significance of tribocorrosion in biomedical applications: Overview and current status, Advances in tribology 2009.

[54] J. Souza, M. Henriques, R. Oliveira, W. Teughels, J. Celis, L. Rocha, Do oral biofilms influence the wear and corrosion behavior of titanium?, Biofouling 26 (4) (2010) 471–478. doi:10.1080/08927011003767985.

[55] V. Leung, B. Darvell, Artificial salivas for in vitro studies of dental materials, Journal of Dentistry 25 (6) (1997) 475–484. doi:10.1016/S0300-5712(96)00068-1.

[56] I. Demetrescu, C. Pirvu, V. Mitran, Effect of nano-topographical features of Ti/TiO2 electrode surface on cell response and electrochemical stability in artificial saliva, Bioelectrochemistry 79 (1) (2010) 122–129. doi:10.1016/j.bioelechem.2010.02.001.

[57] Y. Bai, Y. Wang, Y. Cheng, F. Deng, Y. Zheng, S. Wei, Comparative study on the corrosion behavior of Ti-Nb and TMA alloys for dental application in various artificial solutions, Materials Science and Engineering: C 31 (2011) 702–711. doi:10.1016/j.msec.2010.12.010.

[58] R. Holland, Corrosion testing by potentiodynamic polarization in various electrolytes, Dental Materials 8 (4) (1992) 241–245. doi:10.1016/0109-5641(92)90093-R.

[59] Z. Zhou, J. Zheng, Tribology of dental materials: A review, Journal of Physics D: Applied Physics 41 (2008) 113001. doi:10.1088/0022-3727/41/11/113001.

[60] M. Barry, D. Kennedy, K. Keating, Z. Schauperl, Design of dynamic test equipment for the testing of dental implants, Materials & Design 26 (3) (2005) 209 – 216. doi:10.1016/j.matdes.2004.07.001.

[61] D. Manfredini, C. E. Poggio, F. Lobbezoo, Is bruxism a risk factor for dental implants? a systematic review of the literature, Clinical implant dentistry and related research 16 (3) (2014) 460–469. doi:10.1111/cid.12015.

[62] M. Gallas, M. Abeleira, J. Fernandez, M. Burguera, Three-dimensional numerical simulation of dental implants as orthodontic anchorage, The European Journal of Orthodontics 27 (2005) 12–16. doi:10.1093/ejo/cjh066.

[63] G. Papavasiliou, P. Kamposiora, S. Bayne, S. Felton, Three-dimensional finite element analysis of stress-distribution around single tooth implants as a function

of bony support, prosthesis type and loading during function, The Journal of Prosthetic Dentistry 76 (1996) 633–640. doi:10.1016/S0022-3913(96)90442-4.

[64] M. Sevimay, F. Turhan, M. Kilicarslan, G. Eskitascioglu, Three-dimensional finite element analysis of the effect of different bone quality on stress distribution in an implant-supported crown, The Journal of prosthetic dentistry 93 (2005) 227–234. doi:10.1016/j.prosdent.2004.12.019.

[65] A. Ribeiro, Influence of pH and corrosion inhibitors on the tribocorrosion behaviour of titanium in different tribological geometries, Ph.D. thesis (2007).

[66] A. Fernandes, F. Vaz, E. Ariza, L. Rocha, A. Ribeiro, A. Vieira, J. Rivière, L. Pichon, Tribocorrosion behaviour of plasma nitrided and plasma nitrided + oxidised Ti6Al4V alloy, Surface and Coatings Technology 200 (22) (2006) 6218–6224. doi:35400011546919.0110.

[67] M. Metikos-Hukovic, A. Kwokal, J. Piljac, The influence of niobium and vanadium on passivity of titanium-based implants in physiological solution, Biomaterials 24 (2003) 3765–3775. doi:10.1016/S0142-9612(03)00252-7.

[68] M. Pourbaix, Electrochemical corrosion of metallic biomaterials, Biomaterials 5 (3) (1984) 122–134.

[69] D. Brunette, P. Tengvall, M. Textor, P. Thomsen, Titanium in medicine, Vol. 35, Springer Berlin, 2001. doi:3-540-66936-1.

[70] M. Nakagawa, S. Matsuya, T. Shiraishi, M. Ohta, Effect of fluoride concentration and pH on corrosion behavior of titanium for dental use, Journal of dental research 78 (1999) 1568–1572. doi:10.1177/00220345990780091201.

[71] A. Wiegand, W. Buchalla, T. Attin, Review on fluoride-releasing restorative materials-Fluoride release and uptake characteristics, antibacterial activity and influence on caries formation, Dental Materials 23 (2007) 343–362. doi:10.1016/j.dental.2006.01.022.

[72] Y. Oshida, C. Sellers, K. Mirza, F. Farzin-Nia, Corrosion of dental metallic materials by dental treatment agents, Materials Science and Engineering: C 25 (2005) 343–348. doi:10.1016/j.msec.2004.11.004.

[73] S. Fragou, T. Eliades, Effect of topical fluoride application on titanium alloys: A review of effects and clinical implications, Pediatric Dentistry 32 (2010) 99–105.

[74] P. Watson, H. Pontefract, D. Devine, R. Shore, B. Nattress, J. Kirkham, C. Robinson, Penetration of fluoride into natural plaque biofilms, Journal of dental research 84 (2005) 451–455. doi:10.1177/154405910508400510.

[75] S. Kumar, T. Sankara Narayanan, S. Saravana Kumar, Influence of fluoride ion on the electrochemical behaviour of beta-Ti alloy for dental implant application, Corrosion Science 52 (5) (2010) 1721–1727. doi:10.1016/j.corsci.2010.01.008.

[76] A. Robin, O. Carvalho, Influence of ph and fluoride species on the corrosion behavior of Ti-xNb-13Zr alloys in ringerŠs solution, Advances in Materials Science and Engineeringdoi:10.1155/2013/434975.

[77] M. Sakairi, M. Kinjyo, T. Kikuchi, Repassivation behavior of titanium in artificial saliva investigated with a photon rupture method, Electrochimica Acta 56 (2011) 1786–1791. doi:10.1016/j.electacta.2010.08.090.

[78] L. M. Fais, R. B. Fernandes-Filho, M. A. Pereira-da Silva, L. G. Vaz, G. L. Adabo, Titanium surface topography after brushing with fluoride and fluoride-free toothpaste simulating 10 years of use, Journal of dentistry 40 (4) (2012) 265–275. doi:10.1016/j.jdent.2012.01.001.

[79] L. Joska, J. Fojt, Corrosion behaviour of titanium after short-term exposure to an acidic environment containing fluoride ions, Journal of Materials Science: Materials in Medicine 21 (2) (2010) 481–488. doi:10.1007/s10856-009-3930-y.

[80] E. S. Khoury, M. Abboud, N. Bassil-Nassif, J. Bouserhal, Effect of a two-year fluoride decay protection protocol on titanium brackets, International Orthodontics 9 (4) (2011) 432–451. doi:10.1016/j.ortho.2011.09.005.

[81] H. Uhlig, Mechanism of fretting corrosion, J. Appl. Mech 21 (1954) 401.

[82] S. Watson, F. Friedersdorf, B. Madsen, S. Cramer, Methods of measuring wear-corrosion synergism, Wear 181 (1995) 476–484.

[83] M. Godet, The third-body approach: A mechanical view of wear, Wear 100 (1984) 437–452. doi:10.1016/0043-1648(84)90025-5.

[84] N. Diomidis, J. Celis, P. Ponthiaux, F. Wenger, A methodology for the assessment of the tribocorrosion of passivating metallic materials, Lubrication Science 21 (2009) 53–67. doi:10.1002/ls.73.

[85] D. Landolt, S. Mischler, Tribocorrosion of passive metals and coatings, Woodhead Publishing Series in Metals and Surface Engineering, 2011. doi:978-1-84569-966-6.

[86] S. Mischler, Triboelectrochemical techniques and interpretation methods in tribocorrosion: A comparative evaluation, Tribology International 41 (2008) 573–583. doi:10.1016/j.triboint.2007.11.003.

[87] P. Ponthiaux, F. Wenger, D. Drees, J. Celis, Electrochemical techniques for studying tribocorrosion processes, Wear 256 (5) (2004) 459–468.

[88] S. da Rocha, G. Adabo, G. Henriques, M. Nóbilo, Vickers hardness of cast commercially pure titanium and Ti-6Al-4V alloy submitted to heat treatments, Brazilian Dental Journal 17 (2006) 126. doi:10.1590/S0103-64402006000200008.

[89] M. Geetha, A. Singh, K. Muraleedharan, A. Gogia, R. Asokamani, Effect of thermomechanical processing on microstructure of a Ti–13Nb–13Zr alloy, Journal of Alloys and Compounds 329 (2001) 264–271. doi:10.1016/S0925-8388(01)01604-8.

[90] A. Ribeiro, L. Vad, L. Rocha, Corrosion and tribocorrosion behaviour of new Ti35Nb5Zr and Ti35Nb10Zr alloys in artificial saliva, in: EUROCORR (Istambul), 2012.

[91] P. Majumdar, S. Singh, M. Chakraborty, Wear response of heat-treated Ti-13Zr-13Nb alloy in dry condition and simulated body fluid, Wear 264 (2008) 1015–1025. doi:10.1016/j.wear.2007.08.005.

[92] J. Ong, L. Lucas, G. Raikar, J. Gregory, Electrochemical corrosion analyses and characterization of surface-modified titanium, Applied surface science 72 (1) (1993) 7–13. doi:10.1016/0169-4332(93)90036-B.

[93] D. Wever, A. Veldhuizen, J. De Vries, H. Busscher, D. Uges, J. Van Horn, Electrochemical and surface characterization of a nickel–titanium alloy, Biomaterials 19 (7) (1998) 761–769. doi:10.1016/S0142-9612(97)00210-X.

[94] M. Esposito, J. Lausmaa, J.-M. Hirsch, P. Thomsen, Surface analysis of failed oral titanium implants, Journal of biomedical materials research 48 (4) (1999) 559–568. doi:10.1002/(SICI)1097-4636(1999)48:4<559::AID-JBM23>3.0.CO;2-M.

[95] J. Y. Park, J. E. Davies, Red blood cell and platelet interactions with titanium implant surfaces, Clinical oral implants research 11 (6) (2000) 530–539. doi:10.1034/j.1600-0501.2000.011006530.x.

[96] M. F. López, A. Gutiérrez, J. A. Jiménez, M. Martinesi, M. Stio, C. Treves, Thermal oxidation of vanadium-free Ti alloys: An X-ray photoelectron spectroscopy study, Materials Science and Engineering: C 30 (2010) 465–471. doi:10.1016/j.msec.2010.01.004.

[97] DoITPoMS, The interactive ellingham diagram, University of Cambridge. URL http://www.doitpoms.ac.uk/tlplib/ellingham_diagrams/interactive.php

[98] N. Diomidis, S. Mischler, N. More, M. Roy, Tribo-electrochemical characterization of metallic biomaterials for total joint replacement, Acta Biomaterialia 8 (2012) 852 – 859. doi:10.1016/j.actbio.2011.09.034.

[99] S. Mischler, S. Barril, D. Landolt, Fretting corrosion behaviour of Ti6Al4V / PMMA contact in simulated body fluid, Tribology-Materials, Surfaces and Interfaces 3 (2009) 16–23. doi:10.1179/175158309X408333.

[100] S. Takemoto, M. Hattori, M. Yoshinari, E. Kawada, Y. Oda, Corrosion behavior and surface characterization of titanium in solution containing fluoride and albumin, Biomaterials 26 (8) (2005) 829–837. doi:10.1016/j.biomaterials.2004.03.025.

[101] M. Lopez, A. Gutierrez, J. Jimenez, Surface characterization of new non-toxic titanium alloys for use as biomaterials, Surface Science (0) (2001) 300–305. doi:10.1016/S0039-6028(00)01005-0.

[102] T. Hanawa, Y. Kohayama, S. Hiromoto, A. Yamamoto, Effects of biological factors on the repassivation current of titanium, Materials transactions 45 (5) (2004) 1635–1639. doi:10.2320/matertrans.45.1635.

[103] D. Kolman, J. Scully, Limitations of potentiostatic repassivation techniques and their relationship to the applicability of the high field approximation to the repassivation of titanium, Journal of the Electrochemical Society 142 (7) (1995) 2179–2188. doi:10.1149/1.2044272.

[104] J. L. Gilbert, C. A. Buckley, E. P. Lautenschlager, Titanium oxide film fracture and repassivation: the effect of potential, ph and aeration, ASTM Special Technical Publication 1272 (1996) 199–218. doi:10.1520/STP1272-EB.

[105] T. Beck, Electrochemistry of freshly-generated titanium surfaces-II. Scraped-rotating-disk experiments, Electrochimica Acta 18 (11) (1973) 807–814.

[106] P. Jemmely, S. Mischler, D. Landolt, Electrochemical modeling of passivation phenomena in tribocorrosion, Wear 237 (1) (2000) 63–76. doi:10.1016/S0043-1648(99)00314-2.

[107] F. Contu, B. Elsener, H. Böhni, A study of the potentials achieved during mechanical abrasion and the repassivation rate of titanium and Ti6Al4V in

inorganic buffer solutions and bovine serum, Electrochimica acta 50 (1) (2004) 33–41. doi:10.1016/j.electacta.2004.07.024.

[108] M. Sakairi, M. Hiroomi, K. Tatsuya, T. Hideaki, Effect of potential, temperature, and fluoride ions on the repassivation kinetics of titanium in phosphate buffered saline solution with the photon rupture method, Laser Chemistry (2009) 436065doi:10.1155/2009/436065.

[109] D. Kolman, J. Scully, On the repassivation behavior of high-purity titanium and selected α, β, and $\beta+$ α titanium alloys in aqueous chloride solutions, Journal of the Electrochemical Society 143 (6) (1996) 1847–1860. doi:10.1149/1.1836914.

[110] T. Beck, Electrochemistry of freshly-generated titanium surfaces II. Rapid fracture experiments, Electrochimica Acta 18 (11) (1973) 815 – 827. doi:10.1016/0013-4686(73)85033-9.

[111] D. Landolt, Corrosion and surface chemistry of metals, EFPL Press, 2007.

[112] R. Wei, M. Gao, Further observations on the validity of bare surface current densities determined by the scratched electrode technique, Journal of The Electrochemical Society 138 (9) (1991) 2601–2606.

[113] R. Oltra, G. Indrianjafy, R. Roberge, Effect of electrical transient coupling phenomena on the initiation of pits by a pulsed laser, Journal of the Electrochemical Society 140 (2) (1993) 343–347. doi:10.1149/1.2221048.

[114] S. T. Pride, J. R. Scully, J. L. Hudson, Analysis of electrochemical noise from metastable pitting in aluminum, aged Al 2% Cu, and AA 2024-T3, Electrochemical Noise Measurement for Corrosion Applications, Special Technical Publication 1277 (1996) 307. doi:0-8031-2032-X.

[115] D. Gorse, C. Boulleret, B. Baroux, Effect of metallurgical factors on the electrochemical noise measured on aisi type 430 stainless steels in chloride-containing media, ASTM SPECIAL TECHNICAL PUBLICATION 1277 (1996) 332–342.

[116] G. Burstein, R. Cinderey, The potential of freshly generated metal surfaces determined from the guillotined electrode - A new technique, Corrosion science 32 (11) (1991) 1195–1211.

[117] G. Frankel, B. Rush, C. Jahnes, C. Farrell, A. Davenport, H. Isaacs, Repassivation transients measured with thin film breaking electrodes, Journal of the Electrochemical Society 138 (2) (1991) 643–644.

[118] R. Bosch, B. Schepers, M. Vankeerberghen, Development of a scratch test in an autoclave for the measurement of repassivation kinetics of stainless steel in high temperature high pressure water, Electrochimica acta 49 (17) (2004) 3029–3038.

[119] G. Burstein, P. Marshall, Growth of passivating films on scratched 304l stainless steel in alkaline solution, Corrosion Science 23 (2) (1983) 125–137.

[120] I. Garcia, D. Drees, J. Celis, Corrosion-wear of passivating materials in sliding contacts based on a concept of active wear track area, Wear 249 (5-6) (2001) 452–460. doi:10.1016/S0043-1648(01)00577-4.

[121] M. Dimah, F. D. Albeza, V. A. Borrás, A. I. Muñoz, Study of the biotribocorrosion behaviour of titanium biomedical alloys in simulated body fluids by electrochemical techniques, Wear 294 - 295 (0) (2012) 409 – 418. doi:10.1016/j.wear.2012.04.014.

[122] T. Hanawa, K. Asami, K. Asaoka, Repassivation of titanium and surface oxide film regenerated in simulated bioliquid, Journal of Biomedical Materials Research 40 (4) (1998) 530–538. doi:10.1002/(SICI)1097-4636(19980615)40:4<530::AID-JBM3>3.0.CO;2-G.

[123] J. R. Kearns, J. R. Scully, P. R. Roberge, D. L. Reichert, J. L. Dawson, Coupling of acoustic emission and electrochemical noise measurement techniques in slurry erosion-corrosion studies, Electrochemical Noise Measurement for Corrosion Applications 1277 (1996) 361. doi:10.1520/STP1277-EB.

[124] P. Wu, J. Celis, Electrochemical noise measurements on stainless steel during corrosion-wear in sliding contacts, Wear 256 (5) (2004) 480–490. doi:10.1016/S0043-1648(03)00558-1.

[125] M. Licausi, A. I. Muñoz, V. A. Borrás, N. Espallargas, Tribocorrosion mechanisms of Ti6Al4V in artificial saliva by zero-resistance ammetry (ZRA) technique, Journal of Bio-and Tribo-Corrosion 1 (1) (2015) 1–11. doi:10.1007/s40735-015-0008-x.

[126] N. Cabrera, N. Mott, Theory of the oxidation of metals, Reports on progress in physics 12 (1) (1949) 163.

[127] D. Landolt, S. Mischler, M. Stemp, Electrochemical methods in tribocorrosion: a critical appraisal, Electrochimica acta 46 (24-25) (2001) 3913–3929. doi:10.1016/S0013-4686(01)00679-X.

[128] H. Mohrbacher, J.-P. Celis, J. Roos, Laboratory testing of displacement and load induced fretting, Tribology International 28 (5) (1995) 269–278. doi:10.1016/0301-679X(95)00005-O.

[129] D. H. Buckley, Surface effects in adhesion, friction, wear, and lubrication, Vol. 5, Elsevier, 1981.

[130] S. Barril, S. Mischler, D. Landolt, Electrochemical effects on the fretting corrosion behaviour of Ti6Al4V in 0.9% sodium chloride solution, Wear 259 (2005) 282–291. doi:10.1016/j.wear.2004.12.012.

[131] T. Quinn, J. Sullivan, D. Rowson, Origins and development of oxidational wear at low ambient temperatures, Wear 94 (2) (1984) 175–191. doi:10.1016/0043-1648(84)90053-X.

[132] S. Bhola, R. Bhola, B. Mishra, D. Olson, Povidone–iodine as a corrosion inhibitor towards a low modulus beta Ti-45Nb implant alloy in a simulated body fluid, Journal of Materials Science: Materials in Medicine (2011) 1–7doi:10.1007/s10856-011-4268-9.

[133] S. Oh, I. Y. Na, K. H. Choi, The effect of curcumin against in vitro adhesion of implant device-associated bacteria on nanosized titanium dioxide, in: Journal of Nano Research, Vol. 23, Trans Tech Publ, 2013, pp. 83–90. doi:1662-5250.

[134] D. Hoeppner, V. Chandrasekaran, Fretting in orthopaedic implants: a review, Wear 173 (1) (1994) 189–197. doi:10.1016/0043-1648(94)90272-0.

[135] D. Nolan, S. Huang, V. Leskovsek, S. Braun, Sliding wear of titanium nitride thin films deposited on Ti-6Al-4V alloy by PVD and plasma nitriding processes, Surface and Coatings Technology 200 (20-21) (2006) 5698–5705.

[136] A. Ewald, S. Glückermann, R. Thull, U. Gbureck, Antimicrobial titanium/silver PVD coatings on titanium., BioMedical Engineering OnLine (2006) 5:22doi:10.1186/1475-925X-5-22.

[137] X. Peng, T. Clyne, Formation and adhesion of hot filament CVD diamond films on titanium substrates, Thin solid films 293 (1-2) (1997) 261–269. doi:10.1016/S0040-6090(96)09116-X.

[138] T. Manhabosco, I. Muller, Tribocorrosion of diamond-like carbon deposited on Ti6Al4V, Springer-Verlag Berlin Heidelberg 33 (2009) 193–197. doi:10.1007/s11249-009-9408-8.

[139] L. Le Guehennec, A. Soueidan, P. Layrolle, Y. Amouriq, Surface treatments of titanium dental implants for rapid osseointegration, Dental materials 23 (7) (2007) 844–854. doi:10.1016/j.dental.2006.06.025.

[140] C. Richard, C. Kowandy, J. Landoulsi, M. Geetha, H. Ramasawmy, Corrosion and wear behavior of thermally sprayed nano ceramic coatings on commercially pure titanium and Ti-13Nb-13Zr substrates, International Journal of Refractory Metals and Hard Materials 28 (1) (2010) 115 – 123, <ce:title>Tribology of Hard Coatings</ce:title>. doi:10.1016/j.ijrmhm.2009.08.006.

[141] D. Starosvetsky, A. Shenhar, I. Gotman, Corrosion behavior of PIRAC nitrided Ti-6Al-4V surgical alloy, Journal of Materials Science: Materials in Medicine 12 (2001) 145–150. doi:10.1023/A:1008922111376.

[142] F. Yildiz, A. Yetim, A. Alsaran, I. Efeoglu, Wear and corrosion behaviour of various surface treated medical grade titanium alloy in bio-simulated environment, Wear 267 (2009) 695–701. doi:10.1016/j.wear.2009.01.056.

[143] E. Krasicka-Cydzik, K. Kowalski, I. Glazowska, Electrochemical formation of bioactive surface layer on titanium, Journal of Achievements in Materials and Manufacturing Engineering 18 (2006) 147–150. doi:10.1016/j.corsci.2015.01.041.

[144] J. Hernández-López, A. Conde, J. De Damborenea, M. Arenas, Correlation of the nanostructure of the anodic layers fabricated on ti13nb13zr with the electrochemical impedance response, Corrosion Science 94 (2015) 61–69.

[145] L. Tan, R. Dodd, W. Crone, Corrosion and wear-corrosion behavior of NiTi modified by plasma source ion implantation, Biomaterials 24 (22) (2003) 3931–3939. doi:10.1016/S0142-9612(03)00271-0.

[146] T. R. Rautray, R. Narayanan, K.-H. Kim, Ion implantation of titanium based biomaterials, Progress in Materials Science 56 (2011) 1137 – 1177. doi:10.1016/j.pmatsci.2011.03.002.

[147] A. Gutiérrez, F. Pászti, A. Climent-Font, J. A. Jiménez, M. López, Comparative study of the oxide scale thermally grown on titanium alloys by ion beam analysis techniques and scanning electron microscopy, Journal of Materials Research 23 (08) (2008) 2245–2253. doi:10.1557/JMR.2008.0281.

[148] H. Güleryüz, H. Çimenoğlu, Effect of thermal oxidation on corrosion and corrosion-wear behaviour of a Ti-6Al-4V alloy, Biomaterials 25 (16) (2004) 3325–3333. doi:10.1016/j.biomaterials.2003.10.009.

[149] M. Jamesh, T. S. Narayanan, P. K. Chu, Thermal oxidation of titanium: Evaluation of corrosion resistance as a function of cooling rate, Materials

Chemistry and Physics 138 (2) (2013) 565–572. doi:10.1016/j.matchemphys.2012.12.020.

[150] D. Velten, K. Schenk-Meuser, V. Biehl, H. Duschner, J. Breme, Characterization of thermal and anodic oxide layers on β-and on near-β-titanium alloys for biomedical application, Zeitschrift für Metallkunde 94 (6) (2003) 667–675. doi:10.3139/146.030668.

[151] I. García, A. Ramil, J. Celis, A mild oxidation model valid for discontinuous contacts in sliding wear tests: role of contact frequency, Wear 254 (5Ű6) (2003) 429 – 440. doi:10.1016/S0043-1648(03)00262-X.

[152] A. Nurul Amin, Titanium alloys–towards achieving enhanced properties for diversified applications, InTech, Rijeka.

[153] G. Lütjering, J. Williams, Titanium, Springer Verlag, 2007. doi:1619-0181.

[154] M. Lopez, J. Jimenez, A. Gutierrez, Corrosion study of surface-modified vanadium-free titanium alloys, Electrochimica Acta 48 (10) (2003) 1395–1401. doi:10.1016/S0013-4686(03)00006-9.

[155] S. Izman, A. Shah, M. R. A. Kadir, E. Nazim, M. Anwar, M. Hassan, H. Safari, Effect of thermal oxidation temperature on rutile structure formation of biomedical TiZrNb alloy, in: Advanced Materials Research, Vol. 393, Trans Tech Publ, 2012, pp. 704–708.

[156] C. Leyens, M. Peters, Titanium and titanium alloys, Wiley Online Library, 2003. doi:3-527-30534-3.

[157] W. Shi, D. H.S., Improvement in the tribological properties of uhmwpe sliding against ti6al4v by surface modification, Journal of Shangai University 9 (2) (2005) 164–171.

[158] S. Kumar, T. S. Narayanan, S. G. S. Raman, S. Seshadri, Thermal oxidation of ti6al4v alloy: Microstructural and electrochemical characterization, Materials Chemistry and Physics 119 (1) (2010) 337–346. doi:10.1016/j.matchemphys.2009.09.007.

[159] B. Zhang, B. Wang, L. Li, Y. Zheng, Corrosion behavior of Ti-5Ag alloy with and without thermal oxidation in artificial saliva solution, dental materials 27 (3) (2011) 214–220. doi:10.1016/j.dental.2010.10.005.

[160] M. Orazem, B. Tribollet, Electrochemical impedance spectroscopy, Vol. 48, Wiley-Interscience, 2008. doi:9780470041406.

[161] A. Bloyce, P.-Y. Qi, H. Dong, T. Bell, Surface modification of titanium alloys for combined improvements in corrosion and wear resistance, Surface and Coatings Technology 107 (2) (1998) 125–132. doi:10.1016/S0257-8972(98)00580-5.